# CHAPTER ONE

# INTRODUCTION

## 1.1. Background of study

Nigeria is presently the world's leading producer of cassava (Phillips et al., 2004; FAO, 2008; Akinpelu et al., 2011). Efforts are geared toward promoting the export of the crop and its by-products. Due to the poor storage characteristics of the cassava tuber in its unprocessed state, it is necessary to process the product into a form that is more easily stored in order to minimize deterioration and losses while in transit. The forms in which cassava can easily be stored and transported without deterioration and losses are as dried pellets, chips, flour, garri and cassava starch.

Rapid population increase has a direct impact on food balance. The quality and quantity of farm produce in these developing countries are deteriorating due to poor processing techniques and unavailability of storage facilities. Research have proved that drying is the most effective and practical means of reducing post-harvest losses in all agricultural products (fruits, vegetables, tubers etc.). Such losses are due to the lack of proper processing and inadequate storage facilities. It has been estimated that in developing countries, losses range between 30 and 40% (Jayaraman and Gupta 1995). In addition, the demand for the year-round availability of seasonal food commodities has increased (Jayaraman and Gupta 1995). There is thus a pressing need to match increased production with efficient, suitable, simple, inexpensive and effective post-harvest preservation technique to minimize loss and ensure the supply and availability of food nutrients. To maintain the needed equilibrium balance between food supply and population growth, there is need to ensure that food losses during production time is reduced to the barest minimum.

Drying offers significant weight and volume savings, minimizing packaging and transportation costs and enabling storage of the product at ambient temperature thereby making the product available all year round (Pangavhane et al, 2002, Sharma, et al, 2009, Rahman et al 1999, Thijsen 1979). These goals can be achieved by supplying the necessary latent heat of vaporization to the water present in the food, and removing the resultant vapour from the food. That is, drying can be technically defined as a process of getting a dry product from simultaneous heat and mass-transfer process to removal of moisture or solute from a solid matrix (Jayaraman et al 1995, Karel et al 2003, Ramaswamy et al 2006). In recent years, drying techniques emerging as outcomes of laboratory-based research may yet prove to have a positive impact on the food industry in terms of scalability, energy efficiency, cost and end-product quality

Different methods of food drying exist. They include: sun drying, osmotic drying, microwave drying and convectional hot-air drying. Among these techniques, convectional hot-air drying has been the most common method employed for food materials. Researchers have reported that the major disadvantage of convectional hot-air drying is its low energy efficiency, which extends the drying time (Jayaraman et al 1995, Lewis et al 1987, Us P et al 2007). This prolonged exposure of food samples to elevated drying temperatures has been reported to be associated with substantial degradation in quality attributes such as colour, flavour, texture, retention of nutrients and reduced rehydration ability (Arabhosseini et al 2007, Bondaruk et al 2007, Young et al 1996).

Many studies conducted on convectional hot-air drying have shown that increasing the air temperature increases the rate of moisture evaporation from the food sample (Akgun et al, 2005, Doymaz et al, 2006, Karabulut et al, 2007, Maskan et al, 2002, Tarigan et al, 2007, Wachiraphansakul et al 2007, Yusheng et al 1988). However,

several researchers reported that this is often accompanied by degradation in the colour quality (browning) of the food (Jamradleodluk et al 2007, Karabulut et al, 2007, Lewis et al 1987, Tarigan et al, 2007). Maintaining the sample temperature at certain levels and at certain moisture contents is a useful strategy for overcoming colour degradation (Chou et al 2001, Chua et al 2000, Devahastin et al, 2004, 1999, Lewiki et al 2006, Mishkin et al 1983). Further studies have indicated that an improvement in colour quality can be achieved through periodical interruptions of the drying process (intermittent drying) or the employment of step-wise temperature profiles (Chua et al 2000, Devahastin et al 1999, Ozilgen et al 1995, Pan et al 1999). However, very few of these studies are based on drying temperatures above 100 ºC. In the current study, continuous drying of cassava chips at heater temperatures above $100^0$C is experimented upon, and the process numerically modeled using finite element method.

Knowledge of the drying kinetics of food materials such as the drying rate, time temperature-moisture content distributions, as well as theoretical and semi-empirical approaches to moisture movement, is essential for the prevention of quality degradation and for the achievement of fast and effective drying. Such information can be used to optimize production processes (Karel et al 2003, Leniger et al 1977, Thijsen 1979). The drying kinetics may be described completely by using their transport properties (thermal conductivity, thermal diffusivity, moisture diffusivity, and interface heat and mass transfer coefficients) together with those of the drying medium (Tiris et al, 1996). In the case of food drying, the drying constant K is used instead of transport properties.

The drying constant combines all the transport properties and may be defined by the thin layer equation.

Thin layer equations describe the drying phenomena in a united way, regardless of the controlling mechanism. They have been used to estimate drying times of several products and to generalize drying curves. In the development of thin layer drying models for agricultural products, generally the moisture content of the material at any time after it has been subjected to a constant relative humidity and temperature conditions is measured and correlated to the drying parameters (Togrul et al, 2006, Midilli et al, 2002).

Although there are many studies of hot air drying of fruits such as grapes (Yaldız, et al 2001), apricots, figs, grapes, plums (Togrul et al, 2006), figs (Doymaz, 2005), apples (Akpinar et al, 2003), prickly pear peel (Lahsasni et al, 2004), Stanley plums (Menges et al, 2006), no studies were found in literature about the numerical modeling of the drying kinetics of cassava pellets in a hot air dryer with forced convection. Hence the need for this research.

About 88% of cassava produced in Africa is consumed by humans, 50 percent of which is processed (Famurewa et al, 2014). Freshly harvested Cassava roots cannot be stored for a long period since they rot within 3 to 4 days after harvesting; this means that roots greater than 48 hours old have little market value and limits the range over which fresh roots can be marketed (Famurewa et al, 2014). Cassava roots are usually bulky with about 60-70 % moisture which makes transportation of the tubers to urban market and export difficult and expensive therefore drying is used as means to reduce spoilage and ease transportation. Cassava chips are unfermented white dried products of cassava with an average diameter of 3 to 5 mm. It is often used as a carbohydrate base, for human consumption, in the animal feed industry, milled into flour for other uses such as in the production of ethanol, cakes, dough-nut and biscuits. Traditionally, it is processed into dried whole roots with undesirable colour, irregular shapes and often contaminated with moulds (Balagopalan et al.,

1988). The quality of the dried chips produced is determined mainly in the drying stage. Undesirable biochemical changes and subsequent contamination and spoilage of the chips can only be prevented if the drying process is fast enough and the final product is dry enough (Maskan, 2000). Heat application to food during drying helps to achieve this. Though sun drying is the common method of drying of cassava in the tropics, this has a main disadvantage of slowness of the drying process due to the ambient temperature that is used for drying. Therefore there is need for alternative drying methods which is faster and provides extra advantage of providing uniformity of drying (Minguez-Mosquera et al., 1994; Tiris et al., 1994; Ayensu 1997).

Drying behaviour is basically influenced by a number of internal characteristics and thermo physical properties (such as density, permeability, porosity, sorption-desorption) and external parameters (such as temperature, velocity, and relative humidity of the drying medium) (Kaya et al., 2007). Drying kinetics of food crops is generally affected by factors which include drying temperature, pretreatment method, relative humidity, and product sizes (Ade-Omowaye et al., 2002; Kudra, 2004) and are crop specific. Many researchers have carried out studies on the drying characteristics and kinetics of various food crops (Sacilik et al., 2006; Doymaz, 2007; Vengaiah and Pandey, 2007; Goyal et al., 2008; Therdthai and Zhou, 2009). Physical and thermal properties of agriculture products such as heat and mass transfer, moisture diffusion, energy of activation, and energy consumption are required for ideal dryer design (Akpinar et al., 2003 a & b; Babalis and Belessiotis, 2004; Goyal et al., 2007). Mathematical modelling of drying processes and equipment is an important aspect of drying technology; its purpose is to allow design engineers to choose the most suitable operating conditions, size of the drying equipment and drying chamber accordingly to meet desired operating conditions.

The application of heat during drying affect quality of products. The drying kinetics for cassava chips need to be determined in order to stabilize variation in the quality of dried cassava chips. For these reasons, as well as the fact that most previous research on drying has concentrated on low air temperatures, this study considers the feasibility of using high temperatures for the drying of cassava pellets. Though, still within the recommended temperature range of drying diascoras.

## 1.2. Statement of Problem

In Nigeria, cassava is increasingly becoming a popular cash crop with a large proportion planted purposely for sale to local industries and export. Cassava chips and pellets are the two exportable products that are widely becoming popular in Nigeria. The chips, the most common form in which dried cassava roots are processed and marketed in most exporting countries, are dried irregular slices of the roots that vary in sizes but not exceeding 5cm in length (Raji et al 2008). The major problems associated with cassava chips include: mould formations caused by heating and sweating, resulting from long distance shipment. Chips occupy more space during packaging and transportation thereby resulting in higher cost of handling. Also because of their thin slices and fragile nature, they get broken down into smaller fractions during transportation and handling operations thus failing the international standard required for cassava chips.

As Nigeria props up her desire to be a major exporter of cassava to the international market, the need to improve the uniformity in the shape and size of cassava chips resulted in cassava pellets production. Therefore, research-based knowledge on drying/processing of cassava pellets cannot be overemphasized as it has become the most important form into which cassava could be processed for export. Thus, there is a compelling need for computer simulation of cassava drying, so as to avoid the

currently practiced costly experimental and empirical approaches which would need to consider cassava drying conditions on case-by-case basis.

Pellets are dried and hardened rectangular or cylindrical particulate materials of about 2-8cm long, 0.4-0.8cm in diameter and uniform in appearance and texture (Olm-Olyne, 2004) having about 9% moisture content wet basis which makes for good storability (Onyekwere et al., 1994). They have been observed to have a longer shelf life when dried to 8% moisture wet basis (Raji et al 2008). The advantages derived from processing cassava roots into pellet making them suitable for export include: uniformity in quality, strength (from partial gelatinization of starch and subsequent binding of the gelled starch) (Rajamma et al, 1994), light weight, less storage volume as well as retention of quality during shipment. From the above it is important to note that acceptability of the product in the international market is an important factor that requires extensive study on the drying, handling, processing, cost and time of production.

This study is therefore aimed at mathematical modelling of convective hot air drying of cassava pellets, with a view to delivering good quality products obtainable at the lowest production cost as well as the shortest production time. Results of the numerical and cassava drying kinetics of this study, is expected to perfectly describe the drying dynamics of cassava pellets. This could aid design engineers to choose the most suitable operating conditions, size of the drying equipment and drying chamber accordingly to meet desired operating conditions of cassava pellets production, thereby resolving the challenges of drying, processing, cost and time of production. This agro-industrial development venture will not only provide employment opportunities but also reduce the poverty level in the country. It will also contribute to the country's Economic Recovery and Growth Plan, which seeks to create new jobs in labour-intensive sectors like agriculture, by boosting

agriculture's GDP contribution to more than 8% by 2020, up from its current levels of between 3% and 4% annually (FMARD 2012), and make the country a net exporter of cassava pellets as it holds significant export potential due to its increasing demand in Asia, America and European market (https://oxfordbusinessgroup.com/blog/souhir-mzali/focus-reports/agriculture-africa-2019-special-report).

## 1.3 Aim and Objectives.

The aim of this work is mathematical modelling of convective hot air drying of cassava pellets.

The main objectives of this study are to:

1. Develop 2-Dimensional Numerical Models of coupled heat and mass transfer equations of convective drying for rectangular and cylindrical Cassava slices.
2. Develop a Computational algorithm for solving the mathematical models using the finite element technique
3. Apply the developed model in determining the state variables, surface temperature and moisture content of the samples, as well as the moisture diffusivity coefficient, the shrinkage, and drying rate.
4. Apply the numerical model to predict the effect of fixed and moving boundaries on the drying curve.

## 1.4. Significance of study.

Mathematical modeling of drying processes and equipment is an important aspect of drying technology; its purpose is to allow design engineers to choose the most suitable operating conditions, size of the drying equipment and drying chamber accordingly to meet desired operating conditions. In developing countries, the quality and quantity of cassava products and other agricultural products are deteriorating because of poor processing techniques and shortage in storage facilities. To solve this problem, there is need to develop a drying rate model for cassava pellets that would aid in the design of an industrial dryer so as to reduce losses during production time harvest and post-harvest to ensure that the best processing technique for its preservation is achieved.

## 1.5 Scope of Study

The scope of this research is to experimentally and numerically study the drying process of rectangular and cylindrical geometries of cassava pellets, employing the two-dimensional finite element model developed using Galerkin weighted residual method with a computer code, and using experimentally determined moisture diffusivity, mass transfer coefficient and shrinkage of the samples to describe the drying dynamics.

# CHAPTER TWO

# LITERATURE REVIEW

## 2.1 Drying Process

### 2.1.1 Heat and Mass Transfer

Heat and mass transfer is an essential thermodynamic process in food drying. During hot-air drying, there exist a simultaneous exchange of heat and mass between the food and the drying air. Heat is usually transferred from the food's surroundings to its surface by way of radiation, convection or conduction. In the case of hot air drying, convection is the predominant mechanism (Aguilera et al, 1990, Brennan 2006). This heat transfer to the food surface increases the temperature of the sample been dried and supplies the needed latent heat of vaporization for both the surface water and the water within the product. During this process, the internal moisture (mass) migrates to the surface of the food and then it evaporates to the surrounding hot air (Aversa et al 2007, Ramaswamy et al 2006, and Wagner et al 2007). Aguilera et al (1990), Al-Duri et al (1992) and Singh et al (1993) reported that the transport of moisture from the product surface to the air and the transfer of heat from the air to the product surface are functions of the existing concentration and/or water vapour pressure, and temperature gradients, respectively.

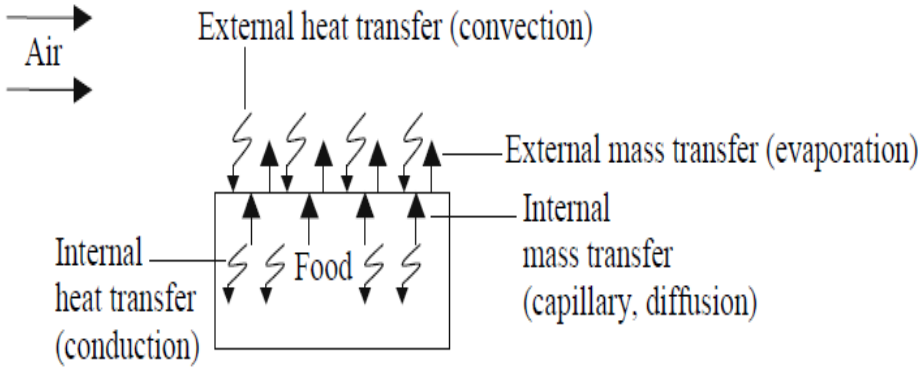


Fig. 2.1: Heat and mass transfer during the drying of a food particle in a hot oven. (Source: Heldman et al 1997)

From the above figure, external heat transfer occurs when convective heat (energy) is transferred from the air to the food's surface, while internal heat transfer occurs when conductive heat is transferred within the food. Internal mass transfer occurs when there is moisture transport within the food toward its external surface. During drying, external mass transfer occurs when there is evaporation and convective transfer of the vapour into the air

The term moisture refers to the volatile part of a food material. It has been used interchangeably in the literature with "water" to describe the amount of water present in foodstuffs (Sokhansanj et al 1995, Young et al 1996).

Transport phenomena thus involve both external and internal resistance to heat and/or mass transfer. Ramaswamy et al (2006) and Singh et al (1993) reported that the factors that slow the rate of these processes determine the drying rate. In other words, the resistance mechanisms control the drying rate. In general, it is accepted that the rate of the drying may be limited either by the rate of internal migration of water molecules to the surface or by the rate of evaporation of water molecules from

the surface into the air, depending on the conditions of drying (Heldman et al 1997, Ibarz et al 2003). This indicates that the resistance to mass transfer is considered to be the primary rate-limiting mechanism and the resistance to heat transfer may hence be neglected. The reason for this is that within the food, heat is usually transported more easily than moisture and thus the temperature gradients inside the food can be assumed to be flat (no resistance to internal heat transfer), especially when compared to the steep moisture content gradient (Karel et al 2003, Marquez et al 2006, Pavon-Melendez et al 2002) . In addition, it is known that heat transfer within the food may be limited by the thermal conductivity of the product as its water evaporates as reported by Donsi et al (1996) and Murphy et al (1999). In conjunction with the external heat transfer, Alzamora et al (1979) concluded that the temperature of the food increases rapidly at the beginning of drying towards the air temperature, indicating a decreasing resistance effect. Wang et al, (1995) attributed this phenomenon to the decrease in the thickness of the samples during drying, which leads to a faster heat transfer within the food. However, the difference between the food and the air temperature becomes negligible (external heat transfer) only after most of the initial water of the food has evaporated (Alzamora et al 1979). The air temperature, air humidity and velocity, and exposed surface area all influence the resistance to external heat and mass transfer whereas the internal mass transfer is only affected by the physical nature of the food, its moisture content and temperature. At the beginning of drying, since the internal resistance in the food is low enough to maintain the surface at saturation, evaporation takes place at a constant rate depending mainly on external heat and mass transfer. When the drying rate starts to decrease due to insufficient water at the surface, resistance to internal mass transfer governs the process.

Most foods therefore switch from an external drying process during the initial stages to an internal drying process as the product dries out (Karel et al 2003 and Ramaswamy et al 2006). In addition, the drying rate in the food sample, which decreases from the very beginning of the process (at a constant temperature), may also indicate that the internal resistance to mass transfer controls the drying (Demirel et al 2003, Marquez et al 2006 and Rahman et al 1999).

## 2.2 Factors Affecting the Rate of Moisture Removal

Factors that influence the drying rate of food have been grouped into two main categories by researchers. viz: factors related to process conditions and those related to the type of food.

### 2.2.1 Factors Related to Process Conditions

#### 2.2.1.1 Drying Temperature

Drying temperature is one of the key factors affecting the rate of moisture removal. The greater the temperature difference between the drying air and the food, the greater will be the heat transfer into the food. This results in a higher driving force (water vapour pressure gradient and/or water concentration gradient between the food surface and the drying air) for moisture removal, which shortens the overall drying time. Increased air temperature improves drying by affecting both external (constant rate period) and internal processes (falling rate periods). However, extremely high temperatures may cause quality loss, especially regarding colour. A practical limit must therefore be found for each food product to maintain maximum product quality (Hallstrom 1992, Heldman et al 1997).

### 2.2.1.2 Relative Humidity

Hallstrom (1992) explained that the amount of moisture in the air, as measured by the vapour pressure or relative humidity, influences the rate of moisture removal from the sample through its effect on external mass transfer. This suggests that relative humidity exerts more influence on drying in the constant-rate period than in the falling-rate period, where internal mass transfer is the controlling mechanism. The effect of relative humidity on external mass transfer is as follows: an increase in the relative humidity of the air decreases the water vapour pressure or water concentration gradient between the food surface and its surrounding air and thus reduces the rate of external mass transfer. Conversely, a decrease in the relative humidity of the drying air increases this gradient between the food surface and its surrounding air and hence enhances the rate of external mass transfer (Heldman et al 1997).

### 2.2.1.3 Air Velocity

The velocity at which the drying air blows across the food surface affects the rate of moisture removal through its impact on external mass transfer. Increasing the air velocity will take more moisture away from the drying surface of the food, preventing the moisture from creating saturated conditions there. This also shortens the duration of the constant rate period although it does not have a significant effect on the falling rate period (Heldman et al, 1997).

Several researchers have studied the effects of air velocity on the drying rate of different food samples (Kashaninejad et al, 2007, Madamba et al, 1996, Marquez et al 2006, Maskan et al, 2002). In these studies, it is revealed that the air velocity, like air humidity, does not influence the drying rate as much as the drying temperature. Studies have shown that a critical air velocity value above which the drying rate

dependence on air velocity becomes negligible. (Babalis et al, 2004, Freire et al, 2001, Kaymak-Ertekan 2002 and Vaccarezza et al 1974). In addition, Iguaz et al, 2003 and Wachiraphansakul et al 2007, reported that the effect of air velocity is more pronounced in the case of low temperature drying.

### 2.2.2 Factors Related to the Food Sample

#### 2.2.2.1 Thickness and Surface Area

The rate at which food can dry is determined by the distance that water molecules have to migrate within a food before evaporating from its surface. In the constant-rate period, smaller pieces have a larger surface area available for evaporation relative to their volume, whereas in the falling-rate period, smaller thickness means a shorter distance for moisture migration to the surface. Thus slicing or dicing into smaller pieces with high surface area will generally facilitate drying (Fellows 2000, Heldman et al 1997).

#### 2.2.2.2 Composition and Structure

The rate of moisture removal from food also depends on the composition and structural properties of the particular food material. For instance, a food material with high concentrations of solutes such as sugars, salts, gums, starches, etc. tends to interact with water molecules in the food and inhibit their mobility to the surface. This causes viscosity in the food to increase, resulting to a decrease in water activity, thereby slowing down the drying rate. Moisture migration within a food product may also occur in different directions depending on the orientation of the food microstructure such as fibers and protein strands. Fibers in celery and protein strands in meat, for example, allow more rapid drying along the length than across the cell structure.

Similarly, moisture is removed more easily from intercellular spaces than from within the cells since there is an additional resistance to water migration across the cell boundary. Blanching and/or reduction in sample size can increase the rate of moisture removal by weakening this resistance. However, such pre-treatments may also result in severe cell rupture and this kind of damage to the cell may adversely affect the texture of the rehydrated product. In addition, the loss of cellular structure, pore formation and shrinkage of the product, which are micro structural changes that occur during the drying of food materials, strongly affect the rate of drying (Fellows 2000, Heldman et al 1997).

#### 2.2.2.3 Internal Mass-Transfer Mechanisms during Drying

Internal mass transfer mechanisms which occur during drying of food exist in different forms. In food materials, moisture exists as bound water within the cell wall and vacuoles, liquid and vapour form in the pores and free water in the capillaries. Due to the differences in capillary attraction and in water vapour pressure and/or concentration, water flows from locations of high moisture content to locations of low moisture content during drying. These mechanisms for moisture within the product moving toward its surface may be summarized as follows:

1) Liquid movement by capillary forces

2) Diffusion of liquids, due to the differences in concentration of solutes at the surface and in the interior of the food

3) Diffusion of liquids which are adsorbed in layers at the surfaces of solid components of the food

4) Water vapour diffusion in air spaces within the food due to the vapour pressure gradients

One or more of these mechanisms may function simultaneously and their relative importance can change as drying progresses. In addition, the drying conditions described in the previous section (drying temperature, air velocity and relative humidity) affect these mechanisms since they alter moisture movement within the food (Fellows 2000, Ramaswamy et al, 2006; Saravacos, 1995).

#### 2.2.2.4 Capillary Movement

Geankoplis (2003) noted that during hot air drying, capillary forces are exerted on the material surface due to evaporation of water from the surface. This tends to pull the unbound water (free water) through the intercellular spaces (pores) and through the surface of the material due to interfacial tension between the water and the food. Hence, the capillary forces act in a direction perpendicular to the surface of the solid (Rahman et al 1999). As the water reaches the surface through the capillaries, pores and cracks on the surface open and air enters the food. Water is then replaced by air entering the food, and wets the surface of the sample. Such redistribution of water lowers capillary force potential (i.e. tension on the surface) slightly. As evaporation at the surface begins, capillary forces again increase until a further replacement of water by air entering the food through pores and cracks with water again wetting the surface. When the surface moisture first depletes, water can no longer be brought to the surface by capillary forces since no air can enter to replace the water. Hence the moisture recedes into the capillaries, and the drying rate falls (Moyers and Balwin 1997).

The driving force for capillary flow is considered to be the suction or the pressure difference between the water and the gas at the curved interfaces present in capillaries (Karel and Lund 2003). For a single capillary, the pressure difference is represented by the height of water given by equation 2.1.

$$h = \frac{2\gamma}{r_{cap} g \rho} \qquad 2.1$$

Capillary radius ($r_{cap}$) affects the water flow in such a way that small capillaries develop greater tensions than the larger ones. The tension is attributed to the concave curvature of the surface. Liquid water in capillaries of very small diameter will exert a lowered vapour pressure. Thus, the large capillaries tend to empty their water content first (Karel et al 2003, Rahman et al 1999).

As in the case of the constant-rate period, Geankoplis (2003) explained further that if the moisture movement follows the capillary flow, the drying rate will vary linearly with moisture content. That is, water moves from the interior of the food at the same rate as it evaporates from the surface and the surface remains wet. Therefore, the internal moisture movement during the constant-rate period is due to the capillary flow as suggested by Lewis (1987). The factors that influence the rate in this period (e.g. air velocity, air temperature and relative humidity of the air) are the same as those for the rate of moisture movement by capillary flow.

**2.2.2.5 Diffusion**

Diffusion is considered to be the main moisture transport mechanism during the falling-rate period in the drying of food materials. Unlike the free-water flow due to the capillary forces in the constant-rate period, moisture diffusion in food samples occurs randomly, responding to concentration gradients perpendicular to the main flow (drying air). It includes liquid diffusion through pores, diffusion of liquids which are adsorbed in layers at the surfaces of the components of the food, and vapour diffusion in air-filled pores (Karel et al 2003, Sablani et al 2000, Saravacos 1995). During the falling-rate period, in addition to diffusion, moisture transport may also take place through other mechanisms such as capillary flow and hydrodynamic flow, depending on the structure of the food material (i.e. size, shape, and connection

of pores in the sample). When there are different transport mechanisms and it is difficult to distinguish between the individual mechanisms, as in the case of falling rate period, the rate of moisture movement is then described by a lumped value, the so-called effective diffusivity ($D_{eff}$), irrespective of which mechanism is really involved in moisture movement. This measure incorporates all possible moisture transport mechanisms in one as reported by Marinos-Kouris et al (1995), Sablani et al (2000), Saravacos et al (2001).

The decrease in moisture concentration during drying leads to an unsteady state condition, i.e. the concentration (dc / dx) or the equivalent moisture content gradient (dW / dx) changes over time (falling-rate period). For such conditions Fick's second law of diffusion as given in equation 2.2 is often applied to analyze moisture transport mechanisms within the sample during the falling-rate period (Kunz 1993, Marinos-Kouris et al, 1995, Okos et al, 2003, Sablani et al, 2000, Sablani et al, 2000, Saravacos et al, 2001, Welti-Chanes et al, 2003).

$$\frac{dW}{dt} = D_{eff} \frac{d^2W}{dx^2} \qquad 2.2$$

Eq. 2.2 expresses how the concentration changes with time t at different positions in the food (Lewis 1987). This differential equation is solved analytically for certain sample geometries under the following assumptions:

- The food sample is one-dimensional
- Moisture diffusivity in the sample is constant
- Free-water content at the surface is essentially zero and moisture is initially distributed uniformly throughout the sample
- The shape and size of the sample remains constant during drying (i.e. there is negligible shrinkage)

- ❖ Heat transfer proceeds very quickly (negligible internal and external thermal resistance)
- ❖ Resistance to mass transfer at the surface is negligible compared to the internal resistance of the sample. That is, internal moisture movement is the main resistance to drying (there is no external moisture movement resistance)

Once the shape of the food product has been determined, eq. 2.2 is simplified and solved to obtain the effective moisture diffusivity ($D_{eff}$). Eqs. (2.3) to (2.5) represent the reduced analytical equations for the sample geometries of sphere, slab and cylinder, respectively (Barbosa-Canovas et al, 1996, Okos et al, 2003, Sablani et al, 2000).

**Sphere:**

$$\frac{W-W_e}{W_0-W_e} = \frac{6}{\pi^2}\sum_{n=1}^{\infty}\frac{1}{n^2}\exp\left(-n^2\frac{\pi^2 D_{eff}t}{r_s^2}\right) \qquad 2.3$$

Examples of products modelled as spheres include grapes (Doymaz 2006), pistachio nuts (Kashanine et al 2007), black tea (Panchariya et al 2002), soybeans (Prachayawarakorn et al 2006), and plums (Sacilik et al 2006).

**Slab:**

$$\frac{W-W_e}{W_0-W_e} = \frac{8}{\pi^2}\sum_{n=1}^{\infty}\frac{1}{(2n-1)^2}\exp\left(-(2n-1)^2\frac{\pi^2 D_{eff}t}{4L^2}\right) \qquad 2.4$$

Food samples assumed to be shaped like a slab geometry include apple and potato cubes (Ahrne et al, 2003), dill and parsley (Doymaz et al, 2006) and red bell pepper cubes (Vega et al, 2007).

**Cylinder:**

$$\frac{W-W_e}{W_0-W_e} = \frac{4}{r_c^2}\sum_{n=1}^{\infty}\frac{1}{\beta_n^2}\exp\left(-\beta_n^2 D_{eff}t\right) \qquad 2.5$$

Pasta (Andrieu et al 1986), raisins (Lomauro et al 1985), rice (Ramseh et al 2003), apple (Srikiatden et al 2005), and potato (Tang et al 2000) have been modelled as cylinders.

For food samples with more complicated geometries, numerical methods such as finite difference, finite element and control volume have been used for the evaluation of effective moisture diffusivity (Rotstein et al 1974, Sablani et al 2000).

Due to long drying times and for purposes of simplification, it is standard procedure to assume that only the first term of the series equations 2.3 to 2.5 is significant; the other terms can be dropped (Mujumdar et al 2003, Okos et al 2003,Sablani et al 2000,Temmerman et al 2007). The effective moisture diffusivity ($D_{eff}$) is then determined typically by plotting experimental drying data in terms of the natural logarithm (ln) of the moisture-content ratio, $W_R = ( W - W_e ) / (W_o - W_e)$ , against time (t). The slope of the drying curve is equal to the quantity $\pi^2 D_{eff} \pi / 4L^2$ in the case of slab geometry in eq. 2.4 from which the value of $D_{eff}$ is then calculated (Okos et al 2003, Sablani et al 2000).

The effective moisture diffusivities are often expressed as a function of moisture content rather than constant values, especially when plotting $\ln[( W - W_e ) / (W_o - W_e)]$ against time yields non-linear drying curves. In this case $D_{eff}$ can be determined by the method of slopes. The method calculates experimental values of $D_{eff}$ at each moisture content level essentially by repeated application of the diffusion eqs. (2.3) to (2.5) to the data, starting with the initial moisture content $W = W_0$ and moisture ratio $W_R = (W - W_e) / (W_o - W_e) = 1$ and continuing until the final moisture content is reached (Karathanos et al 1990, Moyers et al 1997,Saravacos et al 2001). Following this, the experimental drying curve is compared with the theoretical diffusion curve for the given shape of a material, as shown in Fig. 2.2. The slopes of the two curves are estimated at the same moisture-content ratio $W_R = (W - W_e) / (W_o$

$-W_e$) and $D_{eff}$ is calculated from eq. (2.6). Examples of application of this method can be found in the literature for a large variety of food materials such as figs (Bbalis et al 2004), rice (Ramseh et al 2003), apples (Srikiatden et al 2005), and corn starch (Uzman et al 2000).

$$D_{eff} = \left[\frac{(\frac{dw_R}{dt})_{experimental}}{(\frac{dw_R}{df_0})_{theoretical}}\right].L^2 \qquad 2.6$$

$$f_0 = \frac{Dt}{r_s^2}, Fourier\ number\ for\ diffusion \qquad 2.7$$

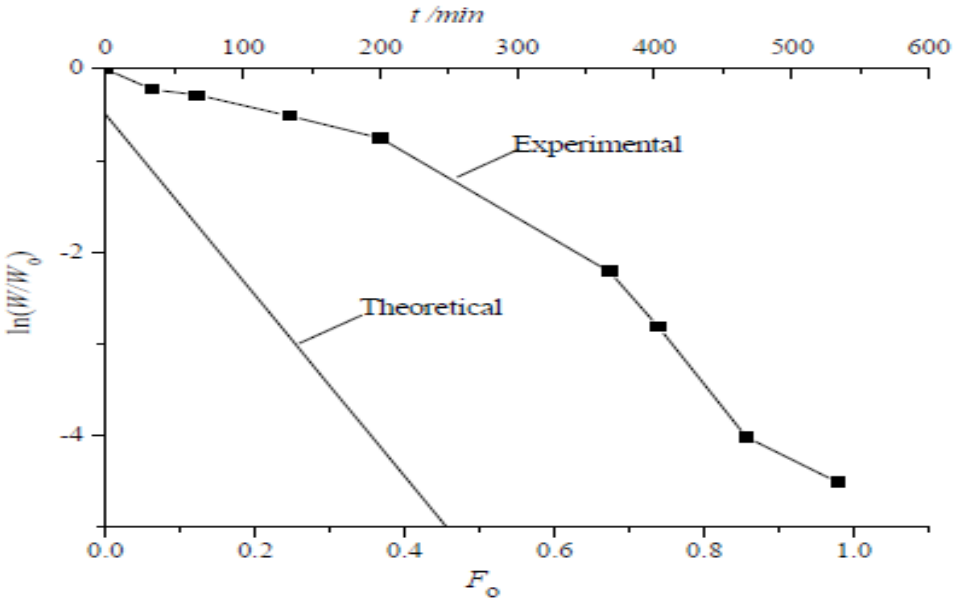


Fig. 2.2: Graphical representation of the method of slopes; adapted from Karathanos et al (1990), Saravacos et al (2001).

Effective moisture diffusivity in food ranges between $10^{-13}$ and $10^{-6}$ $m^2s^{-1}$, with most values in the region $10^{-11}$ to $10^{-8}$ $m^2s^{-1}$ whereas diffusivity in other materials such as sand, clay, wool, silica gel, wood and glass ranges between $10^{-12}$ and $10^{-5}$ $m^2s^{-1}$, with most values in the region $10^{-9}$ to $10^{-7}$ $m^2s^{-1}$ Saravacos et al (2001). These lower diffusivity values in food compared to other materials are ascribed to the

complicated biopolymer structure of food as well as to the stronger binding of water in it (Karel et al 2003, Marinos-Kouris et al, 1995). Saravacos et al, 2002 reported typical effective moisture diffusivity values for various classes of food materials as shown in table 2.1.

Table.2.1: Typical values of effective moisture diffusivity in food materials (Saravacos et al, 2002).

| **Food Material** | **Deff ·10-10/ $m^2s^{-1}$** |
|---|---|
| Highly porous | 50 |
| porous | 10 |
| Nonporous starch/sugar | 1 |
| Nonporous protein/starch | 0.1 |

Moisture diffusivity depends strongly on temperature and moisture content. However, drying itself also causes significant physical changes in the food sample, affecting its moisture diffusivity. For example, during drying, new cracks, pores and channels are formed in the sample. Moisture can then be transported through these at a faster rate in vapour form. Likewise, the presence of small, water-soluble molecules in the sample such as glucose reduces moisture diffusivity, by decreasing the porosity of the sample over the course of the drying process. These effects combine to form the relationship between moisture content and effective diffusivity.

A key assumption of Fick's second law of diffusion, eq. (2.2), for describing the rate of moisture movement within the food sample, is that there is only internal mass transfer during drying. Other transport mechanisms such as external mass transfer and both internal and external heat transfer are neglected. For the analysis of each of these transport mechanisms, corresponding partial differential equations should be

solved numerically. However, this requires considerable computing power and time, and in certain cases, it is not possible to solve them (Fontaine et al 1999, Husain et al, 1972, Marinos-Kouris et al, 1995, Parry, 1985; Pavon-Melendez et al, 2002, Ratti 2001; Simal et al, 2005).

This has led to the development of numerous semi-theoretical models, which propose simple alternatives to eq. (2.2), while still describing the behaviour of moisture loss over time during drying in a satisfactory manner. Among them, the models by Lewis equation. (2.8) and Page equation. (2.9) are the most commonly applied (Queiroz et al, 2004).

$$\frac{w}{w_0} = \exp(-k_{Lewis}.t) \qquad 2.8$$

Queiroz et al (2004) also noted that the Lewis model assumes negligible internal resistance, i.e. no resistance to moisture movement from within the material to the surface of the material. This inadequacies noted in the Lewis model does not provide complete description of mass transfer during drying, however, it is widely used due to its simplicity and computational speed. The drawbacks of eq. (2.8) are that it tends to overestimate the early stages and underestimate the later stages of the drying curve (Akgun et al 2005, Madamba et al 1996). Mascan et al (2001) and Panchariya et al (2002) have applied the Lewis equation respectively to model kiwi and black tea.

To overcome the limitations of the Lewis model, the Page model equation (2.9) offers an empirical modification to the time term by introducing an exponent n.

$$\frac{w}{w_0} = \exp(-k_{Page}.t^n) \qquad 2.9$$

Eq. (2.9) has been used by many researchers to describe and predict the rate of moisture loss during drying for several agricultural products such as noodles (Chen et al 2000), grapes (Doymaz, 2006), rice (Iguaz et al, 2003), Onion Slices (Kumar

et al, 2006), Indian gooseberry (Methakup et al, 2005) and carrots (Prabhanjan et al, 1995).

The parameters $k_{LEWIS}$, $k_{PAGE}$ and $n_{PAGE}$ have been correlated with different process variables such as air temperature and velocity, and sample conditions (e.g. existence of an external skin). It has been shown that the parameter k increases as drying temperature increases, while $n_{PAGE}$ does not demonstrate a clear trend (Methakup et al 2005, Senadeera et al 2003, Simal et al 2005, Tarigan et al 2007). However, the dependence of the drying constant $n_{PAGE}$ on air velocity has been reported in other studies (Chen et al 2000, Queiroz et al 2004). In addition, Karathanos et al (1999) observed an increase in the parameter $n_{PAGE}$ for the existence of an outer skin on the dried fruit, depending on the thickness and type of product. These models assume a direct relationship between moisture content and drying time. That is, they neglect the fundamentals of the drying process and their parameters have no physical meaning. However, they may be used to describe the drying curve for any particular given conditions (air temperature, sample thickness, etc.) of the experimental process (Fortes et al, 1981, Simal et al, 2005). Furthermore, they require less computation time when compared to the purely analytical models and do not make assumptions regarding sample geometry, moisture diffusivity and conductivity (Simal et al, 2005).

## 2.3 Drying of Agricultural crops

After harvesting agricultural products, they have to be stored, which is one of the main stages in any production. During this process, deterioration of considerable amount of the products may occur because of the existence of water in these products. Drying is a conventional method of preserving these products. In some areas around the world, some field products such as wheat, herbs, and raisins are usually spread on the ground for drying by exposure to direct sunlight. This method

has many disadvantages. For example, in most developing countries like Nigeria, providing food is not a problem with regard to the production of enough crops; the problem is its inability to preserve food surplus. Present production is usually much more than the immediate needs; thus, most of the products are wasted because of the short harvest periods, and scarcity occurs during post-harvest periods. Hence, to overcome this problem, drying has been considered as the most efficient preservation technique for most tropical crops (Ekechukwu et al, 1997). Artificial drying has been shown to be more efficient than the other methods of drying, which could not be totally managed. In industrialized countries, the energy consumption for drying is between 7% and 15% of the total energy consumption (Bennamoun et al, 2003). The following are some advantages in grain drying:

- Increase in the quality of the harvested grain by reducing the crop exposure to weather;
- Reduction in the harvesting losses due to head shattering and cracked kernels;
- Reduction in the dependence on weather conditions during harvest;
- Reduction in the size and number of combined harvest equipment and labour required due to extended harvest time; and
- Longer time for post-harvest field works (Kenneth et el, 1994).

Drying has been known to minimize losses of agricultural products from planting to consumption. Among the several methods for preserving agricultural products, increasing their economic lifespan and providing maximum amount of nutrition level, drying is the most used and the most economical method (Pangavhane et al 2002). The following benefits can be achieved using the drying system for agricultural products (Al-Juamily et al, 2007):

- Early harvest;
- Planning of the harvest season;

- Long-term storage without deterioration;
- Advantage in higher price a few months after the harvest;
- Availability of seeds; and
- Better quality product.

The amount of water to be removed from crops can be calculated as:

$$W_r = \frac{M_i - M_f}{1 - M_i} \quad (2.10)$$

Where $M_i$ and $M_f$ are the initial and final moisture contents (in fraction) of the crop on a wet basis. Then, the useful energy required for drying a unit amount (on dry mass basis) of a crop can be obtained using the following relation(Al-Juamily et al, 2007):

$$UE_{dry} = \left(\frac{1 - M_f}{1 - M_i}\right) S(T_d - T_a) + \left(\frac{M_i - M_f}{1 - M_i}\right) h_{fg} \quad (2.11)$$

In the above equation, the first term on the right-hand side represents the useful energy required for sensible heating of the wet crop from ambient temperature ($T_a$) to drying temperature ($T_d$). The second term represents the useful energy required for the evaporation of moisture in the crop, with $h_{fg}$ representing the enthalpy of evaporation of water at the drying temperature. The specific heats of the wet crop was estimated (in MJ/kg $^0$C) using the Siebel's formula (ASHRAE 1974).

Another expression of the useful energy required for drying a unit crop amount on a wet mass basis (Al-Juamily et al, 2007) is suggested as

$$UE_{dry} = \left(\frac{M_i - M_f}{1 - M_i}\right) hfg + S(T_d - T_a) \quad (2.12)$$

An energy evaluation for industrial paddy drying was performed by Jittanit et al (2010). The energy consumption of paddy drying in a large-scale milling plant was investigated, and some experiments were conducted in the laboratory. The results indicated that the specific primary energy consumption in three drying runs was between 3.874 & 4.421 MJ/kg of water evaporated for the whole process. Motevali

et al, (2011) investigated the energy consumption in different drying systems, including hot-air convection, use of micro wave pre-treatment with convection dryer, micro wave drying, vacuum drying, and infrared drying. Pomegranate arils were chosen for testing under diverse circumstances such as different temperature and three air-velocity levels (0.5, 1, and 1.5m/s) with three pre-treatment of the control in the case of convection drying. The following equation is used to compute the energy consumption of the pomegranate arils:

$$E_t = A\rho_a C_a \Delta T t \quad (2.13)$$

where Et is the total energy consumption in each drying round (kWh), A is the cross-sectional area of the container where the sample was placed($m^2$), ρα is the air density($kg/m^3$), t is the total drying time of each sample(h), ΔT is the temperature difference($^0C$), and Ca is the specific heat of air(kJ/kg $^0C$). Then, the specific energy to dry 1kg of pomegranate arils was calculated by $E_{kg} = E_t/W_0$, where $E_{kg}$ is the specific energy (kJ/kg) and $W_0$ is the weight of the sample. The results showed that the energy consumption in convection drying at the maximum condition was approximately 240kWh/kg and was reduced to 160 and 90kWh/kg when 100-and 200-W microwave vacuum dryers were used, respectively.

An investigation was conducted on the drying of onion slices, and the total energy requirement for different inlet air temperature and airflow rate were examined. The results showed that for a change in moisture content from an initial value of 86% (wet basis) to the final value of approximately 7% (wet basis),the energy required per unit mass of moisture/water removed was between 23.548 and 62.117 MJ/kg, whereas the percentage of energy contribution for heating and dehydration was approximately 69% of the total energy consumption (Sarsavadia, 2007). He reported that the variation in the energy required in terms of time at different air temperatures is approximately 2.43 kg/min airflow rate.

Adiletta et al (2018), investigated the influence of an alternative chemical pretreatment on dehydration and rehydration of an Italian ecotype pumpkin. The pretreatment consisted of soaking the slices in a diluted solution of trehalose, sucrose and NaCl. Hot air-drying was performed in a convective dryer at temperatures of 55, 60, 65 and 70°C. Samples treated prior to drying showed a shorter (about 1/4) drying time, less volume shrinkage and colour changes, but showed higher rehydration capacity compared to untreated ones, especially in the range 55-65°C. Moreover, the pretreatment was effective in retention of total phenolic content and antioxidant activity. The Midilli model was the most appropriate for describing drying behaviour, while the Weibull model for rehydration.

Dagde et al (2013), presented an experimental approach to the drying of yam slabs using microwave. The reduction in mass of the yam slab with time at low conditions was investigated. A theoretical model to describe the drying of the yam slab in microwave was developed and validated using the experimental data. The effective diffusivity of water molecules in yam slab in medium low power condition of the microwave oven was estimated to be $5.83 \times 10^{-8}$ $m^2/s$. Simulations of the model reveals that the microwave drying of yam slabs is very sensitive to the thickness of the yam slab and is independent of the moisture content and initial mass of the yam slab. As the thickness of the yam slab increases the rate of drying decreases and therefore the time for complete drying increases.

Jie Chen et al (2013), in their study presented the drying characteristics of fresh Momordica charantia slices at different drying temperatures (50, 60, 70 and 80°C) and different thicknesses (0.5, 0.75 and 1.0 cm). Three mathematical models including Page, Henderson and Pabis and Wang and Singh equations were compared and discussed. The results showed that the Page model provided the best correlation with a regression coefficient $R^2$ of 0.998. The color change of Momordica charantia

slices during hot air drying at different temperatures were also studied by the measuring of color parameters such as whiteness/darkness, redness/greenness and yellowness/blueness. The total color change (ΔE) of the samples was observed to increase as drying temperature increased. Results show that the color of Momordica charantia slices changed sharply when temperature was higher than about 70°C.

Jompob et al (2006) investigated the applicability of simplified mathematical drying models from the research works proposed by several investigators to the drying of some agricultural products. Drying experiments were conducted using a conventional biomass longan dryer (Figure 2.3) at drying air velocity of 1.34m /s and drying air temperature of 80$^{o}$C for red chili peppers, 70$^{O}$C for lemon grass and 60$^{O}$C for leech lime leaves. Drying curves obtained from the experimental data were then fitted to the empirical drying models. Thirteen different mathematical drying models were compared according to their coefficients of correlation in order to estimate the drying curves of those products. The results have shown that among the models, the Midilli et al (2001) model was found to be the best model for describing the drying behavior of red chili peppers and leech lime leaves, whereas the Wangh and Singh model was the most suitable for lemon grass. The results of regression analysis indicated that these models could be used to model the drying behavior which is useful for simulation studies of drying systems.

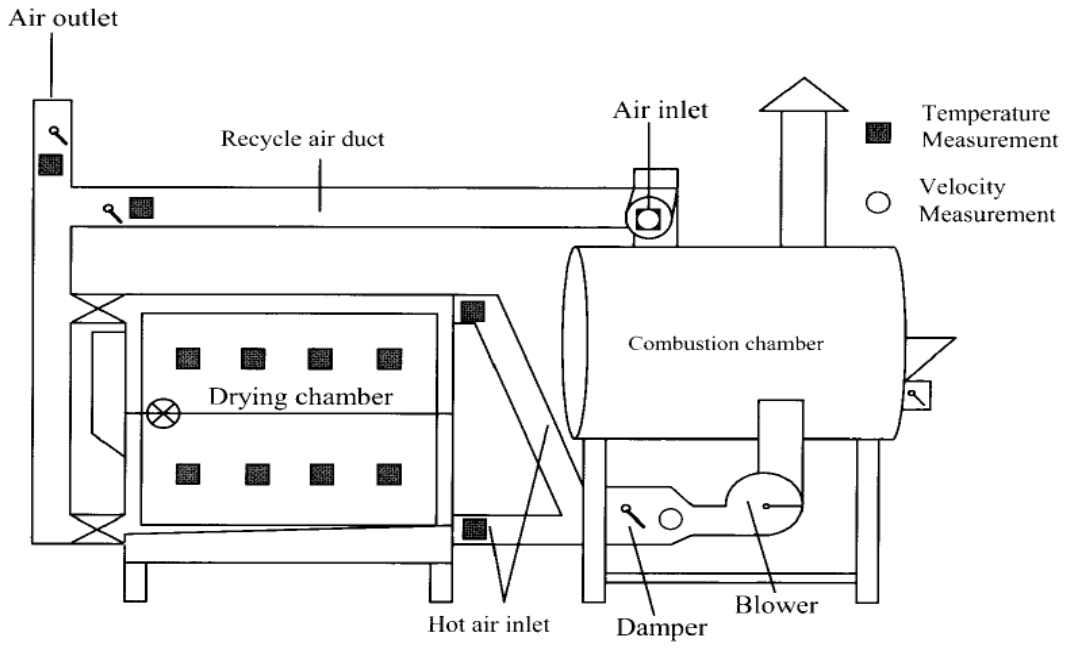


Fig 2.3: The configuration of a conventional biomass longan dryer (Jompob et al 2006).

## 2.4. Different Designs of Drying Chamber

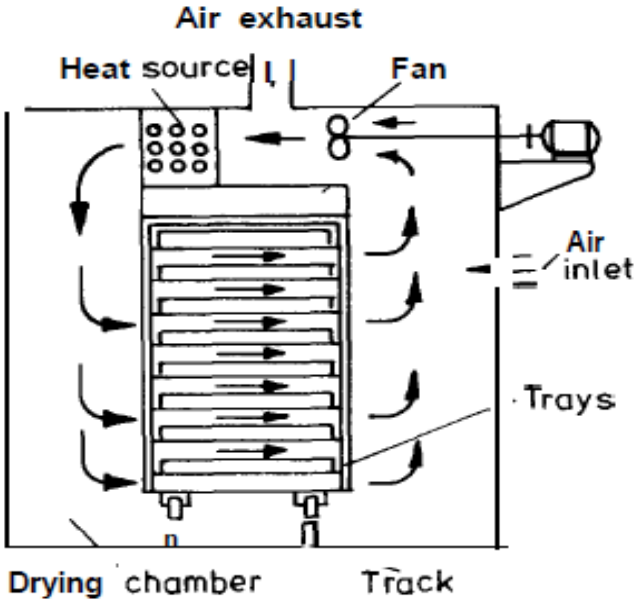


Fig: 2.4. Tunnel drying cabinet (Sayali et al, 2016)

In the design shown in Fig. 2.4, the drying material is spread over trays, and these trays are kept in the tunnel where a constant temperature is maintained with the help of a heat source. Air circulation is maintained with the help of a fan (forced convection). The major drawback in this type of dryer is that the same air is circulated through a cabinet making the initial drying rate faster and better than when the air become moist due to evaporation, which automatically decreases the drying rate.

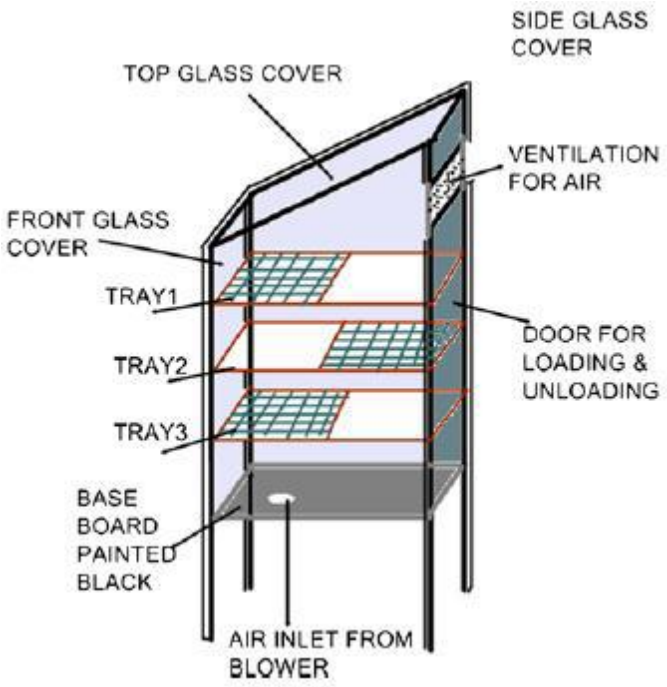


Fig: 2.5.Drying chamber design by C. Pardhi & Bhagoria (Sayali et al, 2016)

A drying chamber design reported by Sayali et al, (2016) is shown in figure 2.5. In this dryer, equal amount of the products to be dried are spread over three trays. Hot air enters from the bottom and comes out from the top opening. The major drawbacks in this design is that the moisture removal rate is highest for tray no. 3 and least for tray no. 1. For tray no. 1. Due to the differences in moisture removal

rate, three different types of dried products are obtained, which are not acceptable. The products of tray no. 1 has higher moisture as compared to the products of tray no. 3.

## 2.5 Review on types of Grain Dryers

Dryers can be categorized in different ways. According to Hellevang (2013), dryers are grouped into natural air/ low temperature, and high temperature dryers; there are also batch, automatic batch and continuous flow dryers; and there are in-bin and column or self-contained dryers. Dryers can also be classified according to the direction of airflow through the grain; cross-flow, counter-flow, and concurrent-flow.

### 2.5.1 Natural air/Low Temperature Drying

Natural air/low temperature drying refers to drying grain using little or no additional heat. Drying takes place in a drying zone which advances upward through the grain (Figure 2.6).

**Advantages:**

• No harvest bottle neck. The bins can be filled at the harvest rate.

• A properly sized system may dry the crop more economically than a high temperature dryer.

**Disadvantages:**

• There is a limit on initial moisture content that can be effectively dried.

• Electrical power must be available at each bin for dryer fan motors.

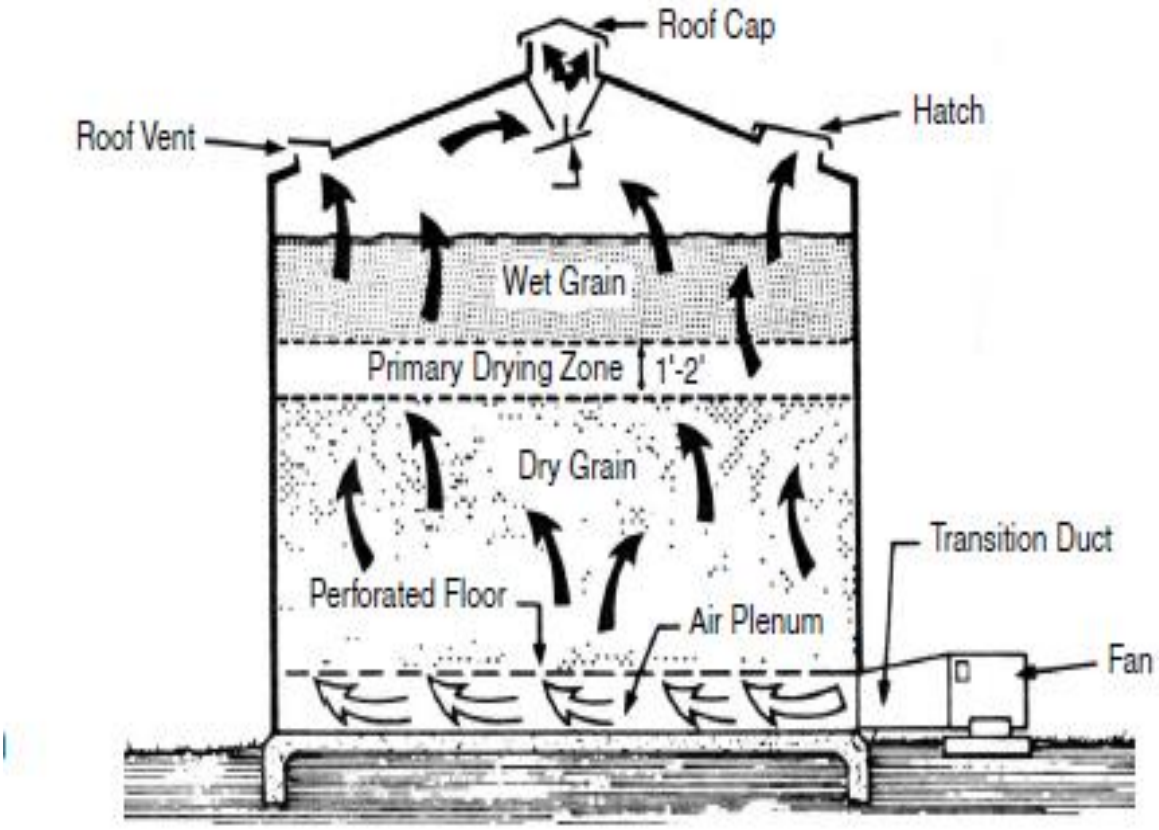


Figure 2.6. A typical bin dryer utilizing natural air/low temperature drying (Hellevang, 2013).

Grains above the drying zone remain at the initial moisture content or slightly above, while grains below the drying zone are at a moisture content in equilibrium with the drying air. Drying may take several weeks depending on the airflow rate, climatic conditions and the amount of water to be removed. Natural air/low temperature drying requires enough airflow to complete drying within the allowable storage time. A well designed perforated floor is recommended for all in-bin drying. Since air does the drying, it is imperative that air reaches all the grain. The size of the perforated floor is dependent on the dryer size and the quantity of grains to be dried. Hence, for faster drying, proper sizing of the floor must be done. Ducts can also be used in place of perforated floor for bin dryers. However, the uniform airflow distribution required

for drying is more difficult to achieve with ducts than with perforated floors. If duct must be used, proper duct spacing must be taken into account during its design. This will ensure that drying can be done successfully within the shortest possible time. As reported by North Dakota State University, AE701, Perforated ducts should be placed on the floor with a maximum centerline spacing equal to one-half the grain depth or the shortest distance to the grain surface. The distance from the duct to the wall must not exceed one-fourth the grain depth at the duct next to the wall. If the duct is longer than 100 feet, it is better to place a fan at each end of the duct.

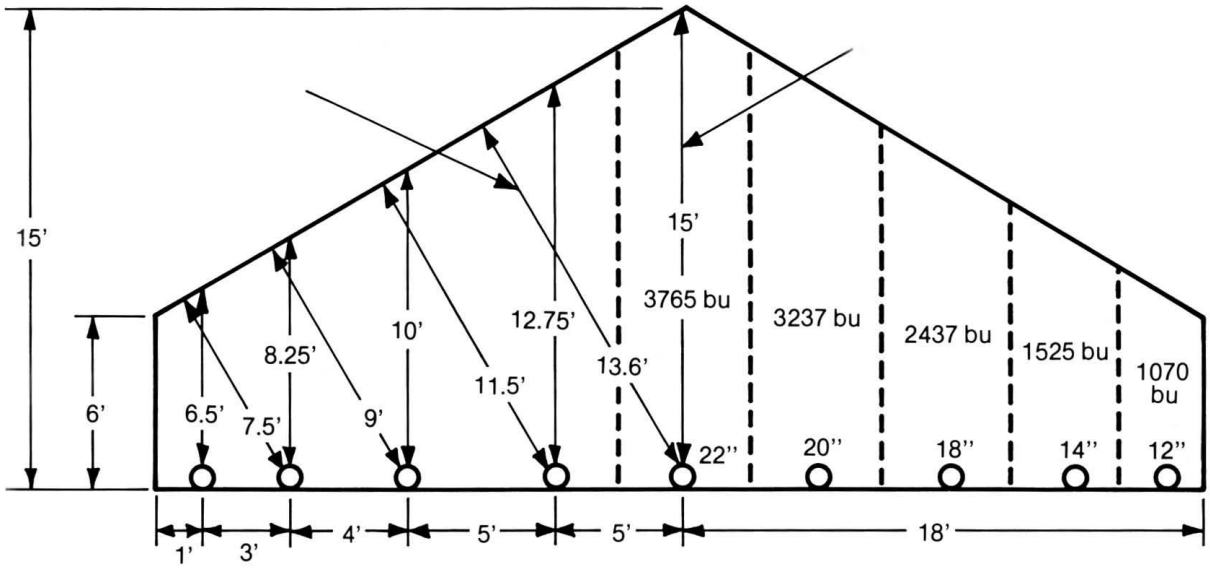


Figure 2.7. A Natural Air/Low Temperature Crop Dryer showing duct size and spacing in a 36' x 72' building with grain 6 feet deep next to the walls and 15 feet deep in the center. (Source: NDSU Extension Bulletin 35, "Natural Air/Low Temperature Crop Drying.")

The greatest risk involved with natural air/low temperature drying occurs if an abnormally warm, damp period of weather occurs after the grain has been placed in the drying bin. This permits rapid mold development while drying speed is increased very little. Layer drying or combination drying, to be described later, are options

used with natural air/low temperature drying when the grain is wetter than the system is designed to handle.

### 2.5.2 Layer Drying

Layer drying is very similar to natural air/low temperature drying except the grain is placed into the drying bin in layers normally about 4 to 5 feet deep depending on the dryer size. In this type of dryer, the grains are fed into the dryer in batches. Firstly, an initial batch or layer of grain is placed in the bin and drying is begun. As soon as drying zone is established and begins to move through the grain, other layers of grain would be added so that a depth of wet grain exists ahead of the drying zone. On a full-bin basis, limiting grain depth to get a higher airflow rate allows drying the grains fed into it at higher moisture contents which may affect the efficiency of the dryer. In designing this type of dryer, the airflow rate and fan size must be carefully considered to ensure optimum performance of the dryer. As shown in Figure 2.8, the actual airflow rate will vary due to individual fan performance.

Due to non-uniformity of the drying front, as drying advances, several points must be checked. The drying front is usually ascertained by probing and measuring the moisture content at various levels. Results obtained from probing, determines when to feed in the next batch of grains to be dried. A common problem with layered drying systems is adding additional wet grain too rapidly, resulting in spoilage of the upper layers.

**Advantage:**

• Grain with a higher initial moisture content can be harvested as compared to the maximum initial moisture content used in full-bin drying.

**Disadvantage:**

• The harvesting schedule may be restricted.

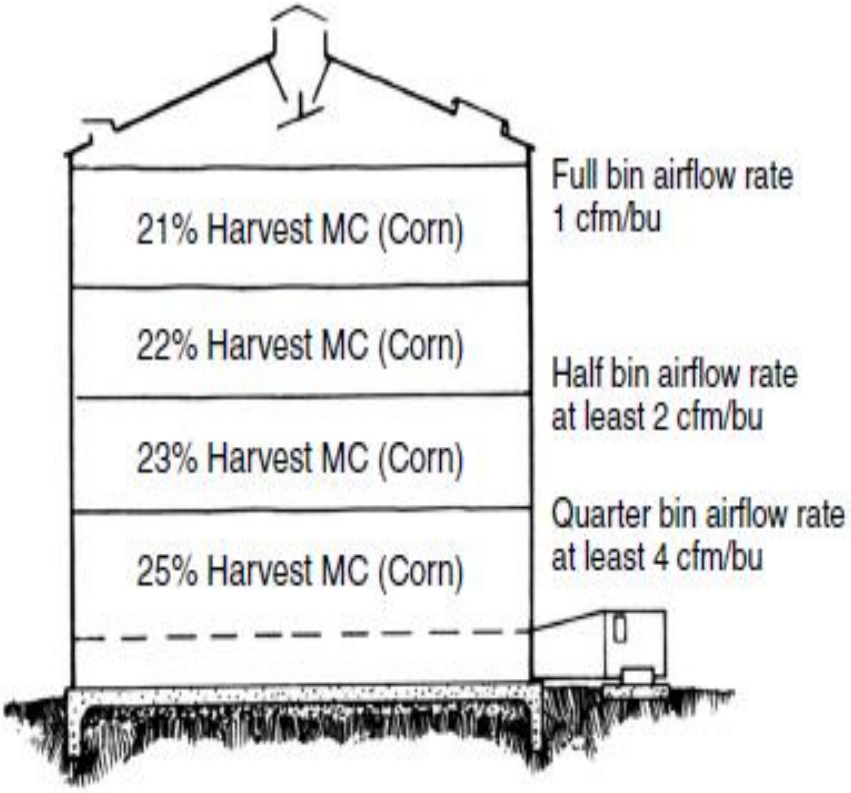


Fig. 2.8: Example of layer drying. The higher airflow rates on a per bushel basis early in the filling permit a higher initial moisture content to be loaded.

### 2.5.3 High Temperature Bin Drying

**Advantages:**

• The bin can be used for storage at the end of the drying season.

• Wetter grain can be dried than can be dried with a natural air or low temperature dryer.

**Disadvantages:**

• A large moisture variation between grain kernels is possible.

• Grain damage may occur from stirring.

### 2.5.4 Batch-in-Bin Drying

This dryer is the simplest dryer. It is usually designed with a storage bin having a perforated floor and a blower to move air through the grain. If the grains just harvested from the field is less than 20 - 22% moisture content, the grain is usually dried with just ambient air, so long as there is enough air flow. The grains must be screened before filling the bin and drying in layers of $0.06m^3$ to $0.09m^3$ at a time will decrease drying times. Ideally, if multiple bins are available, each bin can be filled with a layer of grain before adding more to the first bin filled. During a fall with low humidity, ambient drying will have the highest energy efficiency although it will all be electrical energy. During a fall with damp weather, the grain may not be dried down to storage moisture until spring which will greatly reduce the energy efficiency. If the weather is warm and the grain is high in moisture (20 %+) spoilage can be of concern. To reduce the risk of spoilage and long drying times, a small amount of heat can be introduce with a small resistance heater or a solar collector. Generally the air temperatures are increased up to a maximum of 10°F by these methods while drying times can be reduced significantly especially during damp fall weather where relative humidity exceeds 80%. The basic principle behind the operation of a batch-in-bin dryer is to force relatively large quantities of air through a shallow grain depth so as to obtain a rapid drying speed, thus allowing the producer to accommodate larger harvest rates with other types of in-bin drying.

One reason for the popularity of batch-in-bin drying is the flexibility available when selecting the drying system equipment. Management of a batch-in-bin system is less

critical than in other in-bin drying units since the operator has an opportunity every 24 hours to correct any mistakes. This also allows for some fine tuning of the drying process. The main disadvantage of a batch-in-bin drying system is that the grain must be handled twice. The drying bin must be leveled and unloaded each day; this requires placing the sweep auger in the drying bin at each unloading (unless power sweeps are used) and frequent moving of any portable handling equipment, unless a second auger was purchased to be used exclusively for unloading the drying bin

#### 2.5.4.1 Recirculating Bin Dryer

These are typically small portable dryers that have a central plenum with a column of grain encircling the plenum. They can be manually or automatically loaded and unloaded. Some are powered from a tractor PTO which allows them to be used almost anywhere. The major disadvantage is they require more supervision and labour per bushel than other types of dryers. A well operated batch dryer has approximately the same energy efficiency as a continuous cross flow dryer with cooling section heat recovery. The recirculating bin dryer incorporates a tapered sweep auger which removes grain from the bottom of the bin as it dries (Figure 2.9). The sweep auger is usually controlled by temperature or moisture sensors. When the desired condition is reached, the sensors start the sweep auger, which removes a layer of grain as it rotates. After one complete revolution around the bin, the sweep auger stops until the sensor determines that another layer is dry. The process continues repeatedly until the entire grain is completely dried, after which the dried grain is redistributed on top of the grain surface. The dried grain will be partially rewet by the moist air coming through the grain, which reduces drying efficiency. After all the grain has been dried, the grain is cooled in the bin. The dried and cooled grain is then moved to storage or may be left in the bin. It is common to dry the last bin full of grain using a continuous flow bin dryer as a recirculating bin dryer.

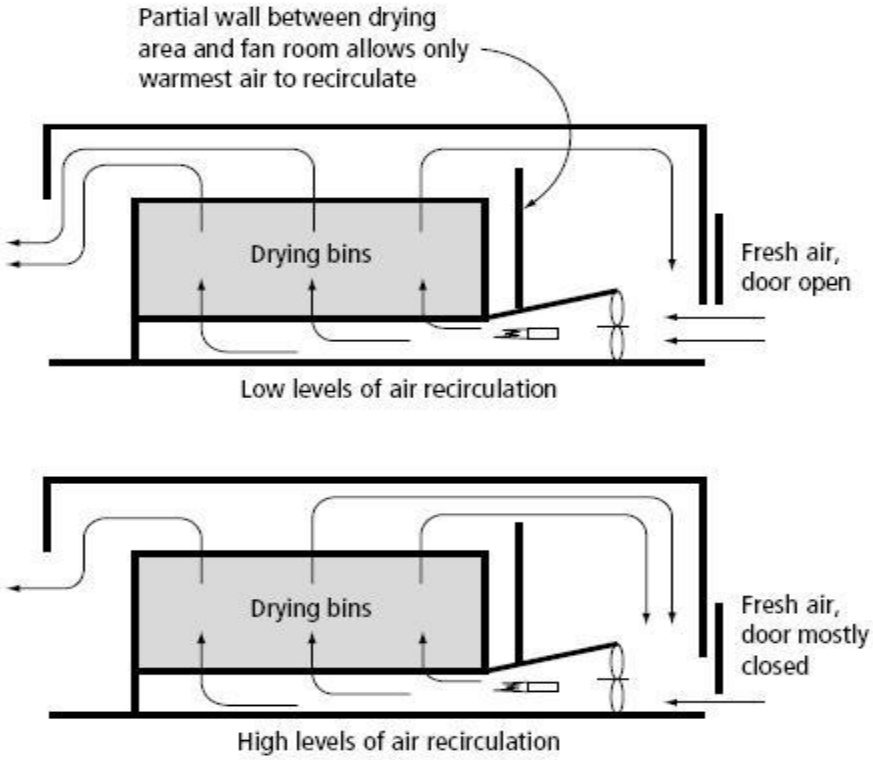


Figure 2.9. High and Low levels of air recirculation grain dryers.

### 2.5.4.2 Continuous Flow Bin Dryer

The continuous flow bin dryer is designed to have a tapered sweep auger whose function is to remove grain from the bottom of the bin as it dries, but the grain is moved to a second bin for cooling (Figure 2.10). Up to 2 points of moisture may be removed in the cooling bin if dryeration is used. (Dryeration is a process where hot grain is removed from the dryer with a moisture content 1 or 2 percentage points above that desired for storage.) Usually, increasing the grain depth will reduce the airflow rate, and the drying rate of a continuous flow bin dryer. In a recirculating batch or continuous flow bin dryer, it is the total airflow capacity that determines the drying rate, not the airflow rate. In this type of dryer, the heat recirculation system guides warm exhaust air directly back into the dryer fan inlet. It works best on continuous flow horizontal or tower dryers operated to dry and cool simultaneously.

Heat Recirculation Performance for a single-stage continuous cross-flow grain dryer, the temperature and relative humidity (RH) of the exhaust air that is warm (at least 20°C-30°C above ambient) with low humidity (40% or less) can be recirculated to reduce energy use. Generally, this is the exhaust air from the lower half of the dryer (including the cooling section).

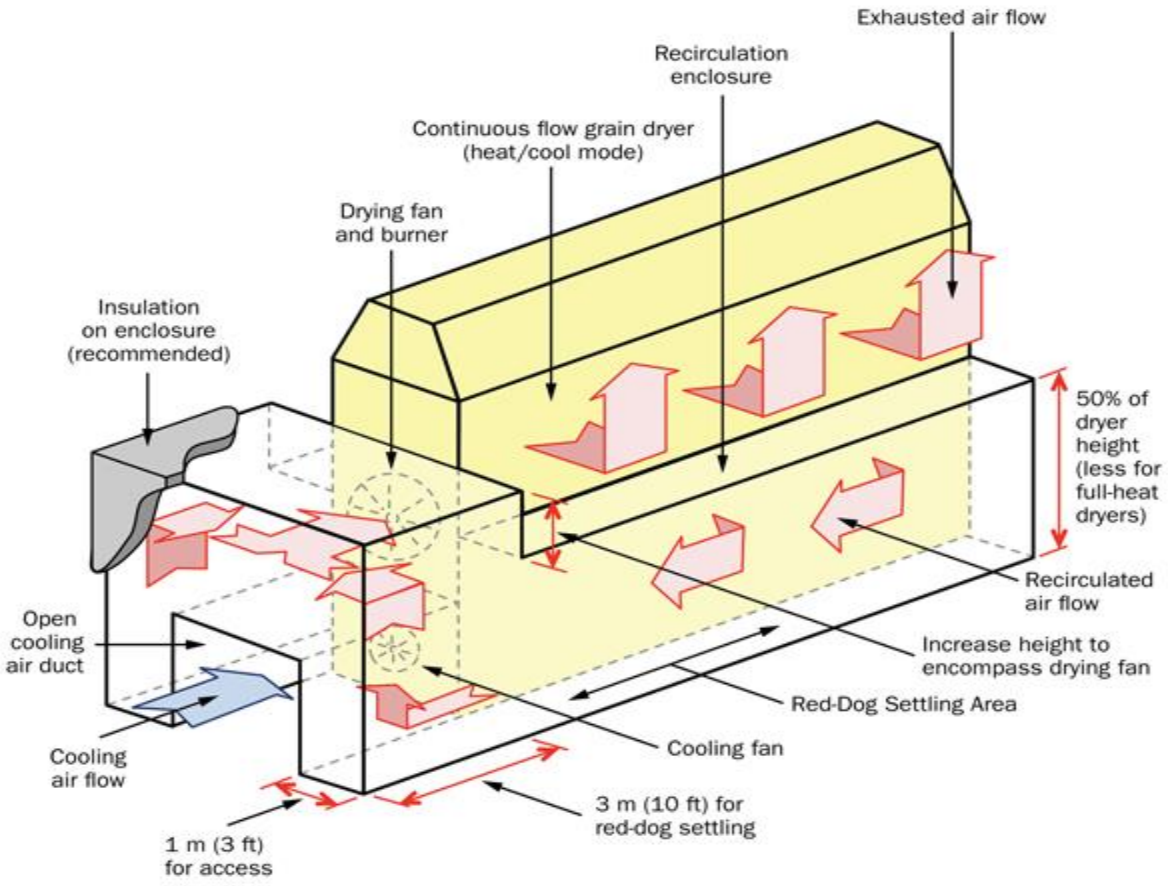


Fig. 2.10: A heat recirculation system on a two-fan continuous flow dryer operating in the heat/cool mode. (Source: Ontario ministry of Agriculture, Food and Rural Affairs. http://www.omafra.gov.on.ca)

### 2.5.5 Column Dryers

Column Dryers are usually designed for plug flow and have a special gas distribution cone to ensure uniform counter-current gas flow up through the material. The effectiveness of this design, results in very low gas flow rates thereby achieving low operating costs. This is especially important when the process gas is nitrogen, steam or other treated gas. Usually, residence time can vary from 1 to 24 hours, depending on the diffusion rate of moisture through the material. Heating coils may be incorporated to enhance thermal input to the material.

The Column Dryer is well suited to process Polymers, Organic Chemicals, and Inorganics. However the feed to the Column Dryer must be non-sticky and in the form of free-flowing crumbs, granules, beads, pellets, or powder and are often employed as a second stage unit. The major advantage is that the dryer does not occupy grain storage space, and its portable units can be moved from one location to another. The major disadvantage is that the heat available in the dryer is not used as efficiently as in deep bed drying.

### 2.5.6 Column Batch Dryers

In column batch dryers, grains are completely filled at one time. The most common batch dryer configuration has two columns surrounding a plenum chamber (Figure 2.11). Several circular-shaped batch dryers are also available. Hot air forced into the plenum from a fan-heater unit passes through the grain-filled columns and dries the grain. This dryer is characterized by high temperatures and high airflow rates. The typical operating sequence is fill-dry-cool-unload. Time for one batch varies, but an average may be two to three hours per batch. Control of the drying sequence can be either manual or automatic.

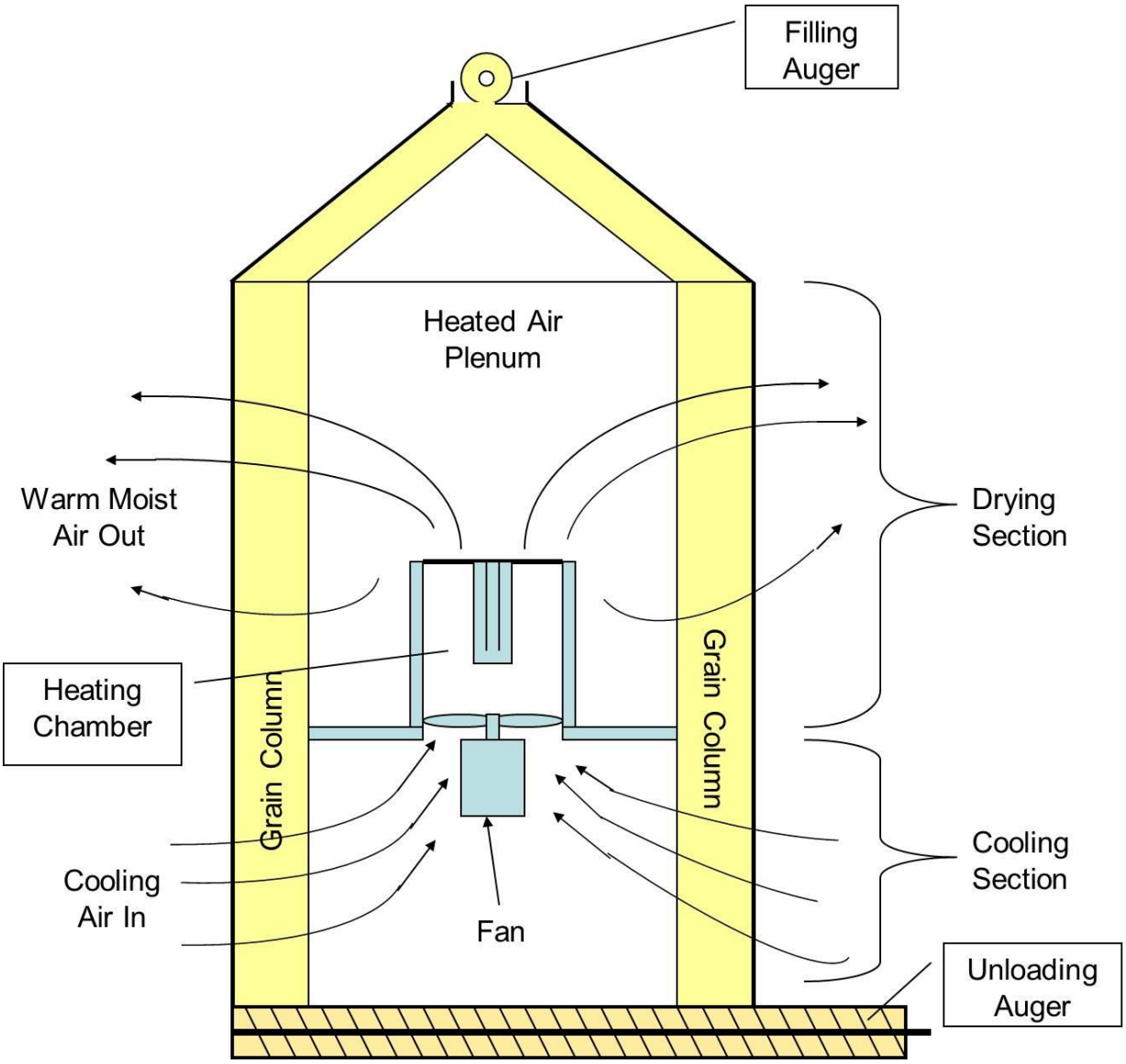


Figure 2.11. Cross-section of a column batch dryer. (Source: Wisconsin Energy Efficiency and Renewable Energy, sasanford@wisc.edu.)

As shown in figure 2.12, a recirculating device may be added to some batch dryers. The aim is to reduce the moisture variation across the column of the dryer. A higher temperature may be used with a recirculating batch dryer when drying some crops. This is because the grains will not be placed next to the heated air for the entire drying cycle and as a result, the grains will not be as hot as the heater temperature.

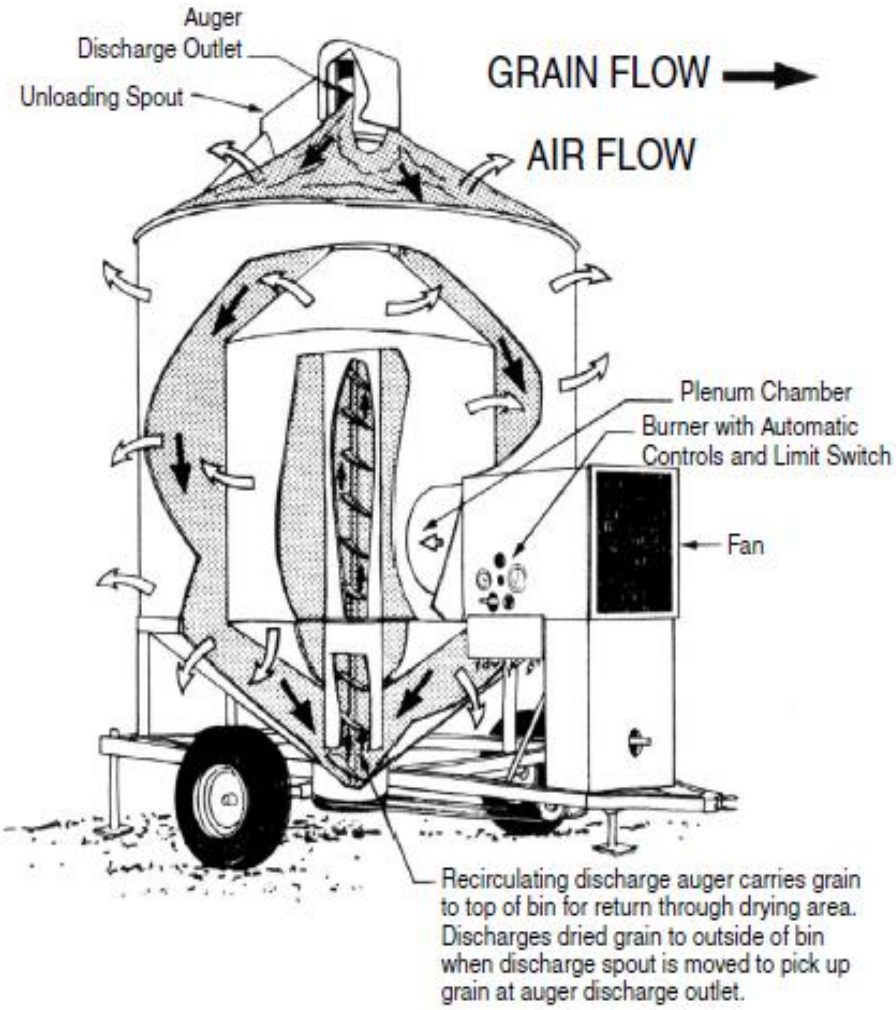


Figure 2.12. Recirculating batch dryer (North Dakota State University, AE701 October 2013 (Revised))

### 2.5.7 Continuous Flow Drying

In a cross-flow dryer, the grain flows by gravity from a holding bin into the drying zone consisting of several screened grain columns. Hot air is then forced perpendicularly from the air plenum through the grain in the columns. In the cooling section, similar process occurs where ambient air is employed. Usually, the width of the grain columns in a cross-flow dryers is between 0.25 and 0.45m and the length of grain columns in the drying section is between 3 and 30 m. In the cooling section, the columns are about 1–10 m long, depending upon the size of the dryer (Brooker et al. 1992). The type of grain to be dried and the grain quality requirements determines the drying air temperature to be set. For food grains, the temperature ranges between 60°C and 75°C, while for feed grains, it is between 80°C and 110°C. The airflow rate varies from 15 to 30 $m^3$/min-$m^2$. One or two fans are often employed in a conventional cross-flow dryer, depending on its size. The residence of grain in crossflow dryers is controlled by the speed of the unloading augers and can be adjusted from zero to the maximum capacity of the dryer. The throughput rates vary according to the size of the dryer, plenum temperature, type of grain being dried, the ambient conditions, and if the dryer is being used in either full or partial heat mode. Because the hot air flows perpendicular to the direction of grain flow, a drying front exists and grain is over-dried at the near side and under-dried at the far side of the grain columns. In extreme cases, the moisture differential between the near side and the far side of the columns can be as high as 8% after cooling (Brooker et al. 1992). Finally, grain is mixed during unloading which equalizes grain moisture contents. Some cross-flow dryer manufacturers have designed an optional grain-turning mechanism. This device is normally positioned about midway along the vertical extent of the dryer heating zone and simply shifts grain from the inner area of the column to the outer area and vice-versa. This reduces the uneven drying problem,

but does not eliminate it. Other manufacturers have used a number of baffles across the depth of grain columns to mix the grain while it flows down. However, the incorporation of mixing mechanisms is uncommon.

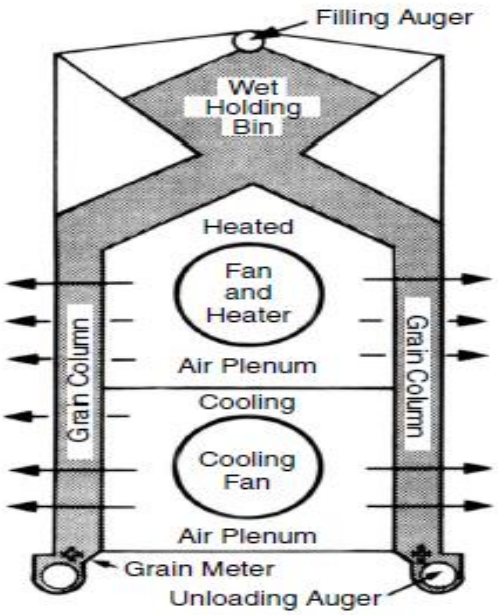


Figure 2.13. Cross-flow dryer with forced-air drying and cooling (Hellevang, 2013).

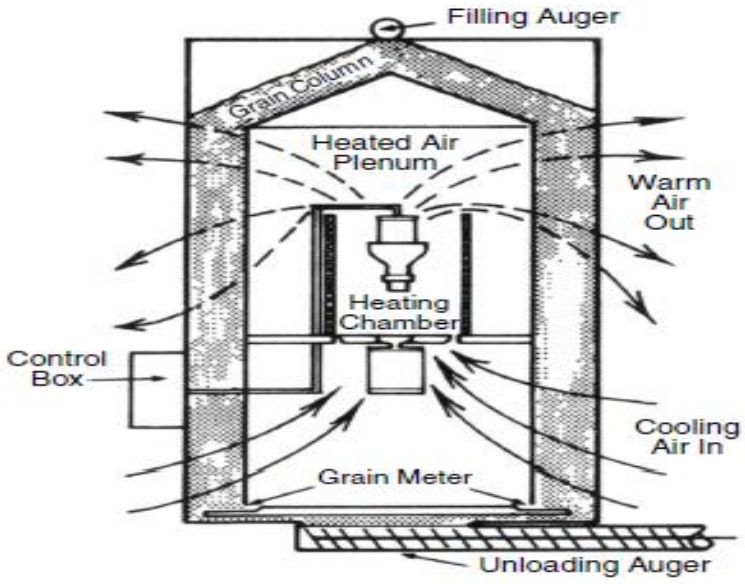


Figure 2.14. Cross-flow dryer with reverse-flow cooling (Hellevang, 2013).

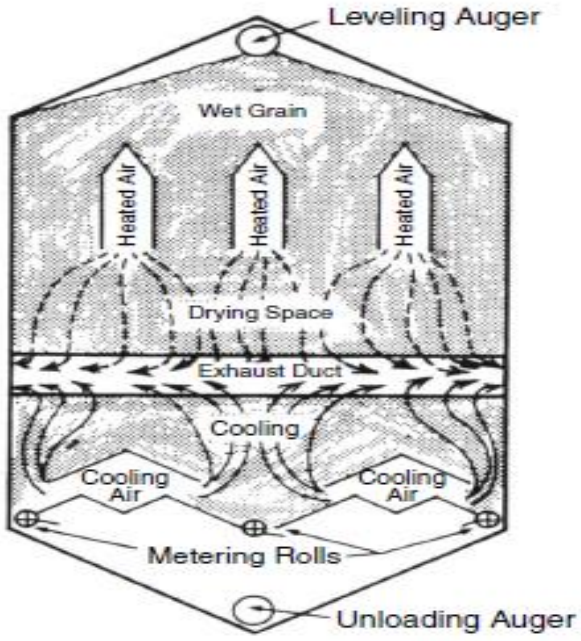


Figure 2.15. Schematic of a concurrent-flow dryer with counter-flow cooling (Hellevang, 2013).

The mixed flow dryer shown in Figure 2.16 is another type of dryer used in drying of grains. In this type of dryer, the grain flows over alternating rows of heated air supply ducts and air exhaust ducts. This is to ensure proper mixing of the grain and alternate exposure to hot drying air which has been cooled by previous contact with the grain. It promotes moisture uniformity and nearly equal exposure of the grain to the drying air.

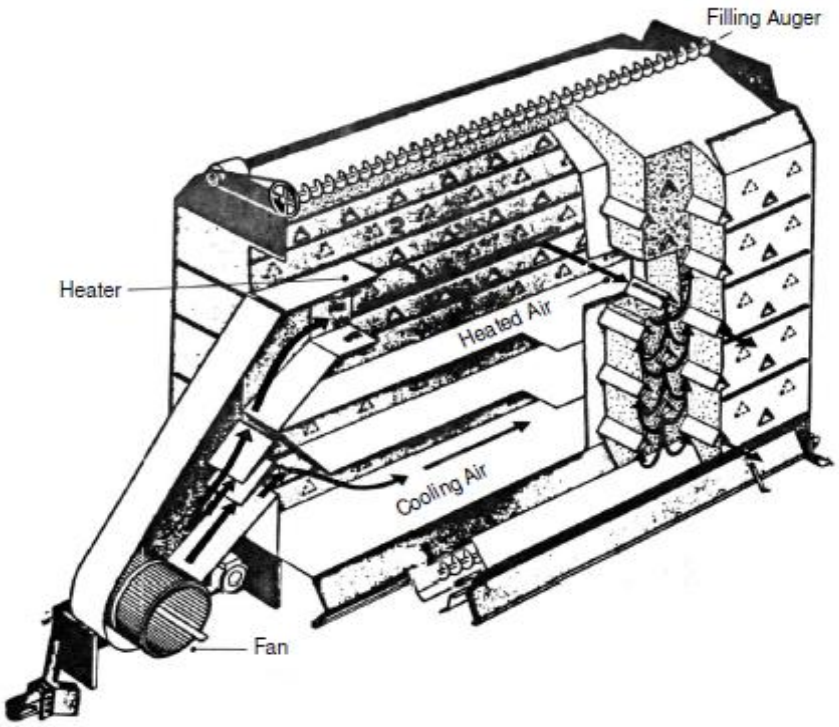


Figure 2.16. Mixed-flow dryer (NDSU Extension Bulletin 2013)

### 2.5.8 Combination Drying

A drying system where high temperature is used to dry the crop to a certain level before natural air/low temperature applied to complete the drying process is referred to as combination drying. This system is used to increase the capacity of the high temperature drying equipment for increased energy efficiency. However, when conditions are not suitable to start drying with a natural air/low temperature drying system, the crop is dried from the harvest moisture content to a level acceptable for natural air/low temperature drying, then it is moved to the natural air/low temperature dryer and drying is completed. Combination dryer is advantageous because it increases drying rate of high temperature dryer by about 300%, and also increases energy efficiency. Its major disadvantage is that it requires natural air/low temperature drying to complete drying, and also requires more grain handling.

## 2.6. A review of Solar Drying Technologies

Solar energy is environment friendly; it is renewable and can serve as a sustainable energy source. It is certainly becoming an important part of the future energy structure with the increasingly drying up of the terrestrial fossil fuel. However, the major challenges in identifying suitable applications using solar energy as the heat source are the lower energy density and its seasonal geographical dependence. Consequently, exploring high efficiency solar energy concentration technology is necessary and realistic (Xie et al., 2011). Solar energy is free, environmentally clean, and therefore is recognized as one of the most promising alternative energy recourse options. In near future, the large-scale introduction of solar energy systems, directly converting solar radiation into heat, can be looked forward. However, solar energy is intermittent by its nature; there is no sun at night. Its total available value is seasonal and is dependent on the meteorological conditions of the location. Unreliability is the biggest retarding factor for extensive solar energy utilization. Of course, reliability of solar energy can be increased by storing its portion when it is in excess of the load and using the stored energy whenever needed. (Bal et al, 2010).

Solar drying is a potential decentralized thermal application of solar energy particularly in developing countries (Sharma et al., 2009). However, so far, there has been very little field penetration of solar drying technology. In the initial phase of dissemination, identification of suitable areas for using solar dryers would be extremely helpful towards their market penetration.

Solar drying is often differentiated from “sun drying” by the use of equipment to collect the sun’s radiation in order to harness the radiative energy for drying applications. Sun drying is a common farming and agricultural process in many countries, particularly where the outdoor temperature reaches $30^0$C or higher.

However, weather conditions often preclude the use of sun drying because of spoilage due to rehydration during unexpected rainy days. Furthermore, any direct exposure to the sun during high temperature days might cause case hardening, where a hard shell develops on the outside of the agricultural products, trapping moisture inside.

Therefore, the employment of solar dryer taps on the freely available sun energy requires ensuring good product quality via judicious control of the radiative heat. Solar energy has been used throughout the world to dry products. Such is the diversity of solar dryers that commonly solar-dried products include grains, fruits, meat, vegetables and fish. A typical solar dryer improves upon the traditional open-air sun system in five important ways (Sharma et al., 2009):

Megha, et al (2015), extensively reviewed solar drying technologies and reported three major types of solar dryer, viz; direct type solar dryer, indirect type solar dryer and mixed mode solar dryer.

### 2.6.1 Direct type solar dryer

Direct type solar dryer is the simplest type of cabinet dryer (Fig. 2.17). In this type of dryer, moisture is removed from top; air enters into cabinet from below and leaves from top. Cabinet dryer is similar to the open sun drying. The only difference is that the food product in the cabinet dryer is covered with a glass sheet. When sun rays fall on the surface of glass of the cabinet dryer, some light rays are absorbed, some reflected back from the glass, and some are also transmitted. Since part of the sun rays are absorbed by the crop in the cabinet dryer, it causes increase in temperature in the drying chamber. The glass cover reduces direct convective losses to the ambient and plays important role in increasing temperature of agricultural product and cabinet temperature. The temperature recorded in this cabinet dryer is 80˚C. The

cabinet dryer has two major disadvantages. (i) Due to natural convection of air flow, it requires enough drying time thereby resulting to low heat and moisture transfer coefficient. (ii) Efficiency is low.

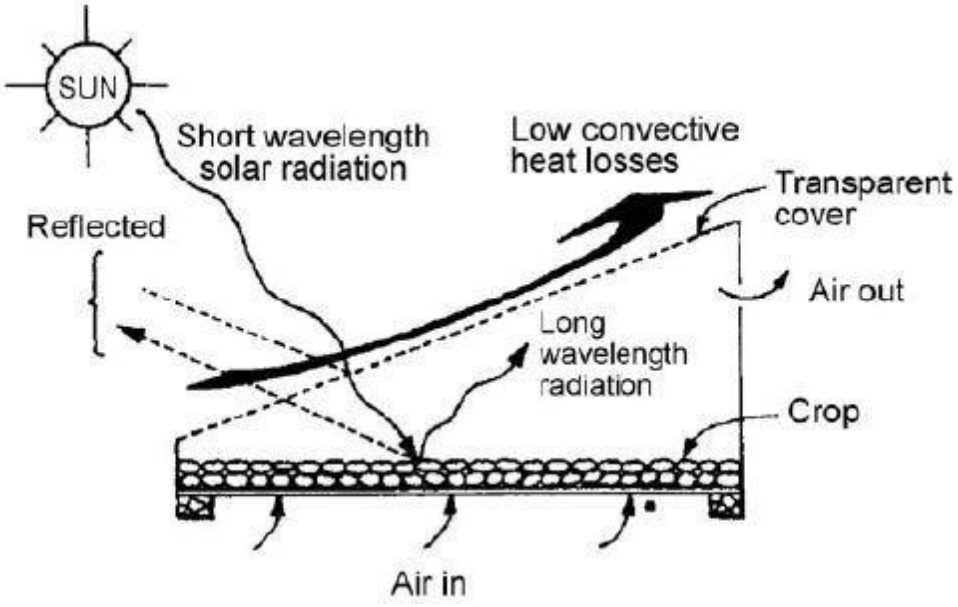


Fig 2.17: Working of Cabinet type of dryer (Source: Hii et al, 2012).

### 2.6.2 Indirect type of solar dryer

This type of dryer differs from direct dryer by heat transfer and vapor removal. In this method atmospheric air is heated in flat plate collector as shown in figure 2.18. This hot air from the flat plate collector then flow in the cabin where products are placed. The moisture from this type of dryer is removed by convection as well as by diffusion. Similarly, instead of flat plate collector, concentrating collector is also used for drying application. Temperature obtained from this type of collector is large as compared to flat plate collector. For fast drying as well as for cloth drying, this type of collector can be used. A small dish type solar air heater connected to a drying chamber for drying apricots was experimented upon. Results show that efficiency improved from 20% at natural flow rate of 0.01kg/sec to 42.6% at a high convective

flow rate of 0.21 kg/sec. apricots took 13 hours for removing moisture from 85% to 8% (Pangavhane, et al 2002).

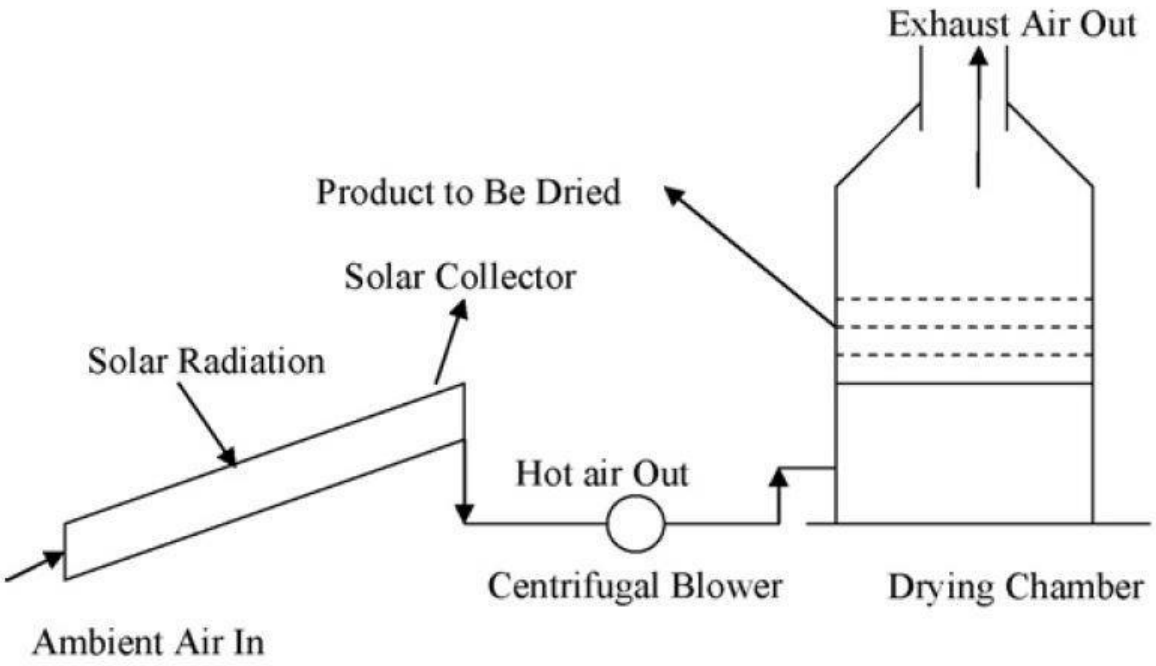


Fig 2.18: Indirect type of solar dryer (Source: Hii et al, 2012).

### 2.6.3 Mix mode solar dryer

Mixed mode solar dryer is the combination of direct and indirect type of solar dryer. Product is dry by direct exposure to the sun light and also by hot air supplier to it. Air is heated in a collector and then this hot air is supplied to the drying chamber and drying chamber top is made of glass cover which can directly absorbs solar radiation. In this way drying rate is higher as compared to direct solar drying. Figure 2.19 shows schematic views of mixed mode natural convection solar crop dryer (MNCSCD). Olalusi and Bolaji (2008) constructed a mixed- mode solar dryer for food preservation. It was found that inside temperature of drying chamber was up to $74^0$C after 12 pm for about 3 hours. Drying rate obtained is 0.62kg/h and system

efficiency obtained is 57.5% (Bolaji et al, 2008). Tripathy and Kumar give information of dryer in which flat plate collectors were placed in series. They used this dryer for drying potato slices of diameter 0.05m and thickness 0.01m (Forson et al, 2007). Various research work related to drying process for agricultural products like mango slices (Bolaji et al, 2008, Bolaji et al, 2005), Banana (El-Beltagi et al, 2007, Babalis et al, 2004), strawberry (Bolaji et al, 2008), grapes (Enibe, 2002, Pangavhane, et al 2002, Sharma et al,1995, ).

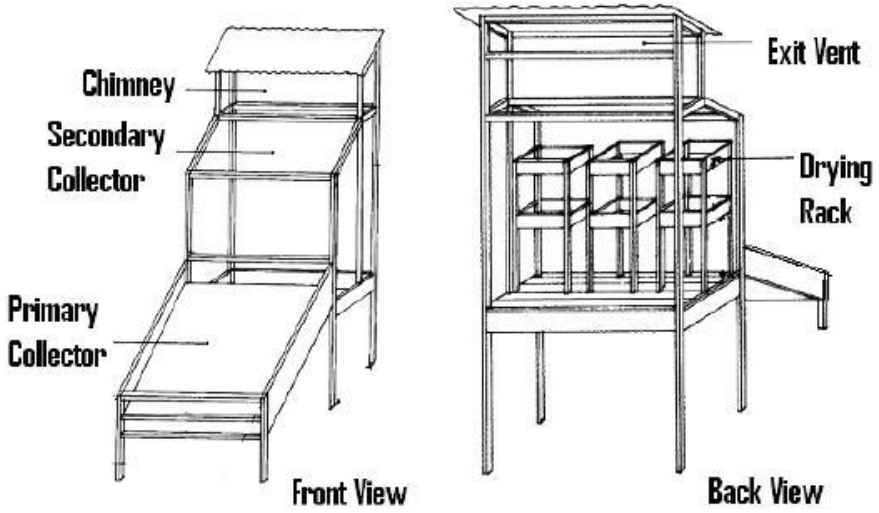


Fig 2.19: Schematic views of the Mixed Mode Natural Convection Solar Crop-Dryer (MNCSCD) (Source: Khalil et al, 2012).

Megha , et al 2015 concluded that time required for drying in mixed mode solar dryer is less than other type of dryer. Force circulation drying gives better result than natural circulation solar dryer.

## 2.7. Solar energy availability for drying

Hot air is a conventional fluid used in all solar powered drying systems. Thus, the amount of extracted solar heat is a significant parameter in the feasibility study of whether sufficient energy is available for a specific application. Generally, the total solar energy absorbed by a solar collector can be calculated by (Karsli , 2007)

$$Q_s = I_t(\tau\alpha)Ac \qquad 2.14$$

where Qs is the rate of solar energy absorbed, It is the isolation or radiation intensity, Ac is the collector area, and τα is the effective transmittance-absorbance product. Basically, τα depends on the transmittance of the transparent covers and on the absorbance of the absorber. Solar energy for drying purposes was investigated in the literature by many researchers, particularly for agricultural purposes. Many potential fields of application are available for solar drying at the medium and medium-high temperature level (80–240 $^{O}$C) (Schweiger , et al, 2000). Kalogirou , et al (2003) investigated the viability of a solar industrial process heat system in a Cyprus industry using the TRNSYS computer program. A simulation of the contribution of the solar processing heat plants under Cypriot environmental conditions was carried out for different collector technologies based on this software. They concluded that the efficiency of the different types of collectors used for drying purposes depends on the temperature difference between the ambient and the collector inlet. Motevali et al (2001) noted that a high irradiation level indicates high collector efficiency and performance. He noted that at two irradiation levels of 500 & 1000 W/m$^2$, Evacuated tube collectors (ETC) appears to be more efficient (80%) than the Flat Plate Collectors (FPCs) and the Stationary Compound Parabolic Collectors (CPCs) with efficiencies of 75% and 72% respectively.

Aderibigbe et al (2016), designed and constructed solar drier using local available materials. The solar dryer consist of the following: (a) a flat plate solar collector with detachable side mirrors, (b) the drying chamber, and (c) the chimney. The solar dryer

works in two stages: (i) the solar heating of the working fluid i.e. the inlet air, and (ii) the circulation of the heated air to extract moisture from the crops in the drying chamber. In his design, a separate solar collector is used to pre-heat the ambient air (the working fluid) drawn into it by natural convection before conveying it to the drying chamber by natural convection. Two design theories were used in the design of the drier, viz; (1) the energy balance equation for the heat absorption process will be obtained by equating the total heat gained to the total heat loss by the heat absorber of the solar collector.

i.e. $IA_C = Q_u + Q_{cond} + Q_{conv} + Q_R + Q_{loss}$ (2.15)

(2) The collector's heat removal factor, FR, is the quantity that relates the actual useful energy gained by a collector to the useful energy gained by the air.

$F_R = \dot{m}\alpha C_{pa}(T_C - T_a)/A_C[\alpha\tau I_T - U_L(T_C - T_a)$ (2.16)

Aderibigbe et al, (2016) estimated the total energy required for drying a given quantity of food items using the basic energy balance equation for the evaporation of water (Youcef-Ali, et al., 2001; Bolaji, 2005):

$M_W L_V = M_a C_p(T_1 - T_2)$ (2.17)

The solar dryer was evaluated and was tested for no load evaluation at different experimental conditions and also tested with up to 5 kg of unripe plantain/banana and yam samples. Results indicate excellent performance, with significant increase in drying air temperature when the side mirrors were attached to the solar collector at 45° to the vertical. The results were compared with traditional method of open air drying. The results indicate that these dryers have good performance.

## 2.8 Numerical Modeling

Computer simulation and mathematical modeling is widely used in drying research to predict dehydration behaviour of materials, design new dryers, and even to control the drying processes, as they both form a powerful method for better understanding the physical process of drying (Naghavi et al 2010). From literature, the main proposed mathematical models used to describe the drying processes of materials are categorized as theoretical, semi-theoretical and empirical models (Hii et al 2009). These models have proved to give good fitting to the experimental data generated from experiments. However, they do not offer any physical meaning (Simal et al 2005). The experimental parameters usually depend on the product, drying technology and processing condition, thereby hindering the understanding of the mechanism that governs the water removal. A part from the empirical and semi-theoretical models, theoretical models are built based on the understanding of the fundamental heat and mass transfer mechanisms that occur during drying. Zare et al, (2006), Zhao et al (2011), Mabrouk et al (2012), Nilnont et al. (2012), Askari et al (2013) have reported computational simulation of various agricultural and food products drying with a remarkable agreement between the theoretical and experimental results.

Models developed theoretically have shown to be realistic and give an accurate explanation of the drying process. However, they require a computing tool and also substantial information about the thermo - physical properties of drying material such as moisture diffusivity, mass transfer coefficient and shrinkage. Therefore, good understanding of these parameters and applying an appropriate numerical method are essential for precise prediction of the process (Lemus-Mondaca et al 2013).

Among the various types of dryers reported in the literature, convective hot air dryers have been to date the most common dryers employed for dehydrating agricultural and food products. Convective dying is considered a simultaneous heat and mass transfer phenomenon wherein moisture transfer occurs in two forms of internal vapour evaporation and surface evaporation. During this process, water is transferred from the product inside to its surface by diffusion and carried from the surface to the air by convection (Sarsavadia et al, 1999). Hassini et al (2007) reported that the moisture diffusivity is a system specific function which represents all moisture gradient driven transfer mechanisms including liquid diffusion, migration in the adsorbed layer, vapour condensation and true diffusion of vapour in the air. For foods, in the falling rate period, it is assumed that moisture transport is controlled by the liquid diffusion (Sharma et al, 2004). Extensive studies have been conducted to determine the moisture diffusivity for various food stuff. Mass transfer between liquid or solid and a gas interface is an important phenomenon for various engineering processes.

Convective mass transfer coefficient is often used to describe and calculate the mass transfer rate at these interfaces (Steeman et al 2009). Convective mass transfer of various materials has been reported in the literature (Lemus-Mondaca et al 2013, Mcminn et al 2003, Kaya 2006, Torki-Harchegani M, 2015). Nilnont et al (2012), Madiouli et al (2012), Brasiello et al (2013) reported that due to moisture evaporation, most fruits and vegetables undergo considerable changes in volume during drying process. Since volumetric shrinkage influences drying behavior of products, it is taken into account in mathematical modeling of such processes for proper prediction of drying curves.

Among the numerical methods available in simulation studies, finite difference method and finite element method are the main methods applied to model heat and

mass transfer. The finite difference method simply formulates the discredited equations set from the transport differential equations and normally is used for simple and regular geometries (Wang et al 2003). The finite element method has better performance in comparison to finite difference method when solving problems with irregular geometries, complex boundary conditions and heterogeneous materials (Janjai et al 2008).

Marcelo et al (2001), modelled the drying kinetics of potatoes taking into account shrinkage they used a natural convection oven with controlled air temperature, vision and weighting system interfaced with computer. Spherical potatoes samples of 10mm diameter were used in the experiments. During drying, the operating conditions were air temperature of 60ºC and absolute humidity of 5 kg$H_2O$/ 100 kg dry air. Shrinkage models' were tested to describe gradually the particle size reduction over time. Based on data analyses, a diffusive model, numerically solved by the method of finite control volumes, to describe the drying kinetics of potatoes considering the effect of shrinkage on mass transfer was proposed. The numerical result showed a good agreement with the experimental judging by the significant correlation coefficient (r = 0.9984) and low maximum experimental error (4.15%) achieved. The shrinkage of spherical potatoes can be described by both tested models: Linear and Kilpaltrick. With respect to model of drying, at the beginning, the diffusive model neglecting the shrinkage of samples fits the experimental data quite well. As the drying progresses, such model overestimates mass transfer phenomenon as it does not take into account the modifications in the internal resistance on mass transfer. However, the model considering the shrinkage presents a better agreement with the experimental data of drying kinetics. This suggests that, Biot number (BiM), in order of magnitude, is not significantly changed (i.e. 50% higher) from beginning to the end of drying (e.g., 20 to 30), the reduction of sample

size has an important effect on predicting drying kinetics. This suggests that model is highly sensitive to dimensionless Biot number (BiM).

Beigi (2016) tried to validate the usefulness of eight mathematical thin layer models to simulate the drying kinetics of Celeriac Slices under Vacuum Drying. The study was aimed at mathematical modelling and determination of mass Transfer parameters of celeriac slices during vacuum drying at different temperatures and vacuum pressures. In describing the drying curves of the samples, Curve fitting tool of MATLAB 7.10 (MathWorks, Inc., Natick, MA) and nonlinear regression technique were applied to fit the models to experimental moisture ratio data. The fit goodness of the mathematical models was evaluated and compared in terms of root mean square error (RMSE) and sum of squares error (SSE). Among the models, the model having minimum RMSE and SSE was selected as the best model to describe the drying curves. After careful examination of the usefulness of the eight mathematical thin layer models to simulate the drying kinetics, the Midilli-Kucuk model best described the drying curves with the minimum values of root mean square error and sum of squares error. The effective diffusivity of the samples was obtained in the range of $2.1908 \times 10^{-10} - 8.9304 \times 10\text{-}10$ ($m^2/s$). Diffusivity increased with increasing drying temperature and decreasing vacuum pressure. The obtained results showed that the convective mass transfer coefficient had ascendant trend during the drying process. Any increment in the drying temperature and vacuum pressure led to an increment and decrement in the convective mass transfer coefficient, respectively.

Salemović et al (2017), presented a mathematical model and numerical analysis of a convective drying process of thick slices of colloidal capillary-porous materials slowly moving through conveyor- belt dryer. A flow of hot moist air was used as drying agent. The drying process has been analyzed in the form of a 2-D

mathematical model, in two directions: along the conveyor and perpendicular to it. The mathematical model consists of two non-linear differential equations and one equation with a transcendent character and it is based on the mathematical model developed for drying process in a form of a 1-D thin layer. The appropriate boundary conditions were introduced. The presented model is seen to be suitable for the automated control of conveyor-belt dryers. The results obtained with analysis could be useful in predicting the drying kinetics of potato slices and similar natural products. The presented original mathematical model describes changes in thick layers of natural materials and it treats heat and mass transfer on the surface and inside the material as one continuum, but with specific differences. It is suitable for the simulation of the drying process of thick materials and for application in automated control of belt conveyer dryers.

The presented results, obtained using potato cubes as drying material, show the differences of the drying kinetic on different layers of the thick drying material, following the changes of the drying agent moisture and temperature as well as the moisture and temperature of drying material. The numerical solution of the mathematical model gives very stable results. It is clearly shown that the increase of enthalpy of the drying agent caused increase of the drying agent absorbing capacity of moisture from drying material. With the increase of enthalpy the heat transfer on the drying material becomes more intensive and the period during which the drying agent is saturated, becomes shorter.

Beigi (2017), conducted an experimental and numerical study to investigate the process of drying potato slices. For simulating the moisture transfer in the samples and predict the dehydration curves, a two-dimensional finite element model was developed and programmed in Compaq Visual Fortran, version 6.5. The model solved the Fick's second law for slab in a shrinkage system to calculate the unsteady

two-dimensional moisture transmission in rectangular coordinates (x,y). Moisture diffusivity and moisture transfer coefficient were determined by minimizing the sum of squares of residuals between experimental and numerical predicted data. Shrinkage kinetics of the potato slices during dehydration was determined experimentally and found to be a linear function of removed moisture. The determined parameters were used in the mathematical model. The predicted moisture content values were compared to the experimental data and the validation results demonstrated that the dynamic drying curves were predicted by the methodology very well.

Haghi (2001), proposed a convective drying model which may be used to describe the drying behavior of leather. Using this model, the calculated transient leather temperature agrees well with experimental values. Variations in temperature and moisture content distribution were solved using the finite-difference method. The effects of operation parameters, such as temperature and humidity in the dryer, initial moisture content of the leather, and heat and mass transfer coefficients were examined using the model. With the model predictions, energy consumption can potentially be reduced by optimizing the drying conditions of the dryer.

Paulo et al (2011) studied and modeled the drying process of corn ears at different air temperatures. The thermodynamic properties associated with the drying process of this product were also determined. Corn ears with initial moisture content of 0.45 dry basis ($kg_w\ kg_{dm}^{-1}$) were dried until they reached a final moisture content of 0.12 ($kg_w\ kg_{dm}^{-1}$) at temperatures of 45, 55 and 65°C. Traditional models used to describe the drying process of several agricultural products were employed to fit the observed data of the drying process of corn ears. The effective diffusion coefficient (Def) was determined by means of an analytical solution of Fick's second law. It was concluded that the Logarithmic model was the one that best fit the observed data

representing the drying process. $D_{ef}$ values increased with temperature increases, ranging from 5.490 x $10^{-10}$ to 1.163 x $10^{-9}$ $m^2$ $s^{-1}$. Based on the dependence of the drying constant of the Logarithmic model with temperature, thermodynamic properties were determined, concluding that the drying kinetics variation is dependent on the energy contributions of the surrounding environment. Based on the values obtained, the Midili and Logarithmic models were considered adequate in describing drying phenomena of corn ears. Paulo et al, (2011) however concluded that, since the Logarithmic model is simpler, it was selected to describe the drying process of corn ears. The diffusion coefficients for corn ears were established as 5.490 x $10^{-10}$, 7.597 x $10^{-10}$ and 1.163 x $10^{-9}$ $m^2$ $s^{-1}$ for temperatures of 45, 55 and 65°C, respectively. The activation energy obtained by the variation of drying constants of the corn ears was 17,644.8 J mol-1 at a temperature range of 45 to 65°C.

Famurewa et al (2014) investigated the drying kinetics of cassava chips using fluidized bed dryer with a view to predicting the most suitable drying model for the drying of cassava. The experiment was carried out using a 4x4x2 factorial; (air velocities, air temperatures, and varieties of cassava) with three replications for each treatment. Fresh cassava tubers were peeled, washed, drained and chipped using manual slicer. A 100 g of the wet chips was then subjected to drying using pre heated fluidized bed drier at a specific temperature and varied air velocity. The change in mass was recorded at constant time interval of 20 minutes until constant weight was achieved. Twelve different mathematical drying models were fitted to the experimental data of the moisture ratio against the time using nonlinear regression analysis by Sigma Plot 10.0 and Microsoft Excel (2010). The models were compared based on their coefficients of determination (R2), reduced chi-squares ($\chi 2$), root mean square errors (RMSE), and mean bias error (MBE). Modified Henderson and Pabis model was found to be the best mathematical model for describing the drying

kinetics of cassava chips having highest value of R2, least values of $\chi 2$, RMSE and MBE.

Based on the results obtained from this study, they concluded that:

- Drying curves of dried cassava chips showed a falling rate-drying period only under the experimental conditions employed for both varieties of species used.
- The highest $R^2$ value, lowest value of $\chi 2$, RMSE and MBE for the thin layer drying process for cassava chips from the two species used was obtained from the Modified Henderson and Pabis model at constant air velocity and varied temperature (40, 50, 60 and 70$^{o}$C). Therefore, the Modified Henderson and Pabis model could adequately describe drying characteristics of cassava chips than the other models.
- Air velocity has effect on the drying process of the chips from both varieties as moisture ratio decreases with increase in air velocity at specific temperature.

Dimitrios et al (2015), developed a numerical model for non-steady heat and mass transfer during convective drying of cylindrical quince slices, with axis parallel to the air flow. The model is based on the numerical solution of the coupled one-dimensional heat and mass transport equations, assuming moisture transport due to Fick's diffusion, with an effective moisture diffusion coefficient derived by fitting the analytical solution of the Fick's law to experimentally derived drying curves, on the basis of an Arrhenius-type temperature dependence. The necessary convective heat and mass transfer coefficients were obtained from CFD calculations of the turbulent flow field around the slices using a commercial CFD package. A new correlation of the Nusselt number, as a function of Prandtl and Reynolds numbers was proposed for the specific geometric flow configuration. The model was validated against experimental data for different air stream velocities (1 and 2 m/s)

and temperatures (40, 50 and 60 °C). The model was found to be robust, computationally efficient and able to capture with sufficient accuracy the time evolution of the temperature and the moisture loss, with a minimum need for experimental adjustment, and hence, is considered suitable from an engineering point of view.

Garcia et al (2014) also developed a rigorous dimensionless analysis of simultaneous heat and mass transfer equations for food drying and simplified for constant properties. From the simplified result, an analytical solution in 1D rectangular coordinate system was obtained. As opposed to Luikov's Equations (LE), the reported solution considers the effect of temperature on interface moisture content. The analytical solution was obtained by Laplace transform and complex inversion integral with space dependent function as initial conditions. The solution behavior compared with some experimental data was detailed, and the potential of the reported solution for the study of interface phenomena and variable mass transfer properties was discussed.

Curcio et al (2016), formulated a conjugated multiphase transport model aimed at predicting the behavior of food convective drying. The model referred to a 3D spatial domain in which two samples were exposed to drying air, flowing around the foods. The system of non-linear, unsteady-state, partial differential equations modeling the simultaneous transfer of momentum, heat and mass, occurring in both the drying chamber and the food samples, was solved by a finite element formulation. The study was intended to cover missing aspects in scientific literature dealing with food drying modeling. It represents, in fact, one of the first attempts to rigorously describe, for given process operating conditions, the transport phenomena involved during drying process of irregular-shaped vegetables, considered as multiphase hygroscopic porous media with different characteristics. In addition, one of the

major contributions offered by this work regarded the possibility of identifying, on food samples surfaces, the points where the local values of both water activity and temperature might determine an inefficient or, even, an unsatisfactory abatement of microbial population, thus causing microbial spoilage.

Computer-aided engineering (CAE) can benefit food product, process and equipment design by enabling mechanistic understanding and speeding up optimization. Datta (2016) reported a comprehensively big picture of CAE in terms of its conceptual frameworks, challenges, developments under way, and achievements so far. While not intended to be a comprehensive review of all models, he focused on mechanistic (physics-based as opposed to data-driven) models that apply to the transformations inside the solid food itself (as opposed to its processing environment) that could perhaps also be captured by the term "product engineering." His work also leans on the practical aspects of implementation of CAE in a food product context by focusing on approaches and workarounds possible today. He asserted that framework discussions go beyond product modeling to its quality and safety modeling. He also reported that generic software tools have become more powerful and easy to use, however, in order to use them for food applications; one needs a framework for modeling various food process, quality and safety that provides an appropriate mathematical description of the reality. Challenges in implementing the frameworks and the workarounds were presented in his report. The goal is to help widen acceptance of the CAE approach in both research and education in the food sector, helping it reap the benefits of CAE like other sectors.

In "3D model-based simulation analysis of energy consumption in hot air drying of corn kernels" by Zhang et al (2013), to determine the mechanism of energy consumption in hot air drying, it simulates the interior heat and mass transfer processes that occur during the hot air drying for a single corn grain. The simulations

are based on a 3D solid model. The 3D real body model is obtained by scanning the corn kernels with a high-precision medical CT machine. The Fourier heat conduction equation, the Fick diffusion equation, the heat transfer coefficient, and the mass diffusion coefficient are chosen as the governing equations of the theoretical dry model. The calculation software, COMSOL Multiphysics, was used to complete the simulation calculation. The influence of air temperature and velocity on the heat and mass transfer processes was discussed.

Zare et al (2006), developed a computer program for simulating a non-equilibrium partial differential equation model for drying rough rice in a deep bed batch dryer. The model consists of four non-linear partial differential equations as a result of the heat and mass balances, together with an appropriate empirical thin layer equation. The set of equations was solved using a finite difference method. Validation of the computer simulation was done in a laboratory scale rough rice batch dryer under various conditions, which included combinations of two parameters: drying air temperature and mass flow rate. There was good agreement between the simulated and measured average moisture content values along the depth of the dryer bed during the drying process.

Liu et al (2015), studied he concept and the model of water potential, which were widely used in agricultural field, and have been proved to be beneficial in the application of vacuum drying model and have provided a new way to explore the grain drying model since being introduced to grain drying and storage fields. Aiming to overcome the shortcomings of traditional deep bed drying model, for instance the application range of this method is narrow and such method does not apply to systems of which pressure would be an influential factor such as vacuum drying system in a way combining with water potential drying model. The study established a numerical simulation system of deep bed corn drying process which has been

proved to be effective according to the results of numerical simulation and corresponding experimental investigation and has revealed that desorption and adsorption coexist in deep bed drying.

ElGamala et al (2013), carried out a CFD simulation to predict the convective heat and mass transfer coefficients in the rice bed, and correlations were developed for the convective heat and mass transfer coefficients as a function of drying air flow rate. The developed correlations were used to extend the coupled CFD and diffusion model developed by ElGamal et al (2013) for thin layer rice drying to volumetric heat and mass transfer in a deep-bed of rice. All mathematical models were solved using the Comsol Multiphysics® simulation program v4.3 (Comsol Inc, Palo Alto), which uses the finite element method to solve the model equations. The model was used to predict the air temperature, as well as the grain moisture content and temperature at different locations of the dryer during the drying process. The theoretical predictions of moisture and temperature profiles inside a deep-bed of rice were validated by experimental data from literature.

Drying conditions affect the quality of dried soybean seeds. Therefore, an accurate description of the drying rate is required. Rafiee et al (2008), developed a finite element formulation and solution of diffusive moisture transfer equation to improve seed drying simulation of axisymmetric bodies. The Fick's diffusive model was solved. For experiment, thin layer soybean seed, 'Villiamz' variety, was dried at drying air temperatures 30, 40, 50, 60 and 70°C with three replications at a fixed drying air velocity of 1 m/s. Good agreement was observed when the output of the model was compared to that of experimental data. The mean relative deviation modulus (P) and modeling efficiency (EF) were used for comparing simulated and experimental data.

Torki et al (2012) developed a non-equilibrium model, for the numerical simulation of rough rice drying in a deep-bed dryer for predicting the average grain moisture content with time. For the purpose of his research, a laboratory scale deep-bed dryer was designed and built, and the average moisture content of the bed was experimentally determined during the process. The effects of temperature, velocity, and relative humidity of the drying air on the average grain moisture content were also investigated. Relative error and mean relative error were calculated for the simulation results, and found to be in acceptable range (10% -15%, and <10%, respectively). Results showed that the temperature of drying air was the most influential parameter on the drying time. The model proved to be able to predict the variation of the average moisture content with respect to the time with a good accuracy.

Haghi (2001), used the mathematical model derived by Nordon with small modifications to develop a convective drying model which may be used to describe the drying behavior of leather. The driving force determining the rate of mass transfer inside the fabric is the difference between the relative humidities of the air in the pores and the leather. He assumed the rate of moisture exchange to be proportional to the relative humidity difference. In his experimentation, the moisture variations of the surface and the center of the leather were calculated. Initially, the surface moisture content decreased rapidly, but later this rate declined because moisture was transferred to the external air from the leather surface. The center moisture content remained constant for a short time, and then decreased rapidly because the moisture content difference between the surface and the interior of the leather became large. After drying out, both center and surface moisture contents converged to reach the external air moisture content. The mathematical model was used to predict the effects of many parameters on the temperature variation of the

leather. These parameters include the operation conditions of the dryer, such as the initial moisture content of the leather, heat and mass transfer coefficients, drying air moisture content, and dryer air temperature. The mathematical model developed can be used to predict transient variations in temperature and moisture content distribution of leather in the dryer with reasonable accuracy. With the model, the effect of the temperature and humidity of the dryer, the initial moisture content of leather and the heat and mass transfer coefficients can be predicted for leather. Also, with the model predictions, energy consumption can potentially be reduced by optimizing the drying conditions of the dryer. Using this model, the calculated transient leather temperature agrees well with experimental values. Variations in temperature and moisture content distribution were solved using the finite-difference method. The effects of operation parameters, such as temperature and humidity in the dryer, initial moisture content of the leather, and heat and mass transfer coefficients are examined using the model.

Castell – Palou et al (2012) developed a mathematical model for a cubic shape to predict the drying kinetics and moisture distribution during cheese drying. The model was developed taking into consideration both the external and internal resistances to mass transfer and an effective diffusion dependent on local moisture and temperature. Also, a specific model for sorption isotherms was established from experimental results and used to complete the overall model formulation. The drying experiments were carried out at 6.3, 12.2, and 18.2°C and 1.0 m $s^{-1}$ until a moisture content of approximately 0.30 kg $kg^{-1}$ (db) was reached. Moisture distribution was experimentally measured from the center of the cheese cube to the center of the surfaces and to the vertexes using a time-domain nuclear magnetic resonance (TD-NMR) method. The proposed model was solved using a finite element method and validated by comparing the experimental moisture profiles with those simulated by

the model. A satisfactory simulation was obtained for both the drying curves and the moisture profiles. For both groups of data, a mean relative error lower than 6% and a percentage of explained variation higher than 97% was achieved.

Irudayaraj et al (2012) presented a finite element procedure for two sets of non-linear coupled drying models for three-dimensional axisymmetric and two-dimensional problems. The models consider temperature and moisture dependent material properties. The two different solution procedures used are the implicit two-level and the explicit three-level time stepping schemes. Application was made to drying of single soybean, barley and corn kernels. The simulation results from the heat and mass transfer models agreed well with the available experimental results. Model one accounts for diffusion of moisture through vapour and liquid phases. Model two assumed that moisture diffuses to the outer boundaries of the kernel in the liquid form and that evaporation takes place only at the surface of the grain. In all simulations, temperature predictions using model one approached the equilibrium temperature faster than model two. The overall grain kernel temperature and moisture predictions from model two were better than model one. The choice of a model depends upon the type of application and availability of material properties.

Haghighi et al (1990) presented a finite element formulation and solution of a set of coupled conductive heat and diffusive moisture transfer equations to improve grain drying simulation of axisymmetric bodies. The model considers the temperature and moisture dependence of the diffusion coefficient, thermal conductivity, and specific heat. It assumes that moisture diffuses to the outer boundaries of the kernel in liquid form and that evaporation takes place only at the surface of grain. Application was made to drying of a barley kernel and predicted results agreed well with the experimental data. The simulated temperature and moisture profiles and gradients are directly usable for stress cracking analyses of grain. The results of the finite

element analysis can be used for grain quality evaluation and drying simulation studies.

Ferguson (2007) presented a novel application of the control volume finite element numerical technique to simulate the high temperature drying of spruce. The numerical treatment of this problem has been studied extensively in the past, however, the basic drawback with previous numerical analyses is that they have been limited to a structured fixed mesh. During drying, timber twists and distorts and to accurately model the drying procedure, it is essential that this behavior is taken into consideration. He reported that the control volume finite element method enables a structured or unstructured mesh to be employed without alteration to the formulation, and lays the foundation for the simulation of the timber deformation.

Zare et al (2006) developed a computer program for simulating a non-equilibrium partial differential equation model for drying rough rice in a deep bed batch dryer. The model consists of four non-linear partial differential equations as a result of the heat and mass balances, together with an appropriate empirical thin layer equation. The set of equations is solved using a finite difference method. Validation of the computer simulation was checked in a laboratory scale rough rice batch dryer under various conditions, which included combinations of two parameters: drying air temperature and mass flow rate. There was good agreement between the simulated and measured average moisture content values along the depth of the dryer bed during the drying process.

Naghavi et al (2010) in his study, developed a non-equilibrium model of the grain fixed deep-bed drying for rough rice. The model was developed by using mass and energy balance inside a control volume of the bed and a proper rate equation for the thin-layer drying. The control volume was composed of two thermodynamic systems: intergranular air and grains. Unlike most of the models reported in the

literature, authors simplified the physical description by neglecting the accumulation terms from the energy and moisture balance equations without a relevant justification. However, Naghavi noted that accurate modeling of the drying process is an important factor from design point of view as well as optimizing the operation. Hence, in his proposed model, the accumulation terms were kept in both energy and mass balance equations. The set of coupled partial differential equations derived from the model was solved simultaneously by using the backward implicit method. Based on the discrete set of equation, a computer program was developed and implemented in MATLAB environment to simulate the grain drying process. The technique was able to predict correctly the temperature of the air and grains, the air humidity and moisture content of the grains at different locations of the dryer at any time. The results of simulation were also compared with the experimental data. The results clearly show that the proposed method can predict the characteristics of the deep-bed dryer with a very good degree of accuracy.

Otuu et al (2013) developed a mathematical model for vertically upward pneumatic conveying drying of cassava cultivar TMe 419. The model was solved using Finite Element approach. His work was based on two-fluid analysis and it used an iterative method to predict the gas phase variables along the flash tube while considering the influence of material on the flow stream. The gas phase variables were generated by a program coded with Comsol Script while the drying variables for a representative cassava particle were determined by finite element method implemented on Comsol Multiphysics Platform. The simulation predicted the state of the moisture along the tube under different conditions thereby providing a tool for research and design of vertical upward conveying dryers. The simulation revealed the state of the particle at different residence time (0.2-3s) and the particle surface temperature was found to increase as residence time increased. Similarly the moisture content was found to

reduce with increasing residence time. Finally the prediction of the tube length was derived simply from the residence time that produced the acceptable final moisture content. The other flow parameters especially those relating to the gas phase were generated from the comsol script program.

## 2.9 Review on Cassava properties

Thermal conductivity (k), specific heat capacity ($c_p$) and thermal diffusivity (d) are important properties in modeling, simulation and control of various food processing operations. Njie et al (1996) investigated the above properties for the following crops: cassava root, yam tuber and plantain fruit. k was measured using a line heat source probe at moisture contents (M) in the range 14-79% wet basis and temperatures near 30°C. The results ranged from 0.16 to 0.57 $Wm^{-1}\ ^0C^{-1}$ for cassava (M = 18- 70%), 0.16 to 0.60 $Wm^{-1}\ ^0C^{-1}$ for yam (M = 0.16-79%), and 0.13 to 0.45 $Wm^{-1}\ ^0C^{-1}$ for plantain (M = 14-57%). $C_P$ was measured with a differential scanning calorimeter between $36^0C$ and 51°C in the M range l0-68%. It increased with M and temperature, and varied from 1.636 to 3.26 kJ $kg^{-1}\ ^0C^{-1}$. "d" of each crop was calculated using k and $C_P$ data predicted by empirical models that were derived from the experimental data. The results were close to those given in the literature for similar foods.

Oladele et al (2007), in his study experimentally determined some engineering properties of cassava tuber samples under five moisture content levels of 70 %, 65 %, 60%, 55 %, and 50 %wet basis. The properties measured were tensile strength, compressive strength and elasticity. Three experimental tools were designed and fabricated using spring balance, hose-clips, and 12Volts motor with reels and rope for the investigations. The IITA improved cassava variety TMS 4(2) 1425 was used in the experiments. Results of the tests indicated that all the properties measured were influenced by the moisture contents of the tuber. The properties investigated

include strength, (shear tensile and compressive) and elasticity, the studies showed that tensile, compressive and shear strength of cassava reduces as the moisture content of the tuber decreases. The degree of elasticity decreases within the range. There is every indication that above statement can be otherwise at moisture content lower than 50% w.b. It was also found that the lower the moisture content the harder the crop is and the more it resists cutting and abrasion. Meaning that cassava tuber mechanical property is moisture content dependent.

Ademosun et al 2012, investigated the effect of physical and mechanical properties of cassava tubers on mechanical peeling and hence provides a basis for cassava peeling mechanization. The tuber used for the experimentations were obtained from soil characterized with sandy loams, moist, high fertility and good farm vegetation ($S_{lmhf}$), and soil characterized with sand, moist, relatively low fertility and poor farm vegetation ($S_{smlf}$). These properties investigated include size of the tuber, $t_l$, proportion by weight of peel, $w_p$, average moisture content of the peel, $m_{ap}$, peel thickness, $t_p$, tuber diameter, $t_d$, tuber surface taper angle, $\alpha$, peel penetration force, F, and peel shearing stress, $t_s$. The results showed that for $S_{lmhf}$; $t_l$ ranged from 140-460mm, $w_p$ ranged from 13.12-20.06%, $m_{ap}$ was 76.27%, $t_p$ ranged from 1.62-4.34mm, $t_d$ ranged from 31.08-136.63mm, $\alpha$ ranged from 9.03-23.130, F ranged from 0.17-1.85N/mm, $t_s$ ranged from 0.85-9.25N/mm2 and quality performance of the machine, QPE, for this tuber ranged from 70.82-96.21%. Similarly, for $S_{smlf}$; $t_l$ ranged from 125-362mm, $w_p$ ranged from 10.52-16.66%, $m_{ap}$ was 70.97%, $t_p$ ranged from 1.22-4.12mm, $t_d$ ranged from 18.86-99.29mm, $\alpha$ ranged from 5.20-12.290, F ranged from 0.13-1.54N/mm, ts ranged from 0.65-7.70N/mm$^2$ and quality performance of the machine, QPE, for this tuber ranged from 67.27-92.25 %. The results confirm influence of physico-mechanical properties of cassava tuber on mechanical peeling.

Oladele 2012, carried out a study to evaluate cassava tuber resistance to Deformation. He investigated hardness and resistant ability of cassava tuber. The study involved the use of laboratory penetrometer and a data lodger. Hand-drilling machine was fitted with a 500mm diameter blade. These devices were powered manually and by application of electricity. Forces were applied by allowing direct cutting of the tubers using rotating sharp blade. The penetrometer was used to test the strength of fresh tuber. The result obtained indicated that cassava tuber hardness increases with the reduction of moisture content. The penetration force of 5.4 Newton at 70% moisture content wet basis was recorded while 9.2 Newton was recorded at 50% moisture content wet basis. The cutting time of 5.3 seconds was recorded for equal size tuber when the moisture was at 70%, at 50% moisture content, 9.7 seconds was recorded. These are useful data in reducing the drudgery involve in transportations and processing. The implication is that all process handling of cassava tuber involving cutting must be carried out when the tuber is still tender.

Jeannine et al, 2015 studied the mechanical properties of cassava starch films as affected by different plasticizers and different relative humidity conditions. The influence of plasticizer type (glycerol and sorbitol), its content (starch: plasticizer ratio of 1:0.15; 1:0.20; 1:0.25 and 1:0.30) and the relative humidity conditions (43, 58, 75 and 85%) on the mechanical properties of cassava starch films was studied. Both plasticizers seemed to integrate homogeneously in the film matrix. The incorporation of different concentrations of plasticizers affected the mechanical properties of the cassava starch films. Plasticizer ratio directly influenced the forced values of the films, they showed significant flexibility when the plasticizer proportion was increased in the formulation. Under conditions of low relative

humidity, sorbitol produced films more resistant to puncture than glycerol. Qualitatively, all the films were less brittle when the plasticizers were incorporated.

Lateef et al 2016, studied the Thermal Properties and Energy Utilization of Cassava Meal in Conductive Rotary Drying. In his study the thermal properties and drying behaviour of cassava meal in a conductive rotary dryer was investigated. Cassava flour and gelatinized garri were produced at drying temperatures of 70°C and 90°C, respectively. The activation energy of cassava meal was 49.52 kJ/mol, and the effective moisture diffusivity, thermal conductivity and heat capacity increased with temperature from $1.74x10^{-10}$ to $4.51x10^{-10}$ $m^2/s$, 0.329 to 0.344 W/m°C and 1.804 to 1.901 kJ/kg°C, respectively. With increase in bulk density of cassava meal from 379.50±2.55 to 464.79±30.38 $kg/m^3$, thermal diffusivity and specific energy consumption decreased from $4.81x10^{-7}$ to $3.89x10^{-7}$ $m^2/s$ and 618.88 to 456 kJ/kg, respectively. The thermal efficiency of the dryer was greater than 31% for both cassava flour and garri. Compared with previous works, performance of the conductive rotary dryer was satisfactory and upgrade of its design will make it suitable for application in the cassava processing industry.

### 2.9.1 Summary of Literature Review

The temporal and spatial variations of moisture content of agricultural products during drying are governed by the laws of diffusion. Diffusion mechanics are expressed in partial differential equations (PDE) and can be solved using the Finite Element (FE) Method. This has been the research practice for decades resulting in FE prediction of drying kinetics of many agricultural products. The kinetics of fruit and vegetable foodstuffs drying were studied in (Vagenas & Marinos-Kouris, 1991) using a 3-dimensional FE model taking into account heat transfer effects based on an overall heat balance. Irudayaraj et al (1992) developed a FE procedure in form of two sets of non-linear coupled drying models for problems of 3-dimensional

axisymmetric and 2-dimensional nature. They considered the material properties as temperature and moisture dependent. Ferguson and Turner (1996) presented a novel application of the hybrid control volume FE scheme for the solution of a timber drying problem on a deforming mesh. Modelling wheat grains as axisymmetric ellipsoids, a 2-dimensional FE model was used to analyze isothermal thin layer drying of wheat (Gastón, et al, 2002). In Ranjan, et al, (2004), a 2-dimensional FE analysis of a set of transient coupled heat and diffusive moisture transfer equations was presented. A 2-dimensional FE analysis was developed in Janjai, et al, (2008) for simulation of drying of mango. Janjai et al (2008) presented a 2-dimensional FE model to simulate drying of longan fruit. A so-called Generalized Conjugate Model was developed by De Bonis et al, (2008) to study the effect of air temperature together with other variables on drying process of fresh-cut vegetable slices. Janas et al (2010) developed a physical FE model of heat and mass transfer in a maize kernel on the bases of Fick and Fourier equations. Their real 3D geometry of maize, which was used to build the mesh needed for the FEM computations, was obtained by Nuclear Magnetic Resonance (NMR) imaging. They were able to correctly describe the evolutions of maize moisture and salt-soluble protein content during fluidized-bed drying with a constant drying air temperature between 50 °C and 100 °C. The moisture diffusivity, shrinkage, equilibrium moisture content and finite element solution drying of coffee were studied in (Nilnont et al., 2012). Computational modelling of the moisture transport phenomena occurring during convective drying of prunes was presented in (Henry et al, 2012). The author developed a mathematical model (transient non-linear partial PDE) to describe the coupled heat, mass and momentum transfer processes occurring in convective drying of prunes. The model was solved using the FE method coupled to the Arbitrary Lagrange-Eulerian (ALE) procedure to account for the shrinkage phenomenon using a commercial package (COMSOL Multi-physics™, Comsol AB, Stockholm,

Sweden). A mathematical model for a cubic shape cheese was proposed and solved using FE method to predict the drying kinetics and moisture distribution during cheese drying (Castell-Palou et al., 2012). A novel application of ultrasound to assist in convective food drying was modelled and tested in (Sabarez, et al, 2012). Perussello et al (2013), presented a detailed procedure for determining the thermophysical properties of yacon (Smallanthus sonchifolius) for use in FE simulation of drying. Recently, drying models in form of coupled heat and mass transfer equations were developed for different fruits and vegetables based on moisture-dependent and temperature-dependent effective diffusivities and solved using COMSOL Multiphysics FE simulation software. As a result, 3-dimensional moisture profiles were developed to reveal the spatial moisture distributions in the samples during drying (Khan, et al 2017).

## 2.10 Knowledge gap

The above comprehensive review shows that FE modelling of cassava drying dynamics has not received the attention of the research community. Of all food crops in Nigeria, cassava is the best candidate for such attention since it is the most produced and consumed food crop in Nigeria, especially in the central and southern parts where about 90% of cassava produced in Nigeria is processed into food (mostly garri). Raw cassava and its various processed forms are dried for storage. Moreover, as Nigeria props up her desire to be a major exporter of cassava to the international market, the need for research-based knowledge of cassava pellets cannot be overemphasized. Considering the enormity of cassava needing drying in Nigeria, experimental and empirical approaches which would need to consider cassava species and drying conditions on case-by-cases basis will be very costly for the industry. Thus there is a compelling need for computer simulation of cassava drying. This is the aim pursued in this work using the FE method.

In this work, a 2- dimensional model will be formulated using Finite element and Finite difference methods. The formulations would yield an Nth order unsteady-state partial differential equations, which would be solved by means of Galerkin Weighted Residual Method. This approach has never been used in describing the drying kinetics of cassava pellets.

The drying dynamics dictated by Fick's second law equation for the 2-dimensional element which are influenced by both initial condition and Neumann boundary condition would be used to trace the boundary of the product and air interface during the drying process using MATLAB. This approach has never been used in the simulation of drying kinetics of cassava pellets.

The state variables, surface temperature and moisture content of the samples, as well as the shrinkage, and drying rate would be determined using the formulated model. The numerical model will be used to predict the effect of fixed boundaries on the drying curve. The relative drying curve, drying rate and surface temperature of the numerical simulation would be compared to see if it is in good agreement with the experimental data analyzed. This will validate the model developed using finite element and finite difference methods. This has not received the attention of the research community.

In both, the numerical and the experimental method, comparison will be made to know if increasing the drying parameters has positive effect on the quality of the product and the drying kinetics in the range chosen for this study.

# CHAPTER THREE

# MATERIALS AND METHODS

## 3.1 Materials

### 3.1.1 Dryer Set up

The experiments were conducted using a laboratory scale conventional double layer convective hot air dryer. The air is provided by a fan. The air flow speed was kept constant at 4m/s. The relative humidity was controlled through a data logger controller. Throughout the experimental run, the sample weights were continuously recorded at predetermined time (20mins) intervals until no noticeable differences between subsequent readings were observed.

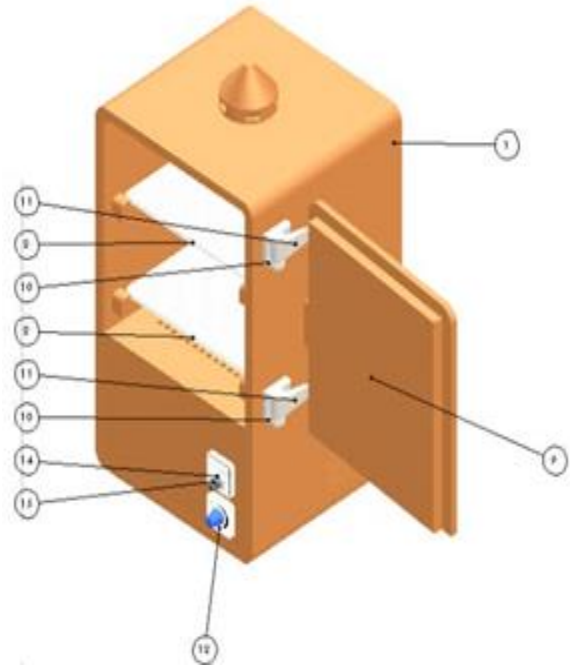

| ITEM NO | PART NAME | QTY |
|---|---|---|
| 1 | Chamber | 1 |
| 2 | Sampling Trays | 2 |
| 3 | Base Damper | 1 |
| 4 | Blower Housing | 1 |
| 5 | Blower shaft | 1 |
| 6 | Fan Blade | 1 |
| 7 | Heater stand | 2 |
| 8 | Heating Coil | 1 |
| 9 | Chamber door | 1 |
| 10 | Hinge | 2 |
| 11 | Hinge 2 | 2 |
| 12 | Switch Hub | 1 |
| 13 | Switch Knob | 1 |
| 14 | Temperature Gauge | 1 |
| 15 | Temperature Knob | 1 |
| 16 | Temperature Gauge Timer | 1 |

Fig 3.1: A Schematic of the Dryer Set-up

## 3.2 Methods

TMS 30572 specie of Cassava tubers identified at Department of Crop Science, Faculty of Agriculture, Nnamdi Azikiwe University were harvested from a farm in Nnamdi Azikiwe University, Awka, Anambra State. They were peeled, chipped and dried at varying temperatures and air velocities to obtain dried cassava chips. The test trials done were triplicates to obtain accurate drying process data. In carrying out the experiment, the Cassava tubers were hand peeled and cut into slabs with a rectangular mold (40 mm×20 mm×10 mm) designed for the purpose. For each drying experiment, approximately 100 and 800 g of the samples were spread on the weighing tray and sampling trays, respectively. The initial moisture content of the cassava sample was determined by drying 10 g of the fresh samples at 103 °C until constant weight is attained. Prior to each experiment, the samples were left at room temperature for 2 h to reach thermal equilibrium with the environment. Two trays were placed in the drying chamber. During the drying experiments, one of the trays was used to monitor dehydration behavior (weighting tray) and the other was used to determine shrinkage kinetic (sampling trays) of the samples.

For each drying experiment, 8 pieces of the cut sample were placed in small wire gauze with a known weight inside the drying tray. The remaining samples were spread in the drying tray inside the drying chamber. The airspeed of the fan was kept constant at 4 m/s throughout the experiment while the temperature of the heater was set at 110$^{o}$C. The samples were left to dry to a constant weight. The loss in weight of the sample in the wire gauze was taken at interval of 10 minutes, and the shrinkage rates were determined at the same time by inserting a piece of the sample taken from the drying tray into a 100 mL measuring cylinder containing toluene at a known level. The volume of toluene displaced was measured. The experiments were replicated twice. The sample mass was measured by a digital mass measuring scale

with an accuracy of 0.001g. The whole procedures was repeated for cassava pellets cut with a circular mold of radius 16mm and height 10mm, which gave approximate volume with the rectangular mold. For both the rectangular and circular moulds, the experiments were repeated at heater set temperatures of 120, 130, 140, and 150 $^{o}$C following the procedure as shown in figure 3.2.

### 3.2.1 Dryer Calibration

The dryer was calibrated to ascertain the accurate hot air temperature for every heater temperature been set to be used for the drying process. A linear relationship between heater temperature $T_h$ and hot air temperature $T_a$ (eqn.3.1) with $R^2$ valve of 0.9685 was developed and used in the drying process. With the aid of equation 3.1, heater temperatures of 110°C, 120°C, 130°C, 140°C, and 150°C gave corresponding hot air temperatures of 66°C, 70°C,75°C,78°C, and 81°C respectively.

$$T_a = 24.7230 + 0.3757T_h \qquad 3.1$$

### 3.2.2 Kinetics of Cassava Drying

Logarithmic kinetic model, given generally in equation (3.2), for moisture ratio is calibrated using nonlinear regression methods and was used in determining the experimental moisture ratio as a function of drying time.

$$\chi = a\exp(-kt) + \mathrm{c} \qquad 3.2$$

The coefficients $a$, $k$ and c are the parameters of the model the choice of which determines the accuracy of the kinetics models. Logarithmic kinetic model is known for high accuracy.

### 3.2.3 Experimental Procedure

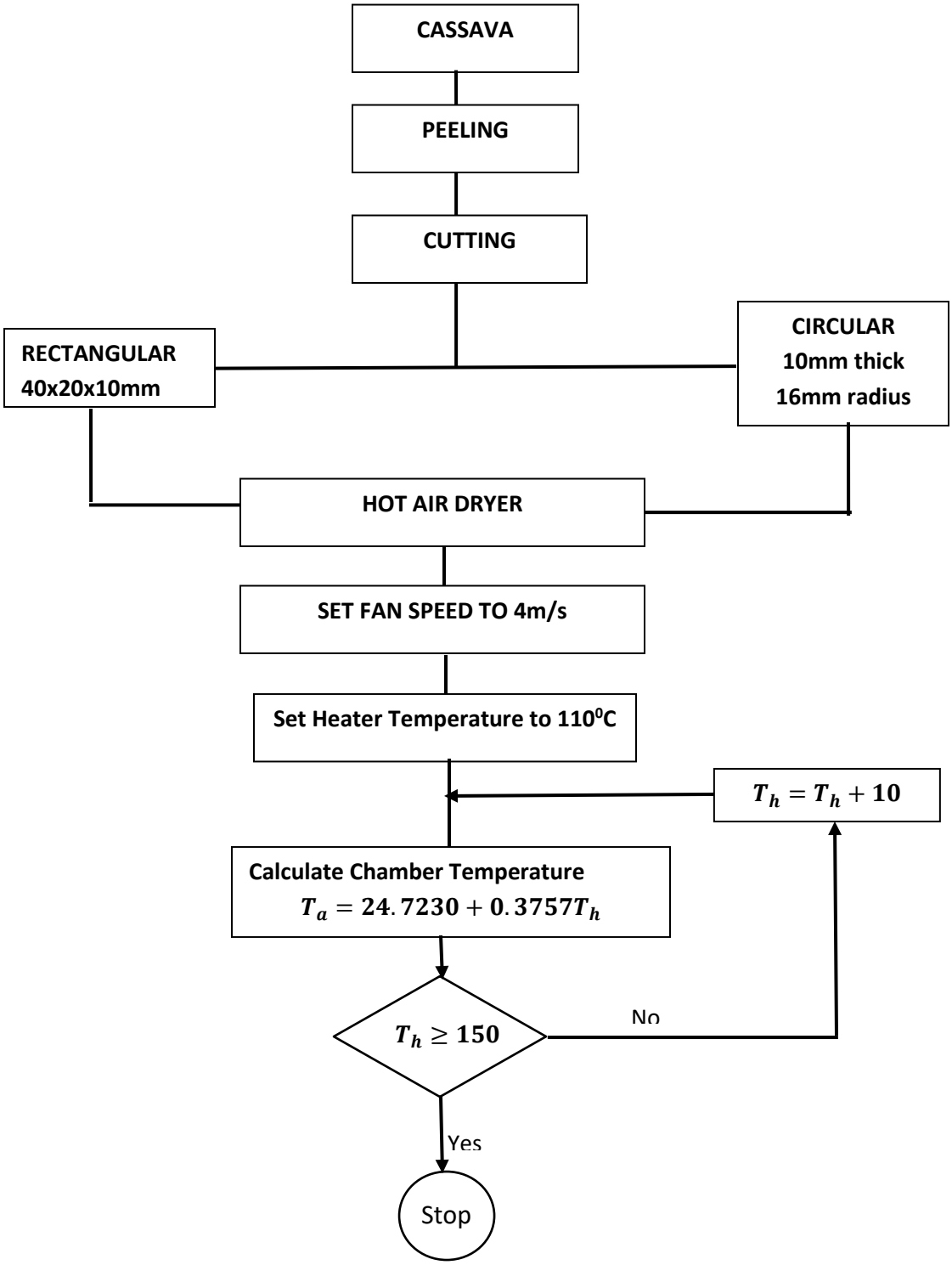


Fig 3.2: A Summary of Experimental Procedure

## 3.3. Analysis of the Drying data

### 3.3.1. Moisture Content

Moisture content was calculated using Eq. (3.3) (Torki-Harchegani et al, 2015):

$$M = \left(\frac{(M_0+1)W}{W_0} - 1\right) \quad (3.3)$$

Where M and Mo are the moisture content at any given time ($kg_{water}/kg_{dry\ matter}$) and the initial moisture content ($kg_{water}/kg_{dry\ matter}$), respectively and W and $W_o$ are the mass of samples at any given time (t) and the initial mass of fresh samples (g), respectively. In drying processes, it is more advantageous to express the water content of a material in dry basis form. This is due the fact that the dry matter remains constant during drying, therefore it can be used as a reference point (Helman et al 1997, Ramaswamy et al, 2006).

### 3.3.2. Drying rate

The drying rate is computed as the decrease in water concentration between two subsequent measurements divided by the elapsed time between the measurements as shown in the following equation. Drying rate was computed using Eq. 3.4. (Beigi, 2017) :

$$DR = -\frac{M_{t+dt}-M_t}{\Delta t} - 1 \quad (3.4)$$

The drying rate data from the different drying tests would be analyzed relative to moisture content. In addition, the drying rate (DR) is expressed as ($g_{water}/(g_{dry\ matter}$)), Mt and Mt+dt are the moisture contents at t and t+dt respectively, and t is the drying time (s), which is independent of the surface area because shrinkage complicates the measurement of the outside surface area of the sample (Karathanos, et al 1997).

### 3.3.3 Effective Moisture Diffusivity

The effective moisture diffusivity was determined experimentally using Fick's second law of diffusion for rectangular and cylindrical geometries as shown in eqns. 3.5.

$$\frac{\partial M}{\partial t} = \text{Div}\left[D_{eff}(T)\text{grad}(M)\right] = D_{eff}(T)\left(\frac{\partial^2 M}{\partial x^2} + \frac{\partial^2 M}{\partial y^2}\right) \quad (3.5)$$

The Crank's series solution for variation with time of moisture ratio for an infinite slab is

$$MR = \frac{8}{\pi^2}\sum_{n=0}^{\infty}\frac{1}{(2n+1)^2}\exp\left(-\frac{(2n+1)^2\pi^2 D_{eff}t}{4H^2}\right) \quad (3.6)$$

where $H$ is half thickness of the sample and moisture ratio MR is given as

$$MR = \frac{M-M_{eq}}{M_0-M_{eq}} \quad (3.7)$$

The first term of the series can give acceptable results for long drying periods

$$MR = \frac{8}{\pi^2}\exp\left(-\frac{\pi^2 D_{eff}t}{4H^2}\right) \quad (3.8)$$

In logarithmic form, Equation (3.7) becomes

$$\ln(MR) = \ln\left(\frac{8}{\pi^2}\right) - \frac{\pi^2 D_{eff}}{4H^2}t \quad (3.9)$$

By plotting $\ln(MR)$ against $t$, a straight line is obtained with the slope $S = -\frac{\pi^2 D_{eff}}{4H^2}$ such that $D_{eff} = -\frac{4H^2}{\pi^2}S$

### 3.3.4 Finite Element Formulation

Schematic diagrams of the cassava samples are presented in Figures 3.3 and 3.4 for unsteady two-dimensional mass transfer during convective drying. The theoretical or numerical modeling and simulation to be developed will be validated by experimental work that was carried out for different drying parameters of heater temperatures (150°C, 140°C, 130°C, 120°C, 110°C) which gave corresponding hot air temperatures (81°C, 78°C, 75°C, 70°C, and 66°C) and hot air velocities 4m/s at a constant relative humidity.

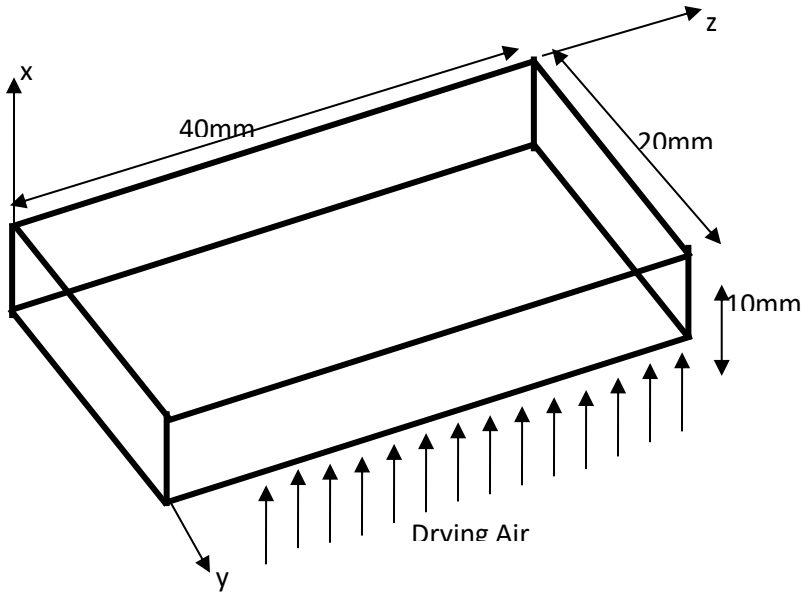


Fig. 3.3: Schematic diagram of the rectangular geometry of the cassava slice

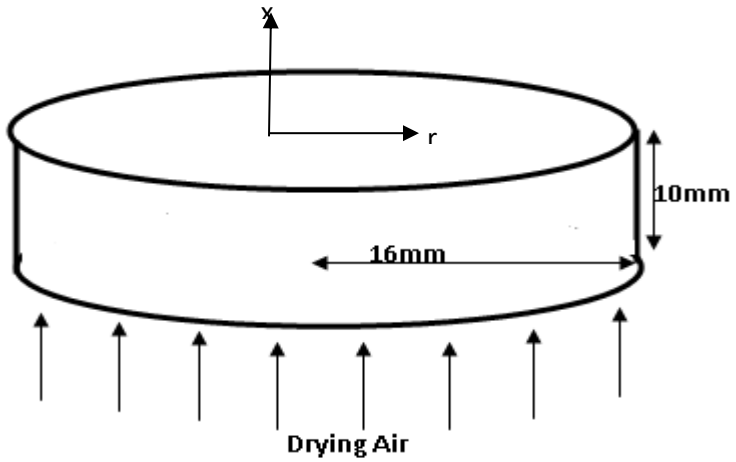


Fig. 3.4: Schematic diagram of the circular geometry of the cassava slice

Drying is synonymous with water diffusion thus it is a mass transfer process governed by Fick's second law. With regards to the water diffusivity, Fick's second law for a 2-dimensional element (Eqn 3.10) would be used to define the mass transfer process, by assuming isotropic behavior of the samples.

$$\frac{\partial M}{\partial t} = \mathrm{Div}\left[D_{eff}(T)\mathrm{grad}(M)\right] = D_{eff}(T)\left(\frac{\partial^2 M}{\partial x^2} + \frac{\partial^2 M}{\partial y^2}\right) \tag{3.10}$$

In carrying out the Finite Element formulations, the following assumptions were made:

- ❖ No heat is generated inside the sample during the drying process
- ❖ Two dimensional equations sufficiently describe the process for small thickness of the drying samples,
- ❖ Initial moisture content inside the sample is homogeneous,
- ❖ Material to be dried is isotropic
- ❖ Shrinkage is neglected.

The drying dynamics dictated by equation (3.10) are influence by both initial condition and Neumann boundary condition. The initial condition is given as $M(t=0) = M_0$ while the Neumann boundary condition is given as

$$-D_{eff}(T)\frac{\partial M}{\partial n} = h_m(T,t)\left[M_{surf} - M_{eq}\right] \tag{3.11}$$

Where $M_{surf}$ represents the surface moisture content and $M_{eq}$ represents the equilibrium moisture content which is a function of seasonal and climatic conditions. In what follows, the 2-dimensional FE formulation for drying of rectangular shaped potatoes as presented in (Beigi, 2017) is adapted here for drying of cassava pellets with rectangular and circular shapes. The typical 2-dimensional finite element used here, the triangular element, is reviewed. The field of $M$ in the $x-y$ plane of a triangular element is given by

$$M = N_1M_1 + N_2M_2 + N_3M_3 = \mathrm{NM}^e \tag{3.12}$$

Where the shape functions are contained in $\mathrm{N} = \{\xi \quad \eta \quad 1-\xi-\eta\}$ and the nodal vector given as$\mathrm{M}^e = \{M_1 \quad M_2 \quad M_3\}^T$. The spatial variables $x$ and $y$ are also interpolated similarly, thus

$$x = N_1x_1 + N_2x_2 + N_3x_3 = \mathrm{Nx}^e \tag{3.13}$$

$$y = N_1y_1 + N_2y_2 + N_3y_3 = \mathrm{Ny}^e \tag{3.14}$$

Differentiating the field variable *M* with respect the local spatial variables $\xi$ and $\eta$ gives

$$\frac{\partial M}{\partial \xi} = \frac{\partial M}{\partial x}\frac{\partial x}{\partial \xi} + \frac{\partial M}{\partial y}\frac{\partial y}{\partial \xi} \tag{3.15}$$

$$\frac{\partial M}{\partial \eta} = \frac{\partial M}{\partial x}\frac{\partial x}{\partial \eta} + \frac{\partial M}{\partial y}\frac{\partial y}{\partial \eta} \tag{3.16}$$

which in vector-matrix form reads

$$\begin{Bmatrix} \frac{\partial M}{\partial \xi} \\ \frac{\partial M}{\partial \eta} \end{Bmatrix} = \mathrm{J}\begin{Bmatrix} \frac{\partial M}{\partial x} \\ \frac{\partial M}{\partial y} \end{Bmatrix} \tag{3.17}$$

Where the Jacobian matrix J is given as

$$\mathrm{J} = \begin{bmatrix} x_1 - x_3 & y_1 - y_3 \\ x_2 - x_3 & y_2 - y_3 \end{bmatrix} = \begin{bmatrix} x_{13} & y_{13} \\ x_{23} & y_{23} \end{bmatrix} \tag{3.18}$$

Therefore,

$$\begin{Bmatrix} \frac{\partial M}{\partial x} \\ \frac{\partial M}{\partial y} \end{Bmatrix} = \mathrm{J}^{-1}\begin{Bmatrix} \frac{\partial M}{\partial \xi} \\ \frac{\partial M}{\partial \eta} \end{Bmatrix} = \frac{1}{\det \mathbf{J}}\begin{bmatrix} y_{23} & -y_{13} \\ -x_{23} & x_{13} \end{bmatrix}\begin{Bmatrix} 1 & 0 & -1 \\ 0 & 1 & -1 \end{Bmatrix}\mathrm{M}^e = \mathrm{B}_T\mathrm{M}^e \tag{3.19}$$

Where$|\det \mathbf{J}| = 2A_e$, where $A_e$ is the area of the triangular element, and $\mathbf{B}_T$ can be written as

$$\mathrm{B}_T = \frac{1}{\det \mathbf{J}} \begin{Bmatrix} y_{23} & -y_{13} & y_{13} - y_{23} \\ -x_{23} & x_{13} & x_{23} - x_{13} \end{Bmatrix} = \frac{1}{\det \mathbf{J}} \begin{Bmatrix} y_{23} & y_{31} & y_{12} \\ x_{32} & x_{13} & x_{21} \end{Bmatrix} \tag{3.20}$$

The Galerkin method of weighted residual is widely used to solve this type of field problem. The Galerkin method leads to solving the problem

$$\iint \varphi \left[ D_{eff}(T) \left( \frac{\partial^2 M}{\partial x^2} + \frac{\partial^2 M}{\partial y^2} \right) - \frac{\partial M}{\partial t} \right] dA = 0 \tag{3.21}$$

Where $\varphi(x, y)$ is the weight field function which vary according to

$$\varphi = \mathrm{N}\varphi \tag{3.22}$$

$$\begin{Bmatrix} \frac{\partial \varphi}{\partial x} \\ \frac{\partial \varphi}{\partial y} \end{Bmatrix} = B_T \varphi \tag{3.23}$$

Equation (3.20) is then re-written to become

$$\iint D_{eff}(T) \left[ \frac{\partial}{\partial x} \left( \varphi \frac{\partial M}{\partial x} \right) - \frac{\partial \varphi}{\partial x} \frac{\partial M}{\partial x} \right] dA + \iint D_{eff}(T) \left[ \frac{\partial}{\partial y} \left( \varphi \frac{\partial M}{\partial y} \right) - \frac{\partial \varphi}{\partial y} \frac{\partial M}{\partial y} \right] dA - \iint \varphi \frac{\partial M}{\partial t} dA = 0 \tag{3.24}$$

$$\iint D_{eff}(T) \left[ \frac{\partial}{\partial x} \left( \varphi \frac{\partial M}{\partial x} \right) + \frac{\partial}{\partial y} \left( \varphi \frac{\partial M}{\partial y} \right) \right] dA - \iint D_{eff}(T) \left[ \frac{\partial \varphi}{\partial x} \frac{\partial M}{\partial x} + \frac{\partial \varphi}{\partial y} \frac{\partial M}{\partial y} \right] dA - \iint \varphi \frac{\partial M}{\partial t} dA = 0 \tag{3.25}$$

Using the Gauss divergence theorem transforms the area integral on the right-hand-side of equation (3.25) to boundary integral, such that

$$\iint D_{eff}(T) \left[ \frac{\partial}{\partial x} \left( \varphi \frac{\partial M}{\partial x} \right) + \frac{\partial}{\partial y} \left( \varphi \frac{\partial M}{\partial y} \right) \right] dA = \int D_{eff}(T) \left[ \varphi \frac{\partial M}{\partial x} n_x + \varphi \frac{\partial M}{\partial y} n_y \right] d\Omega \tag{3.26}$$

where $n_x$ and $n_y$ represent the direction cosines of unit normal to the boundary.

Therefore, equation (3.25) becomes

$$\int D_{eff}(T)\left[\varphi\frac{\partial M}{\partial x}n_x+\varphi\frac{\partial M}{\partial y}n_y\right]d\Omega-\iint D_{eff}(T)\left[\frac{\partial\varphi}{\partial x}\frac{\partial M}{\partial x}+\frac{\partial\varphi}{\partial y}\frac{\partial M}{\partial y}\right]dA-$$

$$\iint\varphi\frac{\partial M}{\partial t}dA=0 \qquad (3.27)$$

Considering 2-dimensional geometry of the problem, then

$$\int D_{eff}(T)\left[\varphi\frac{\partial M}{\partial x}n_x+\varphi\frac{\partial M}{\partial y}n_y\right]d\Omega=\int D_{eff}(T)\left[\varphi\frac{\partial\chi}{\partial n}\right]d\Omega \qquad (3.28)$$

Where $n$ is the unit normal to the boundary, therefore, equation (3.24) becomes compactly written as

$$\int D_{eff}(T)\left[\varphi\frac{\partial M}{\partial n}\right]d\Omega-\iint D_{eff}(T)\left[\frac{\partial\varphi}{\partial x}\frac{\partial M}{\partial x}+\frac{\partial\varphi}{\partial y}\frac{\partial M}{\partial y}\right]dA-\iint\varphi\frac{\partial M}{\partial t}dA=0 \qquad (3.29)$$

In light of equations (3.19) and (3.23)

$$\iint D_{eff}(T)\left[\frac{\partial\varphi}{\partial x}\frac{\partial M}{\partial x}+\frac{\partial\varphi}{\partial y}\frac{\partial M}{\partial y}\right]dA=\iint D_{eff}(T)\left\{\frac{\partial\varphi}{\partial x}\quad\frac{\partial\varphi}{\partial y}\right\}\begin{Bmatrix}\frac{\partial M}{\partial x}\\ \frac{\partial M}{\partial y}\end{Bmatrix}dA=$$

$$\iint D_{eff}(T)\varphi^T\mathrm{B}_T^T\mathrm{B}_T\mathrm{M}^e dA \qquad (3.30)$$

Considering the boundary condition, then

$$\int D_{eff}(T)\left[\varphi\frac{\partial M}{\partial n}\right]d\Omega=\int\varphi h_m\left(M_{eq}-M_{surf}\right)d\Omega \qquad (3.31)$$

The forward difference formula gives

$$\frac{\partial M}{\partial t}=\frac{1}{\Delta t}(M_{i+1}-M_i)=\frac{\mathbf{N}}{\Delta t}(\mathrm{M}_{i+1}^e-\mathrm{M}_i^e) \qquad (3.32)$$

Equation (3.29) then becomes

$$\int \varphi h_m\left(M_{eq} - M_{surf}\right) d\Omega - \iint D_{eff}(T)\varphi^T \mathrm{B}_T^T \mathrm{B}_T \mathrm{M}^e dA - \iint \varphi \frac{1}{\Delta t} \mathrm{N}(\mathrm{M}_{i+1}^e - \mathrm{M}_i^e) dA = 0 \quad (3.33)$$

This becomes

$$\sum_e \varphi^{\mathrm{T}} \mathrm{h}_T \, \mathrm{r}_{eq} - \sum_e \varphi^{\mathrm{T}} \mathrm{h}_T \, \mathrm{M}_{surf,i}^{\mathrm{e}} - \sum_e \varphi^{\mathrm{T}} \mathrm{k}_T \, \mathrm{M}_i^{\mathrm{e}} - \sum_e \varphi^{\mathrm{T}} \mathrm{m}_T \, \mathrm{M}_{i+1}^{\mathrm{e}} + \sum_e \varphi^{\mathrm{T}} \mathrm{m}_T \, \mathrm{M}_i^{\mathrm{e}} = 0 \quad (3.34)$$

where

$$\mathrm{r}_{eq} = \frac{h_m M_{eq} l_{23}}{2} \begin{Bmatrix} 0 \\ 1 \\ 1 \end{Bmatrix} \quad (3.35)$$

$$\mathrm{h}_T = \frac{h_m l_{23}}{6} \begin{bmatrix} 0 & 0 & 0 \\ 0 & 2 & 1 \\ 0 & 1 & 2 \end{bmatrix} \quad (3.36)$$

$$\mathrm{k}_T = D_{eff} \boldsymbol{\varphi}^{\mathrm{T}} \mathbf{B}_{\mathrm{T}}^{\mathrm{T}} \boldsymbol{B}_T \quad (3.37)$$

$$\mathbf{m}_T = \frac{A_e}{3\Delta \mathrm{t}} \begin{Bmatrix} 1 \\ 1 \\ 1 \end{Bmatrix} \quad (3.38)$$

and $l_{ij}$ is the length of a boundary element edge between nodes "$i$" and "$j$". The global moisture content vector becomes assembled into an iterative scheme as follows;

$$\mathrm{M}_{i+1} = (\mathrm{M}_T)^{-1}(\mathrm{M}_T - \mathrm{K}_T - \mathrm{H}_T)\mathrm{M}_i + (\mathrm{M}_T)^{-1}\mathrm{H}_T \mathrm{R}_{eq} \quad (3.39)$$

Under the assumption of uniform moisture content of $M_0$ at $i = 0$, that is at $t = 0$, the initial solution $\mathbf{M}_0$ is known. Therefore the first step solution $\mathbf{M}_1$ can be calculated and the iteration continues to the end of the solution history.

### 3.3.5 Flowchart for MATLAB pdetool Simulation

The core Partial Differential Equation (PDE) toolbox algorithm uses the Finite Element Method (FEM) for problems defined on bounded domains in 2-D or 3-D space. In most cases, elementary functions cannot express the solutions of even simple PDEs on complicated geometries. The finite element method describes a complicated geometry as a collection of subdomains by generating a mesh on the geometry. In this work, the matlab partial differential equation toolbox (pdetool) which provides solutions to partial differential equation in two space dimensions and time was employed to solve the developed 2-dimensional partial differential equation (equation 3.38). The constructive solid geometry (CGS) model was used to create the rectangular and circular geometry within the computational domain. The boundary condition was set at Neumann boundary condition and equation 3.10 which satisfies the condition was keyed in. Equation 3.38 was then defined in the graphical user interface (GUI), and the PDE problem and coefficients were then specified. The automated mesh generation tool was then used to create triangular meshes on the created geometry before activating the FEM discretization of the PDE, boundary conditions and interpolation functions to solve the problem. The solution is calculated using the solvepde function and the temperature distribution is plotted using the pdeplot function. The plot selection dialog box solves other physical properties calculated from the solution. More accurate results are obtained by mesh refinement. Mesh refinement causes significant increase in the number of points where the PDE is solved and significant increase in the time required to compute the solution.

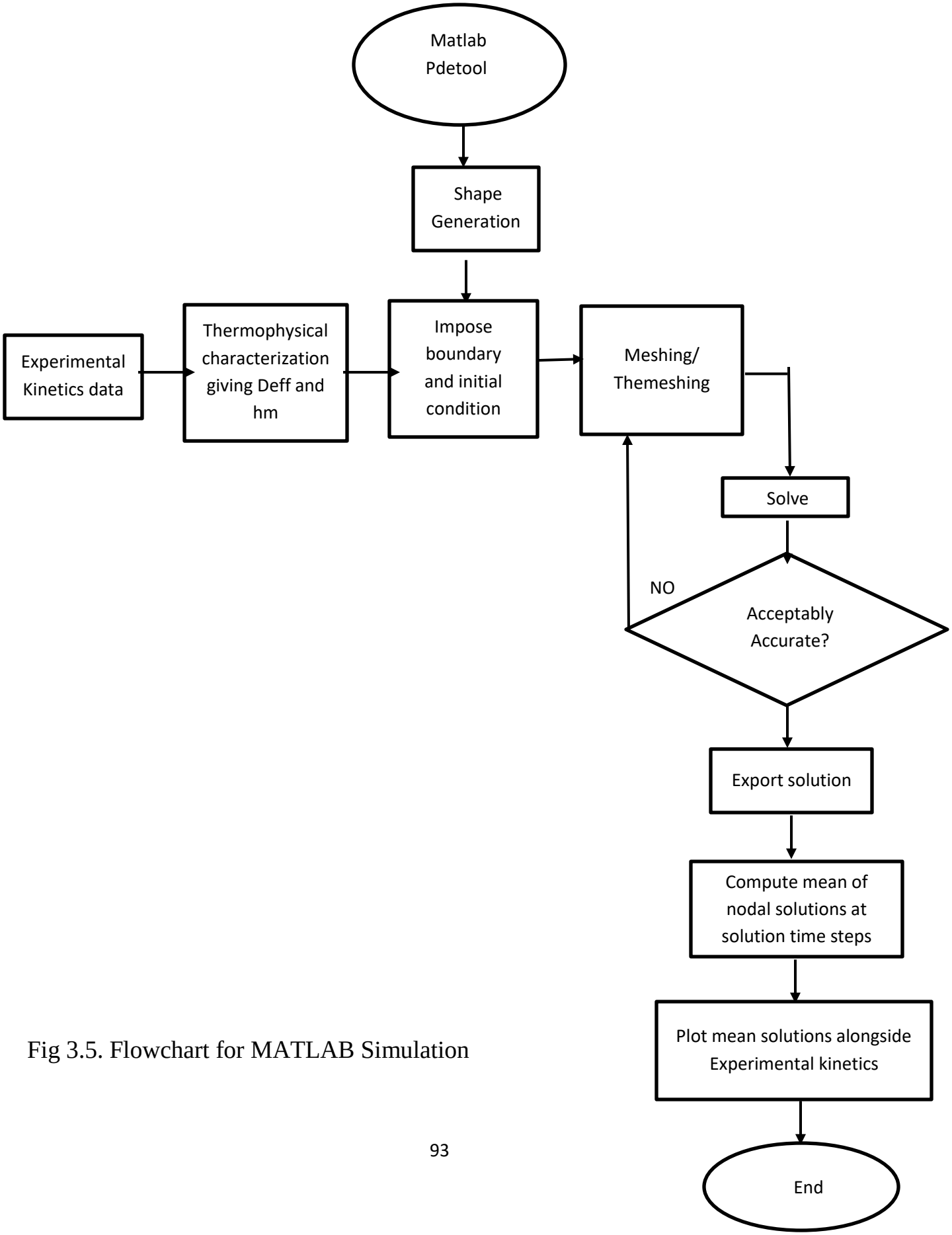


Fig 3.5. Flowchart for MATLAB Simulation

### 3.3.6 Flowchart for MATLAB Simulation at $150^0$ C heater temperature ($81^0$ C hot air)

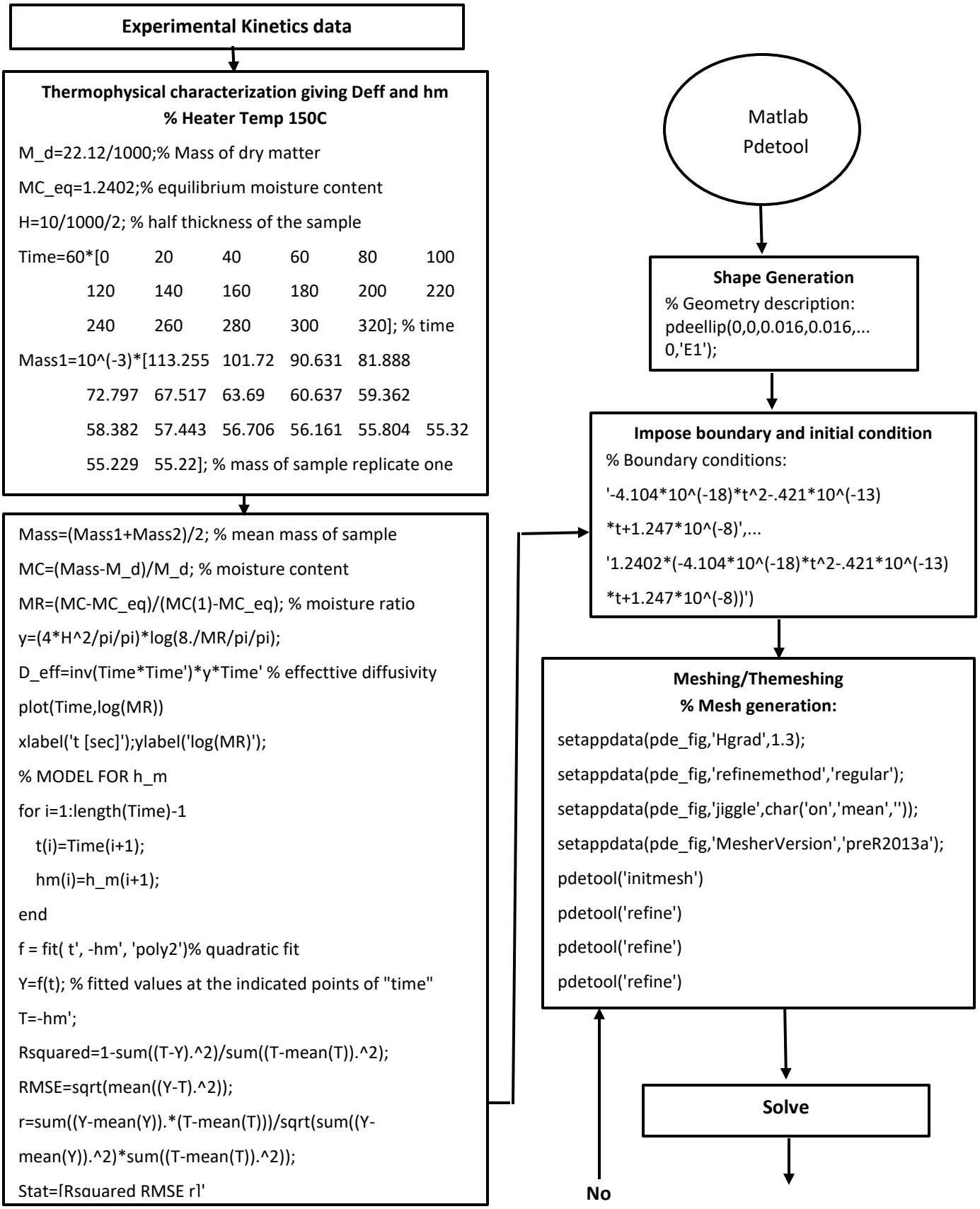

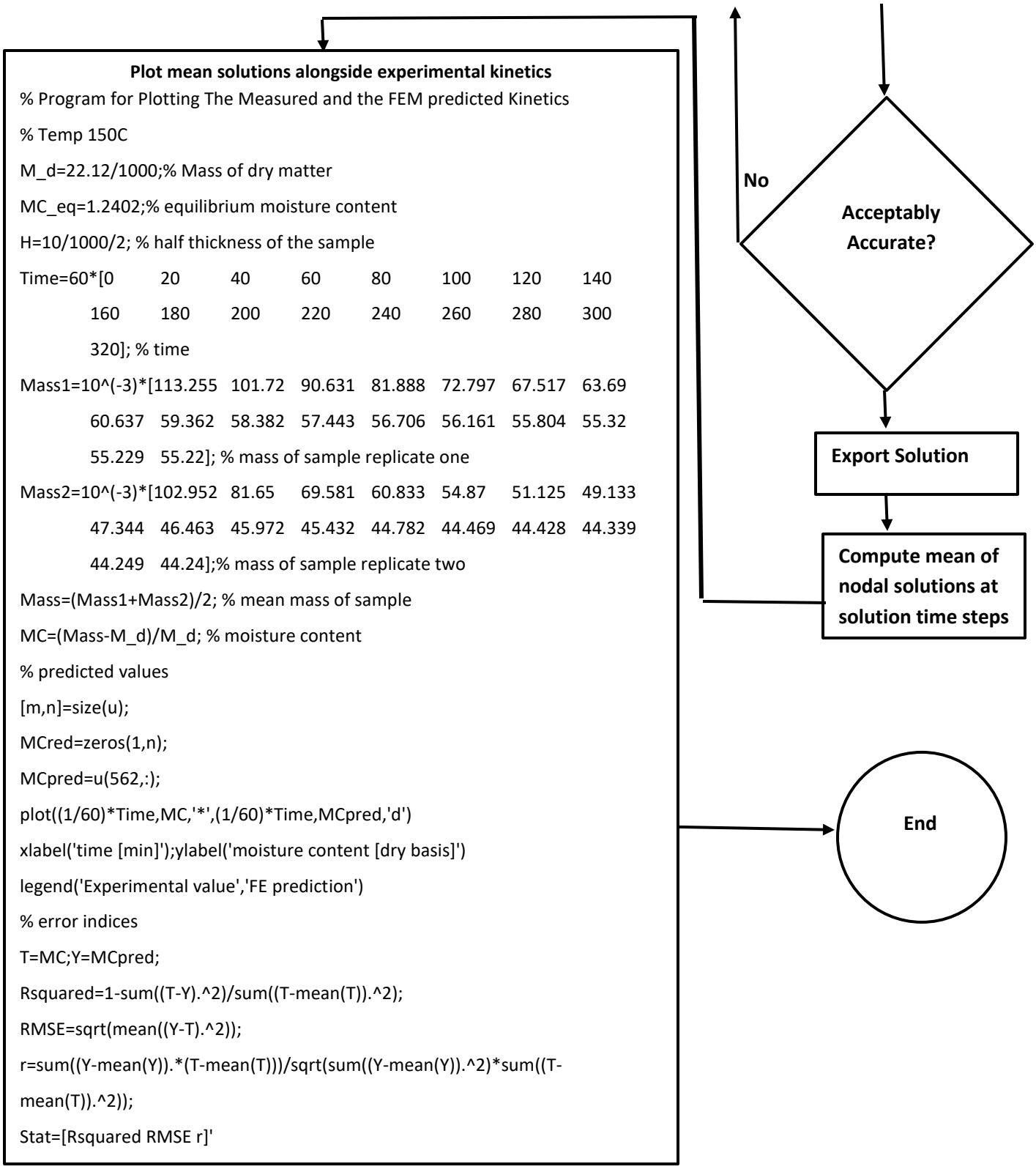


Fig. 3.6. Algorithm for MATLAB Simulation at $150^0$ C heater temperature ($81^0$ C hot air)

### 3.3.7. Constitutive Relationships

The mass transfer source term per unit length can be obtained by multiplying the evaporation rate from a single particle $m_s$ by the number of particles Np in the control volume per unit length, which falls within the hydraulic diameter of the dryer (Levy, et al 1999).

$$S_{mass} = N_P m_s \quad 3.39$$

The mass transfer in equation (3.39) is based on a single stage drying process, where the solid surface is considered to be wetted. Drying starts when the surface of the pellets receives heat from the moving air stream and evaporation commences on the surface. This is referred to as constant-rate drying period.

For a situation that involves molecular diffusion and mass transfer due to forced convection, the following variables are important: mass diffusivity ($D_{eff}$) from vapour component to gas phase, the velocity of the fluid, the characteristic dimension which for this work corresponds to pellets diameter and convective mass transfer coefficient $h_{m.}$

The variables are grouped into the following dimensionless numbers:

Schmidt number

$$S_C = \frac{\mu}{\rho D_{eff}} \quad 3.40$$

Sherwood number

$$Sh = \frac{h_m d}{D_{eff}} \quad 3.41$$

Reynolds number

$$Re = \frac{\rho u d}{\mu} \quad 3.42$$

Linear interpolation (3.43) would be employed in obtaining the needed parameters which would give the needed values for the Schmidt number, Sherwood number and Reynolds number as expressed in equations (3.40), (3.41) and (3.42) respectively.

$$y_2 = \frac{(x_2 - x_1)((y_3 - y_1)}{(x_3 - x_1)} + y_1 \quad (3.43)$$

To interpolate the $y_2$ value:

$x_1$, $x_3$, $y_1$ and $y_3$ need to be entered/copied from the table (Appendix III).

$x_2$ defines the point to perform the interpolation.

$y_2$ is the interpolated value and solution.

After evaluating the correlations above, the Sherwood number is substituted into equation (3.41) and $h_m$ can be solved for.

- For fully developed laminar flow in a circular tube, we have
  Sh = 3.66 (for constant moisture concentration at the wall
  Sh = 4.36 (for constant wall mass tube)
- For fully developed turbulent flow in a circular tube,
  $Sh = 0.023\ Re^{0.83} Sc^{0.44}$
  Since the pellets are arranged in trays in the drying chamber, appropriate correlation for Sh should be determined. The heat transfer analogy would be applied.

# CHAPTER FOUR

## 4.0 Results and Discussions

## 4.1. Thermophysical Characterization of Cassava Samples

### 4.1.1 The Effective Diffusivity

Looking at the boundary condition given in equation (3.10), it is seen that $D_{eff}(T)$ and $h_m(T,t)$ are necessary for numerical solution of the developed FE model. The Crank's series solution for variation with time of moisture ratio for an infinite slab as stated in equation (3.5), when solved and transformed in logarithmic form to Equation (3.8), gave solutions to the effective diffusivity.

By plotting $\ln(MR)$ against $t$, a straight line is obtained with the slope $S = -\frac{\pi^2 D_{eff}}{4H^2}$ such that $D_{eff} = -\frac{4H^2}{\pi^2}S$. The plots are shown in Figures 4.1a to 4.5a for the experimental drying of the rectangular samples as discussed under the experimental procedure. The plots for the five considered heater temperatures exhibited expected trends; lines with negative slopes. The slopes are seen on the inserted linear equations which are lines of best fit from linear regression. The calculated $D_{eff}$ are given in Table 4.1. Also, based on the experiments, the equilibrium moisture content at different times of the days the experiments were conducted are tabulated in Table 4.1 alongside the heater temperatures employed for experiments. Corresponding results for the circular samples are given in Figures 4.1 b to 4.5 b and Table 4.1.

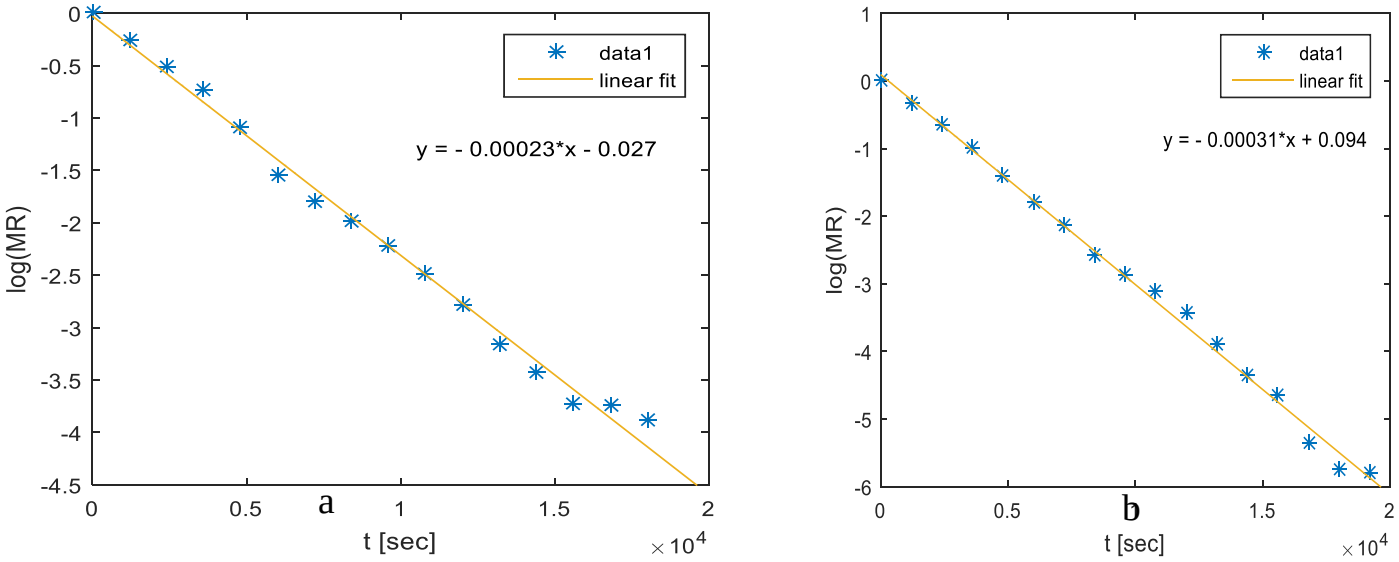


Figure 4.1. The plot of $\ln(MR)$ against $t$ for the Experiment at Heater Temperature of 150°C (81$^0$C air temperature) for (a) the rectangular and (b) the circular samples

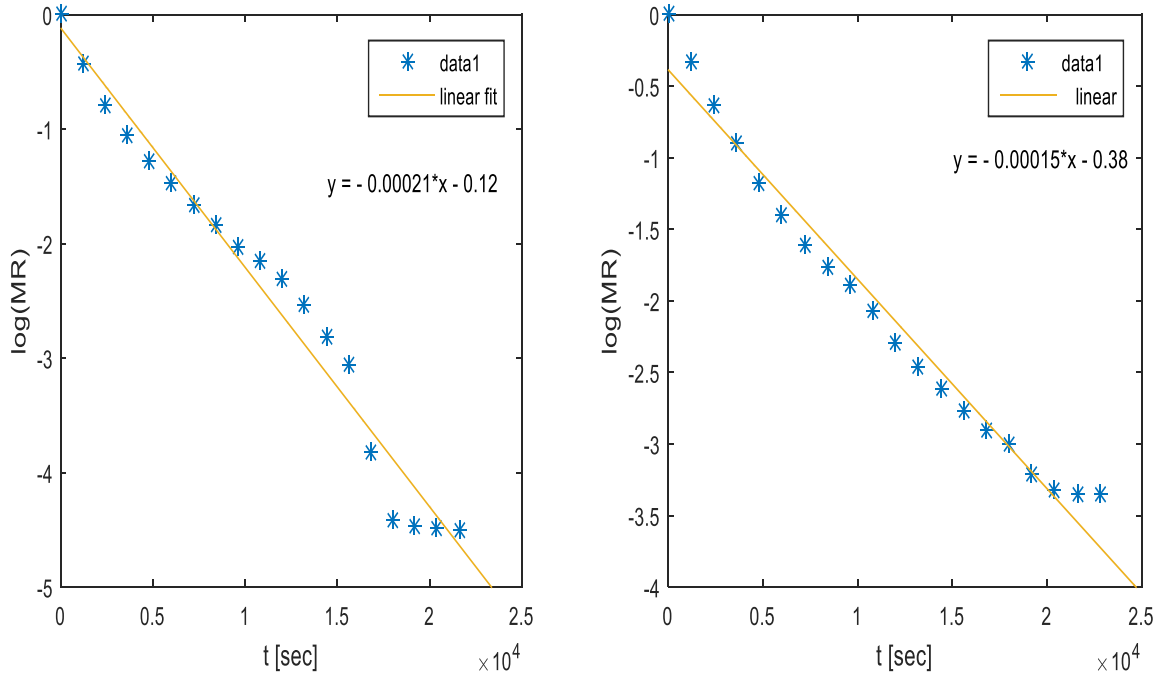


Figure 4.2. The plot of $\ln(MR)$ against $t$ for the Experiment at Heater Temperature of 140°C (78$^0$C air temperature) for (a) the rectangular and (b) the circular samples

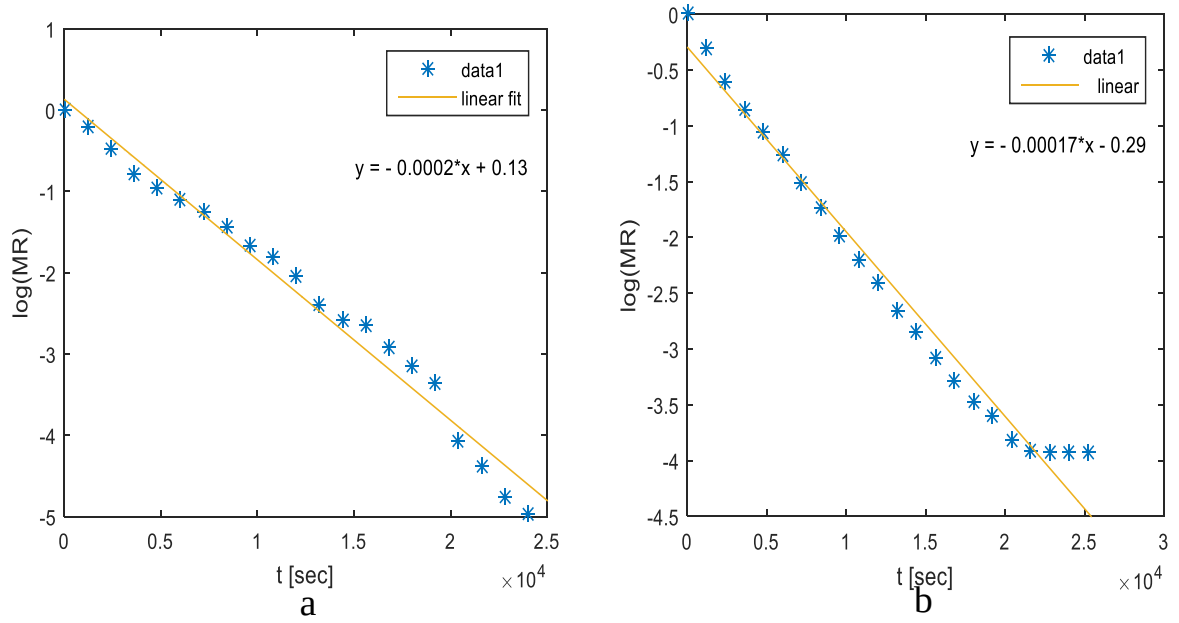


Figure 4.3. The plot of $\ln(MR)$ against $t$ for the Experiment at Heater Temperature of 130°C (75$^0$C air temperature) for (a) the rectangular and (b) the circular samples

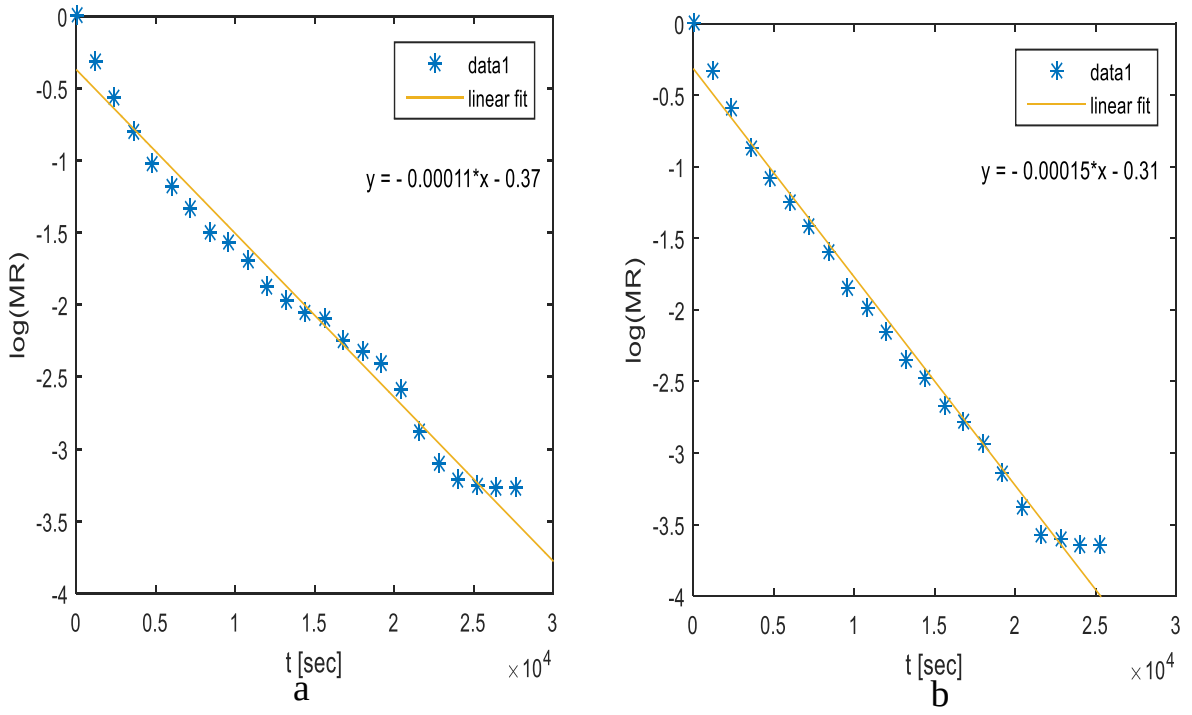


Figure 4.4. The plot of $\ln(MR)$ against $t$ for the Experiment at Heater Temperature of 120°C (70$^0$C air temperature) for (a) the rectangular and (b) the circular samples

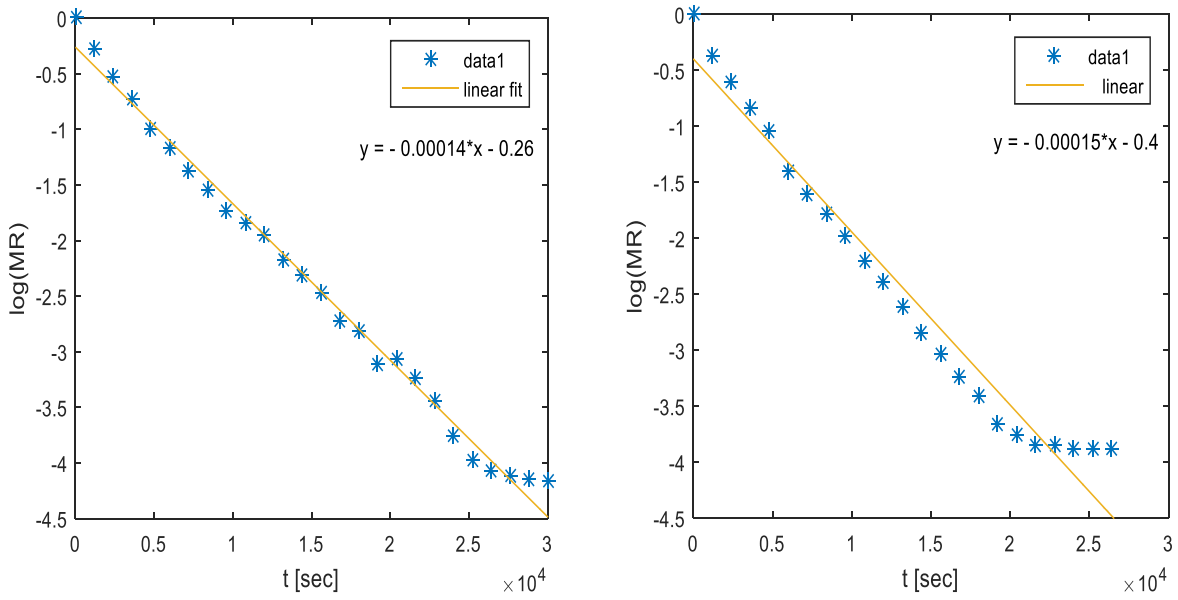


Figure 4.5. The plot of $\ln(MR)$ against $t$ for the Experiment at Heater Temperature of 110°C (66$^0$C air temperature) for (a) the rectangular and (b) the circular samples.

As tabulated in Table 4.1 (Appendix IV), the diffusivity of the rectangular samples were determined to be in range of $2.3304\times10^9$ - $1.4260\times10^9$ $m^2s^{-1}$, and described using a 3$^{rd}$ order polynomial equation ($y = -9E-05x^3 - 0.0343x^2 - 4.4281x + 189.6$) with the value of $R^2 = 0.8989$. The effect of drying air temperature on the moisture diffusivity can be discussed using Figure 4.6. Also, the diffusivity of the circular samples were determined to be in range of $3.1467\times10^9$ - $1.4759\times10^9$ $m^2s^{-1}$, and described using a 3$^{rd}$ order polynomial equation ($y = 0.0001x^3 - 0.0487x^2 - 6.0254x + 246.05$) as a function of air temperature with the value of $R^2 = 0.9402$ as shown in Figure 4.7. The plots clearly explains that the moisture diffusivity of cassava pellets can be expressed as a function of temperature using a 3$^{rd}$ order polynomial equation. Diffusivity range and plots follows the same trend with Beigi 2017.

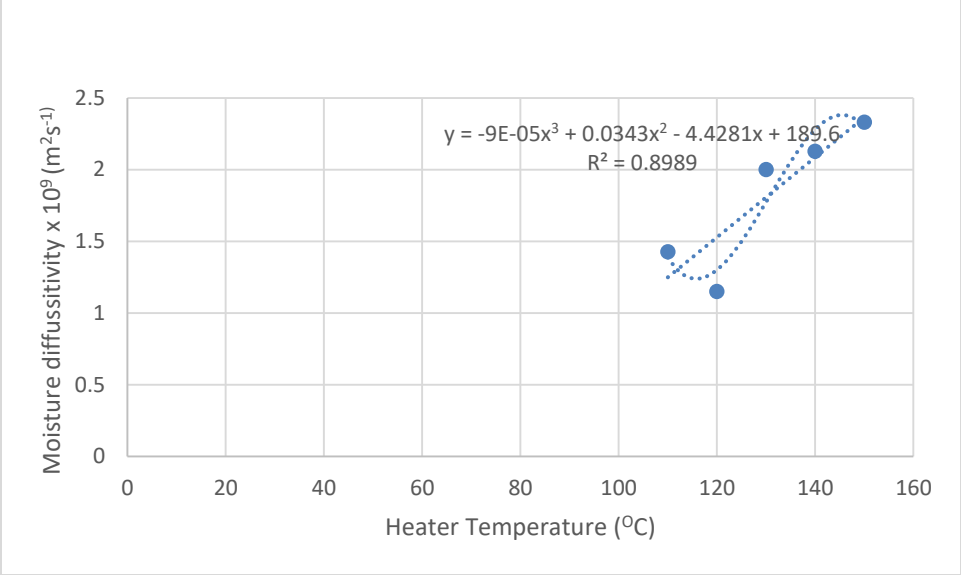


Fig. 4.6: Air temperature effect on effective moisture diffusivity for the Rectangular shape cassava pellets.

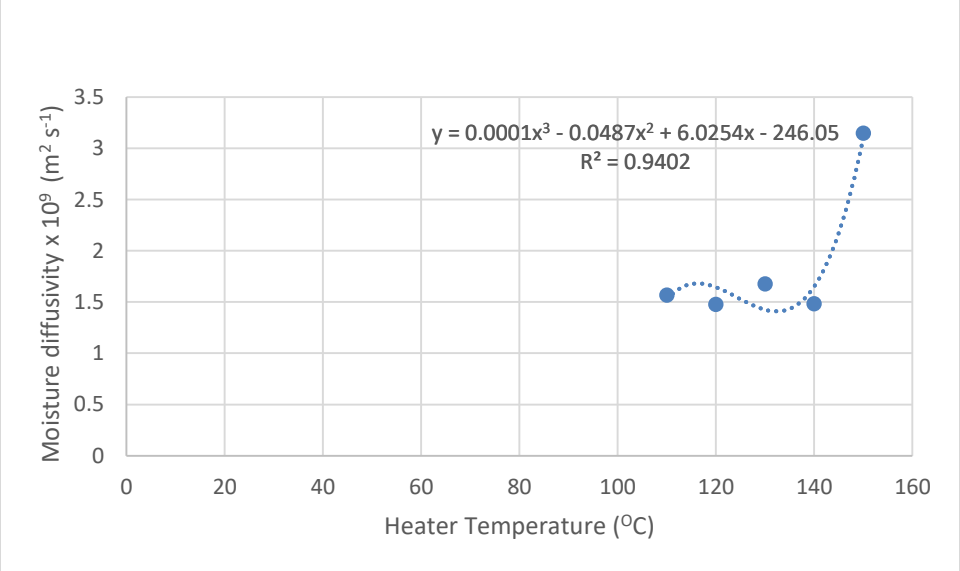


Fig. 4.7: Air temperature effect on effective moisture diffusivity for the Circular shape cassava pellets.

### 4.2.2 Convective Mass Transfer Coefficient

This has been given by (Beigi, 2017) as

$$h_m = \frac{V}{At}\ln(MR) \tag{4.5}$$

Where $V$ and $A$ are the volume and area of the sample respectively. The V were estimated by inserting a sample at intervals inside a calibrated cylinder containing toluene at a known level while noting the volume of toluene displaced. The results are summarized in Tables 4.2 to 4.11 (Appendix IV). In the tables, $n_s$is the number of samples used in the kinetics experiment. Twelve samples were mostly used. It is seen that the convective mass transfer coefficient varies with time. A polynomial of second order has been recently assumed by Beigi (Beigi, 2017). The quadratic models for the convective mass transfer coefficients presented in Tables 4.2 to 4.11(Appendix IV) were developed and tabulated in Tables 4.12 and 4.13 for the rectangular and circular cassava samples. It is seen that the $R^2$ values and correlation coefficients ($r$) are mostly above 0.9 meaning that the convective mass transfer coefficient of the cassava samples is adequately modeled as a quadratic function of drying time for each air temperature. As shown in equations 4.6- 4.10 (rectangular pellets) and equations 4.11- 4.15 (circular pellets).

T=81$^{O}$C $h_m = -4.922 \times 10^{-18}t^2 + 9.929 \times 10^{-15}t + 9.267 \times 10^{-9}$ $R^2 = 0.6310$ (4.6)

T=78$^{O}$C $h_m = 4.27 \times 10^{-17}t^2 - 1.253 \times 10^{-12}t + 1.645 \times 10^{-8}$ $R^2 = 0.9149$ (4.7)

T=75$^{O}$C $h_m = 1.308 \times 10^{-17}t^2 - 3.866 \times 10^{-13}t + 9.221 \times 10^{-9}$ $R^2 = 0.7138$ (4.8)

T=70$^{O}$C $h_m = 1.487 \times 10^{-17}t^2 - 6.495 \times 10^{-13}t + 1.159 \times 10^{-8}$ $R^2$ =0.9747 (4.9)

T=66$^{O}$C $h_m = 8.165 \times 10^{-18}t^2 - 3.945 \times 10^{-13}t + 1.032 \times 10^{-8}$ $R^2 = 0.9575$ (4.10)

T=81$^{O}$C $h_m - 4.104 \times 10^{-18}t^2 - 1.421 \times 10^{-13}t + 1.247 \times 10^{-8}$ $R^2 = 0.8518$ (4.11)

T=78$^{O}$C $h_m = 1.386 \times 10^{-17}t^2 - 6.5 \times 10^{-13}t + 1.301 \times 10^{-8}$ $R^2 = 0.9713$ (4.12)

T=75$^{O}$C $h_m = 1.171 \times 10^{-17}t^2 - 5.486 \times 10^{-13}t + 1.166 \times 10^{-8}$ $R^2 = 0.9491$ (4.13)

T=70$^{O}$C $h_m = 1.278 \times 10^{-17}t^2 - 5.989 \times 10^{-13}t + 1.242 \times 10^{-8}$ $R^2$ =0.9424 (4.14)

T=66$^{O}$C $h_m = 1.223 \times 10^{-17}t^2 - 5.966 \times 10^{-13}t + 1.26 \times 10^{-8}$ $R^2 = 0.9073$ (4.15)

Table 4.12. The quadratic models for the convective mass transfer coefficients at various heater temperatures for the rectangular samples

| Rectangular Samples | | | | | |
|---|---|---|---|---|---|
| Heater Temperature [$^{o}$C] | $M_{eq}$ | $D_{eff} \times 10^9$ | $h_m$ | $R^2$ | $r$ |
| 150 | 0.5400 | 2.3304 | $-4.922 \times 10^{-18}t^2 + 9.929 \times 10^{-15}t + 9.267 \times 10^{-9}$ | 0.6310 | 0.7943 |
| 140 | 0.8380 | 2.1277 | $4.27 \times 10^{-17}t^2 - 1.253 \times 10^{-12}t + 1.645 \times 10^{-8}$ | 0.9149 | 0.9565 |
| 130 | 0.7375 | 2.0004 | $1.308 \times 10^{-17}t^2 - 3.866 \times 10^{-13}t + 9.221 \times 10^{-9}$ | 0.7138 | 0.8449 |
| 120 | 0.9410 | 1.1498 | $1.487 \times 10^{-17}t^2 - 6.495 \times 10^{-13}t + 1.159 \times 10^{-8}$ | 0.9747 | 0.9872 |
| 110 | 1.2376 | 1.4260 | $8.165 \times 10^{-18}t^2 - 3.945 \times 10^{-13}t + 1.032 \times 10^{-8}$ | 0.9575 | 0.9785 |

Table 4.13. The quadratic models for the convective mass transfer coefficients at various heater temperatures for the circular samples

| Circular Samples | | | | | |
|---|---|---|---|---|---|
| Heater Temperature [$^{o}$C] | $M_{eq}$ | $D_{eff} \times 10^{9}$ | $h_m$ | $R^2$ | $r$ |
| 150 | 1.2402 | 3.1467 | $-4.104 \times 10^{-18}t^2 - 1.421 \times 10^{-13}t + 1.247 \times 10^{-8}$ | 0.8518 | 0.9229 |
| 140 | 1.3369 | 1.4830 | $1.386 \times 10^{-17}t^2 - 6.5 \times 10^{-13}t + 1.301 \times 10^{-8}$ | 0.9713 | 0.9855 |
| 130 | 1.4377 | 1.6770 | $1.171 \times 10^{-17}t^2 - 5.486 \times 10^{-13}t + 1.166 \times 10^{-8}$ | 0.9491 | 0.9742 |
| 120 | 1.4367 | 1.4759 | $1.278 \times 10^{-17}t^2 - 5.989 \times 10^{-13}t + 1.242 \times 10^{-8}$ | 0.9424 | 0.9708 |
| 110 | 1.4359 | 1.5665 | $1.223 \times 10^{-17}t^2 - 5.966 \times 10^{-13}t + 1.26 \times 10^{-8}$ | 0.9073 | 0.9525 |

## 4.3. The kinetics of cassava drying

The logarithmic kinetic model was used in determining the experimental moisture ratio as a function of drying time. The estimated parameters and statistical analysis of the model for all the drying condition are presented in Table 4.14 and 4.15 for the circular and rectangular pellets respectively. The model gave consistently high coefficient of determination ($R^2$) values in the range of 0.9949 – 0.9993 for the circular pellets, and 0.9852-0.9967 for the rectangular pellets. This is an indication that the model could satisfactorily describe the fast drying of cassava pellets at heater temperatures above $100^0$C.

### 4.3.1 Results of the drying kinetics of the circular and rectangular cassava Sample

The model parameters and statistical error indicators for the circular and rectangular cassava samples dried at different heater temperatures are summarized in tables 4.14. and 4.15.

Table 4.14. Table of model parameters and statistical error indicators for the circular cassava sample dried at different heater temperatures

| SN | Heater Temp. [$^o$C] | Coeffs. | $R^2$ | RMSE | MBE | MABE | Corr. Coef. |
|---|---|---|---|---|---|---|---|
| 1 | 150 | a = 1.014<br>c = -0.005402<br>k = 0.01706 | 0.9993 | 0.0077 | 0.0000 | 0.0064 | 0.9996 |
| 2 | 140 | a=0.9993<br>c=0.04578<br>k=0.0154 | 0.9970 | 0.0138 | 0.0000 | 0.0119 | 0.9985 |
| 3 | 130 | a= 0.9749<br>c= 0.05159<br>k= 0.01349 | 0.9981 | 0.0112 | 0.0000 | 0.0084 | 0.9991 |
| 4 | 120 | a=0.9345<br>c=0.03656<br>k=0.01344 | 0.9949 | 0.0178 | 0.0000 | 0.0155 | 0.9974 |

| | | | | | | | |
|---|---|---|---|---|---|---|---|
| 5 | 110 | a= 0.9272<br>c= 0.02171<br>k= 0.01389 | 0.9968 | 0.0142 | 0.0000 | 0.0100 | 0.9984 |

Table 4.14. The model parameters and statistical error indicators for the Rectangular cassava sample dried at different heater temperatures

| SN | Heater Temp. [$^{o}$C] | Coeffs. | $R^2$ | RMSE | MBE | MABE | Corr. Coef. |
|---|---|---|---|---|---|---|---|
| 1 | 150 | a = 1.025<br>c = -0.007591<br>k = 0.01369 | 0.9967 | 0.0169 | 0.0000 | 0.0114 | 0.9983 |
| 2 | 140 | a = 0.9945<br>c =0.03706<br>k =0.01677 | 0.9852 | 0.0304 | 0.0000 | 0.0274 | 0.9926 |
| 3 | 130 | a = 0.9820<br>c =0.07305<br>k =0.01111 | 0.9953 | 0.0188 | 0.0000 | 0.0142 | 0.9976 |
| 4 | 120 | a = 0.9749<br>c =0.06146<br>k =0.01273 | 0.9899 | 0.0240 | 0.0000 | 0.0220 | 0.9949 |
| 5 | 110 | a = 0.9443<br>c =0.02557<br>k =0.01179 | 0.9966 | 0.0145 | 0.0000 | 0.0123 | 0.9983 |

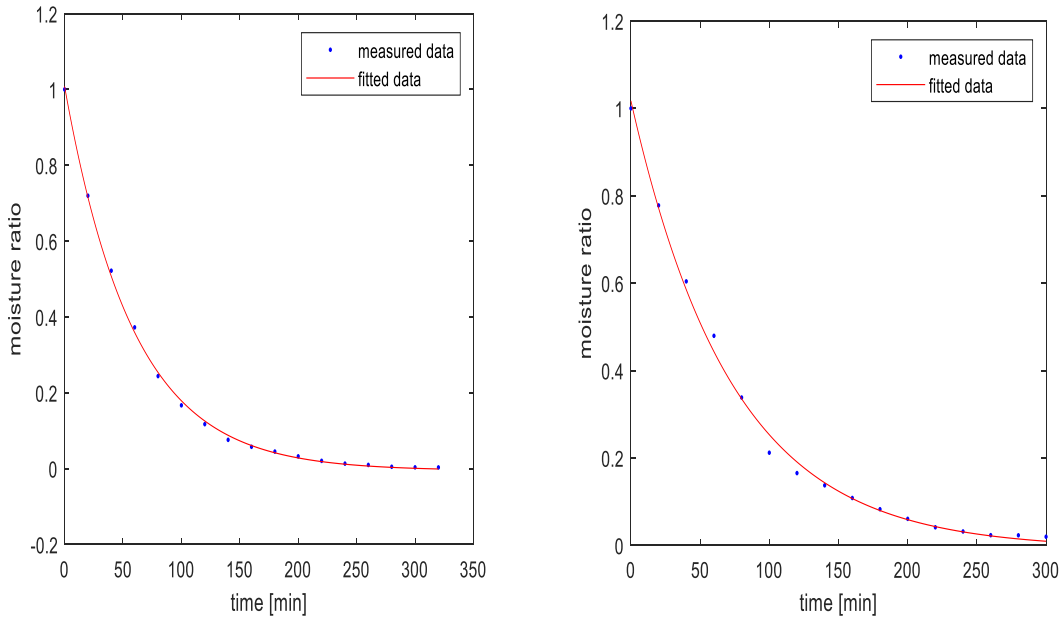


Figure 4.8. Kinetics of measured and fitted moisture ratio at heater temperature of 150$^{o}$C (81$^{0}$C air temperature) for the circular and rectangular cassava samples.

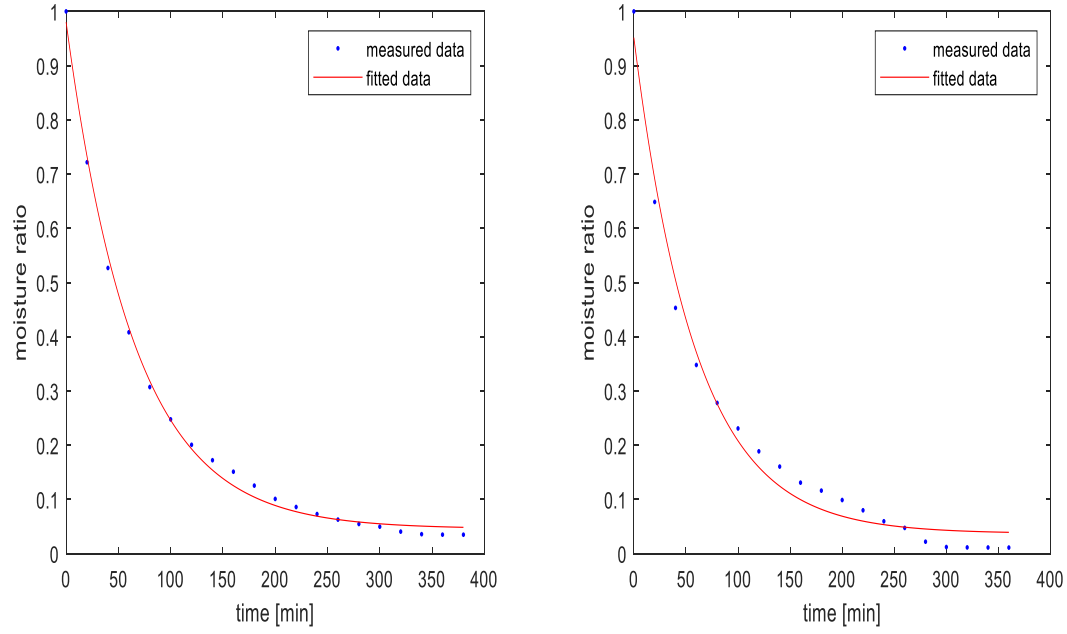


Figure 4.9. Kinetics of measured and fitted moisture ratio at heater temperature of 140$^{o}$C (78$^{0}$C air temperature) for the circular and rectangular cassava samples.

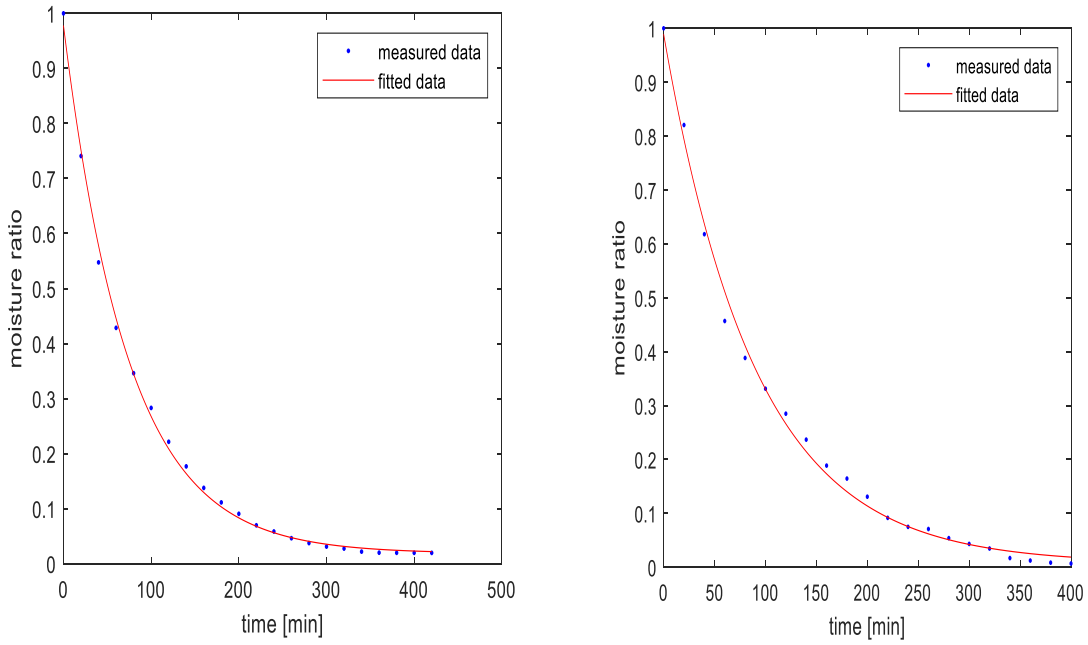


Figure 4.10. Kinetics of measured and fitted moisture ratio at heater temperature of 130$^{o}$C (75$^{0}$C air temperature) for the circular and rectangular cassava samples.

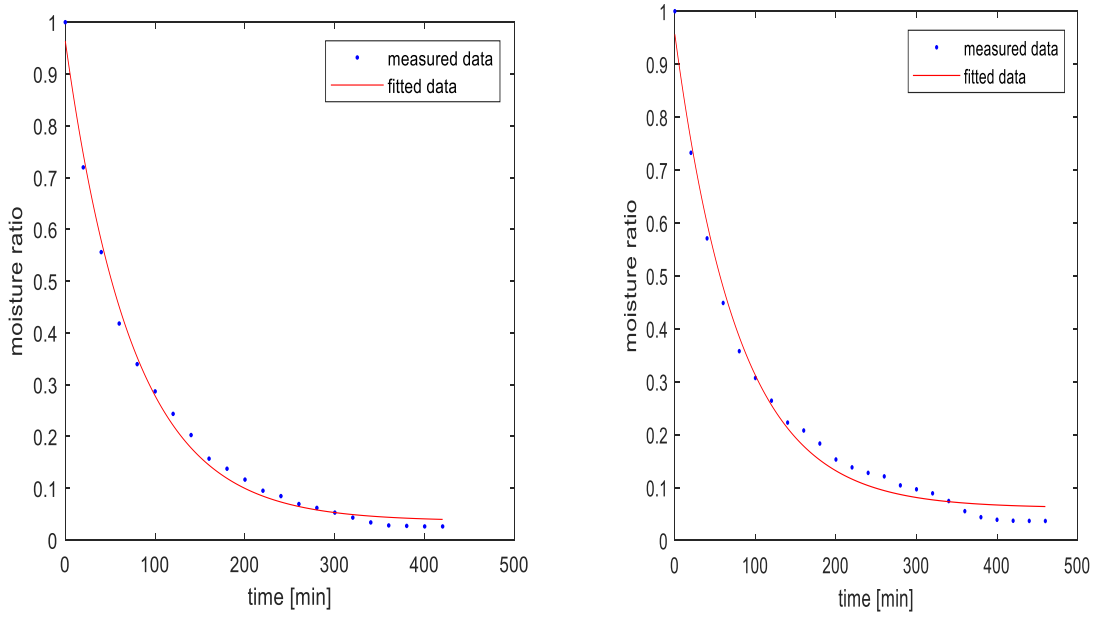


Figure 4.11. Kinetics of measured and fitted moisture ratio at heater temperature of 120$^{o}$C (70$^{0}$C air temperature) for the circular and rectangular cassava samples.

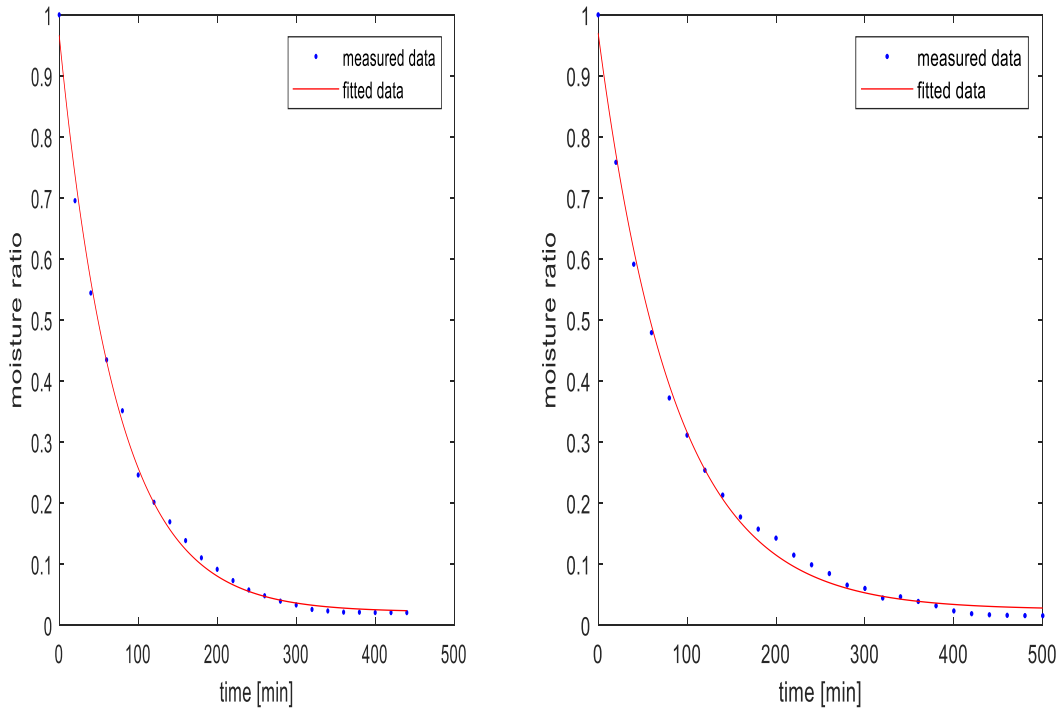


Figure 4.12. Kinetics of measured and fitted moisture ratio at heater temperature of 110$^{o}$C (66$^{0}$C air temperature) for the circular and rectangular cassava samples.

The performance of the lagarithmic model for all the drying temperatures as illustrated in figures 4.8-4.12 proved the accuracy of logarithmic model in describing the drying behaviour of cassava pellets. It is seen that the value of the drying rate constant (k) increased with the increase in temperature. This implies that with increase in temperature, drying curve becomes steeper indicating increase in drying rate. The fitting procedure showed that the results of the logarithmic model could be used to predict the drying behaviour of cassava pellets at heater temperatures above 100$^{0}$C. However, this did not indicate the effect of drying air temperature. To account for the effect of the drying air temperature on the constants “a”, “c” and “k” of logarithmic model, the constants were regressed with respect to heater temperatures. Linear and second order polynomial equations were found to be best fitted for both the

rectangular and circular pellets, for which the $R^2$ value was more than 0.9. This implies that the corresponding equations could be used to indicate the effect of drying air temperature on the constants "a", "c" and "k". The values of these constants could be calculated at any particular temperature using these equations and in turn moisture ratios can also be estimated. From the regression analysis, the accepted logarithmic model constants and coefficients were expressed in terms of the heater or hot air temperature as:

For rectangular pellets:

$$a = 0.0018T + 0.7488 \quad (R^2 = 0.9485) \tag{4.16}$$

$$c = -0.0001T^2 + 0.0378T - 2.3332 \quad (R^2 = 0.9801) \tag{4.17}$$

$$k = 3E - 06T^2 - 0.0007T + 0.0508 \quad (R^2 = 0.9834) \tag{4.18}$$

For circular pellets:

$$a = 0.0024T + 0.06601 \quad (R^2 = 0.9616) \tag{4.19}$$

$$c = -0.0001T^2 + 0.0279T - 1.7354 \quad (R^2 = 0.9002) \tag{4.20}$$

$$k = 4E - 06T^2 - 0.001T + 0.00764 \quad (R^2 = 0.9766) \tag{4.21}$$

Predictions by the logarithmic model are in good agreement with the data obtained from the convective drying experiment. The kinetics results and plots are line with Rayaguru and Routray 2012.

## 4.4. Numerical Solutions

Referring back to the PDE model in Equation (3.9) for moisture diffusion, the Neumann boundary condition in Equation (3.10) and the initial condition is the initial moisture content $M_0$ which is assumed uniform at $t = 0$, numerical solutions are generated from MATLAB programming of the developed models.

### 4.4.1. Rectangular Samples

In finite elements analysis, solutions can be improved by mesh refinement. That is why predictions are generated for a 99-element model, a 367-element model, a 1395-element model and a 5447-element model as shown in Figures 4.13 to 4.16 to show that the solutions progressively fell within the experimental range of moisture content as number of elements increased. The FE predictions at the experimental intervals are compared with the measured values in Figure 4.17. The $R^2$, RMSE and $r$ for the predictions in Figure 4.17 (a) are respectively 0.9340, 0.1924 and 0.9912 for the 1395-element model while the prediction accuracy improved to 0.9958, 0.0483 and 0.9984 for the 5447-element model. Marked improvement in accuracy is recorded on mesh refinement. Using the 5447-element model, FE predictions at the experimental intervals are compared with the measured values in Figures 4.18 to 4.21 and the corresponding statistical goodness of fit values are presented in Table 4.16. All the $R^2$ values in the tables are above 90% where majority were up to 99% indicating high accuracy of FE prediction of cassava drying.

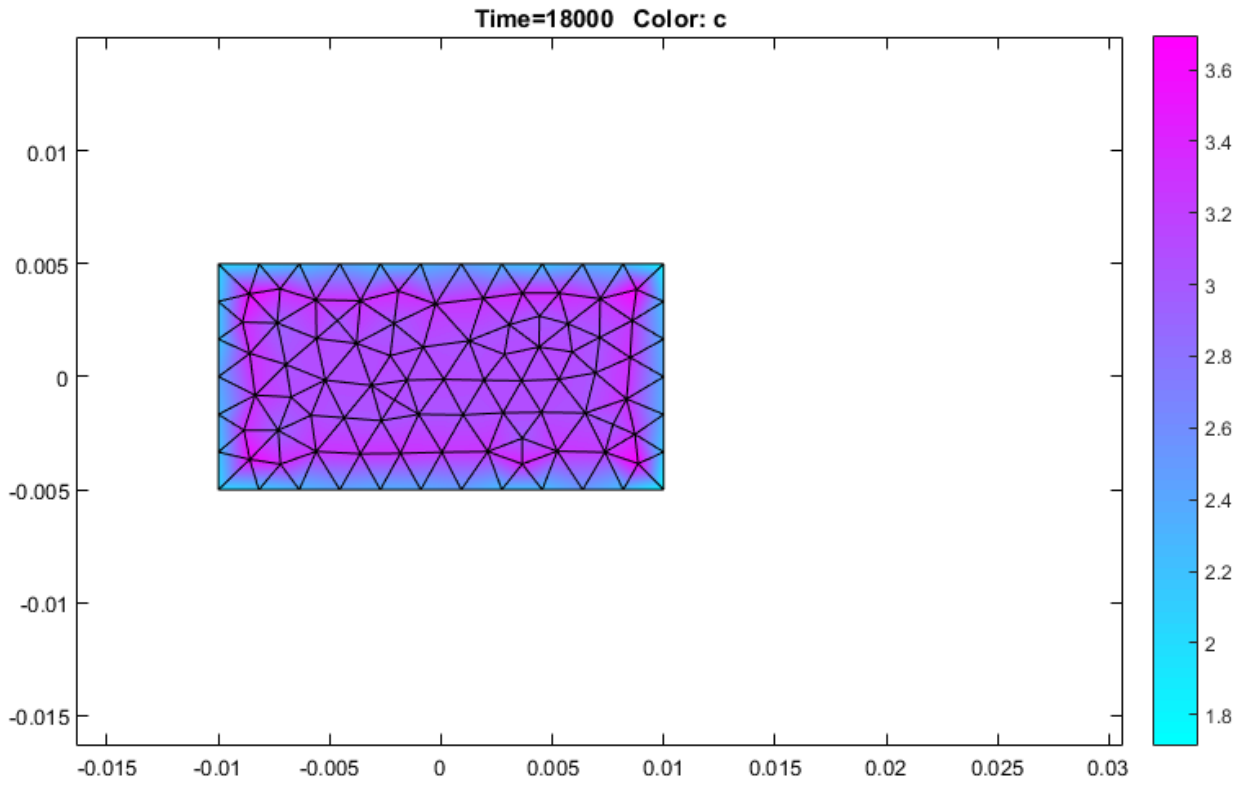


Figure 4.13. Solution showing the colour bar for 99-Finite Element model

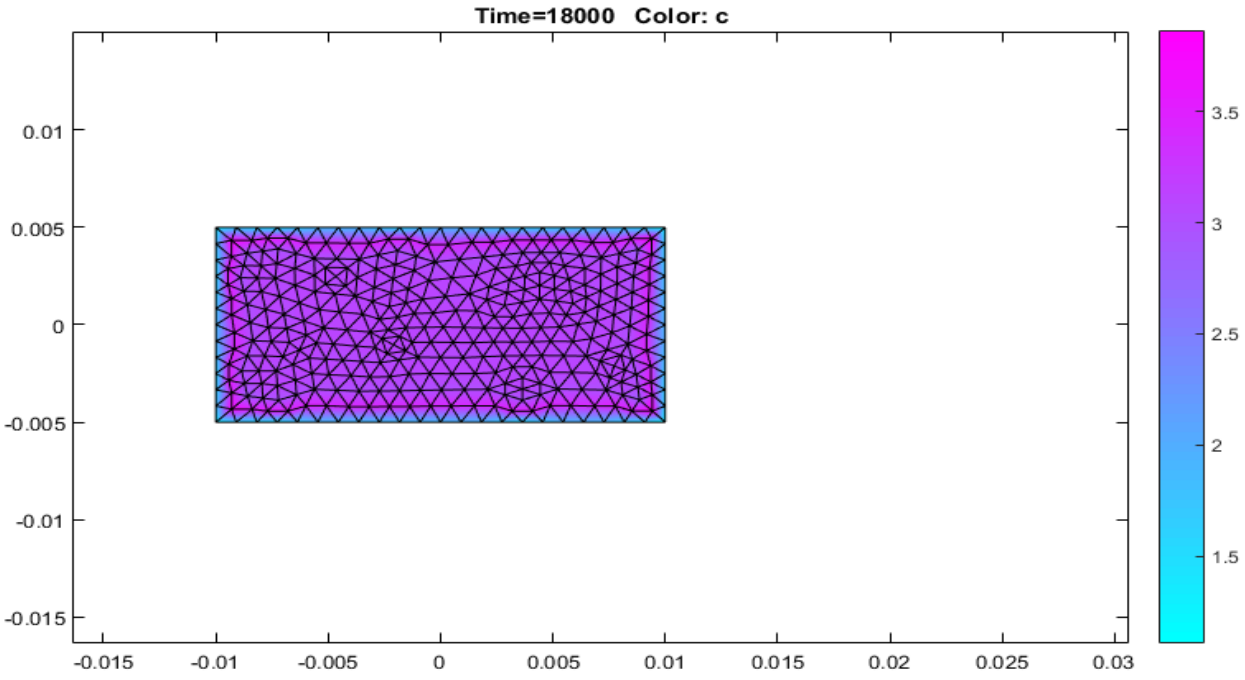


Figure 4.14. Solution showing the colour bar for 367-Finite Element model

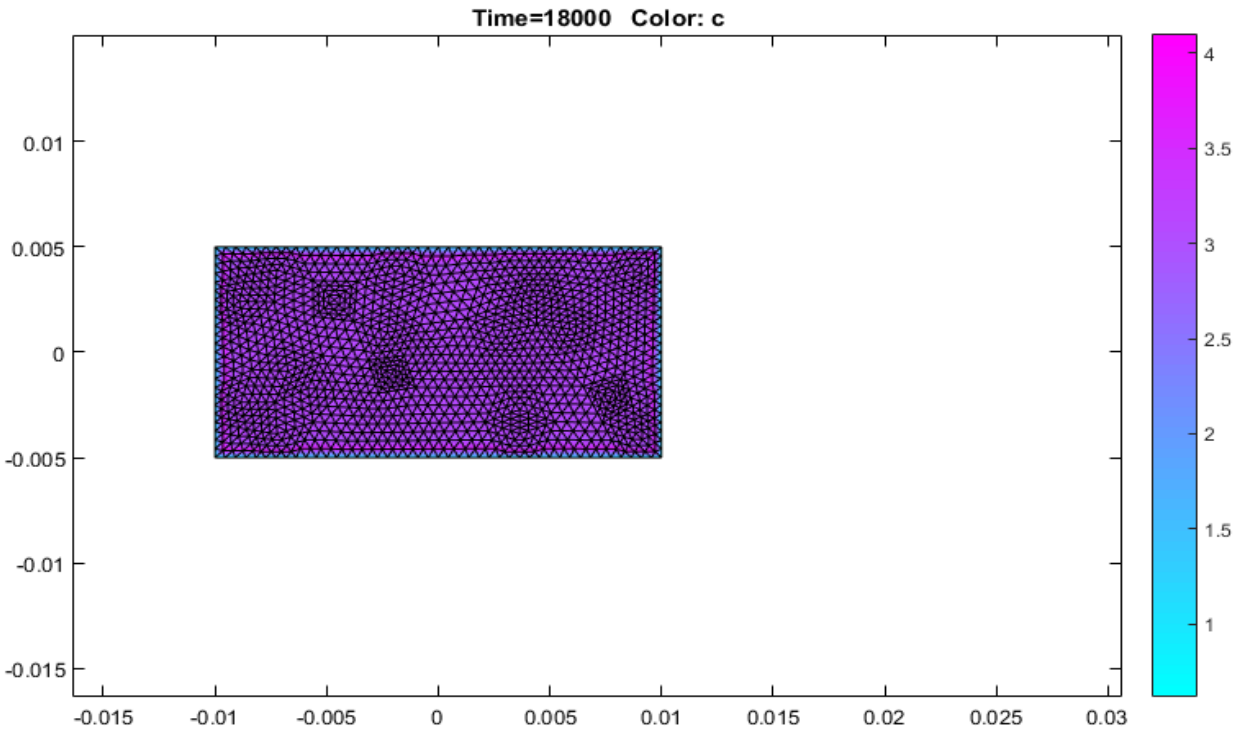


Figure 4.15. Solution showing the colour bar for 1395-Finite Element model

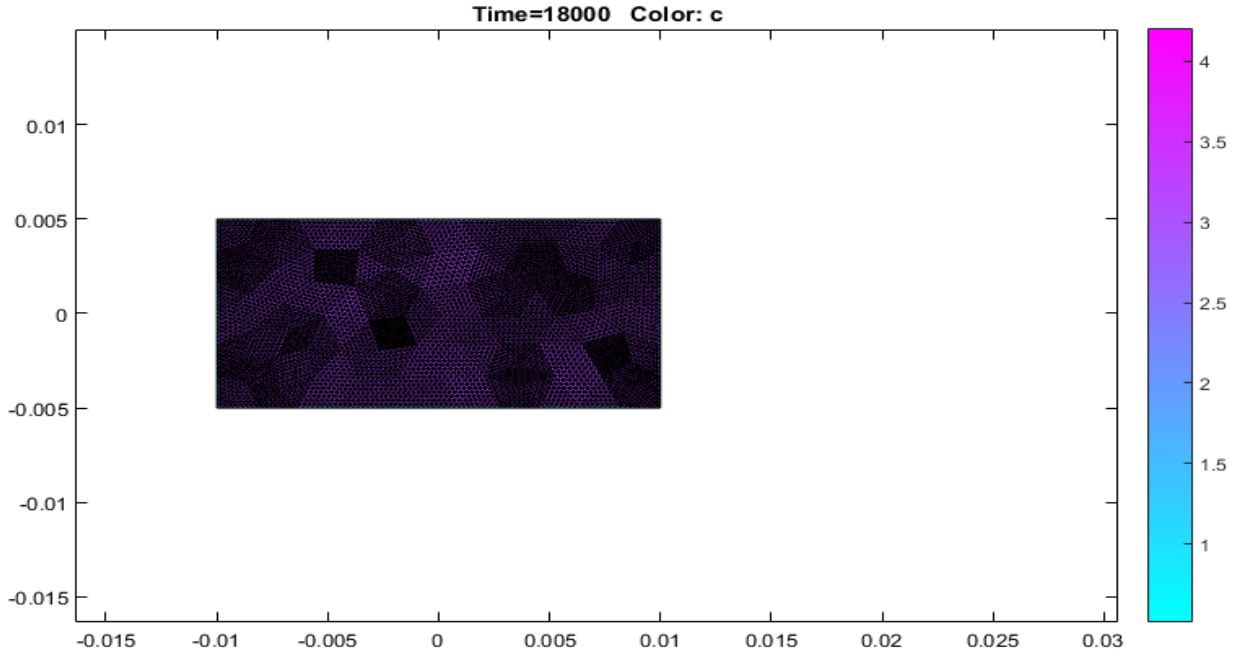


Figure 4.16. Solution showing the colour bar for 5447-Finite Element model

(a)

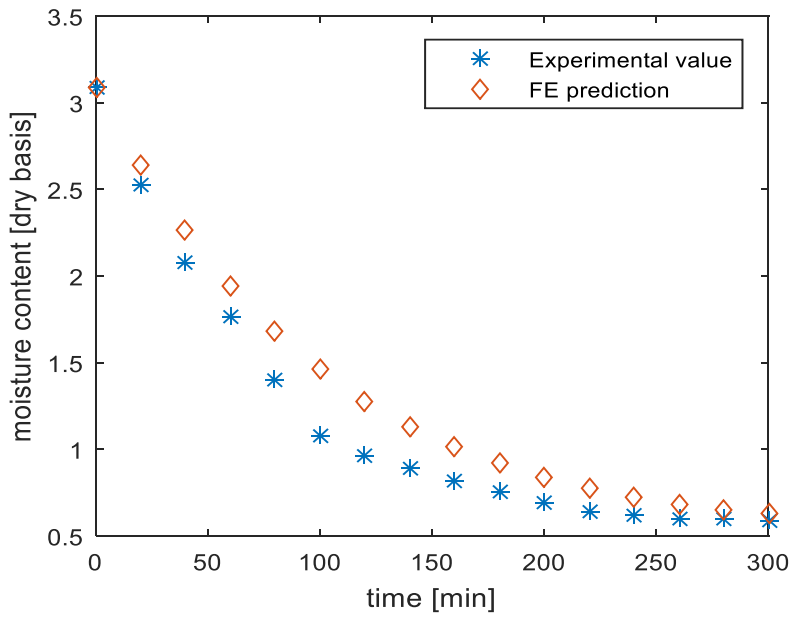


(b)

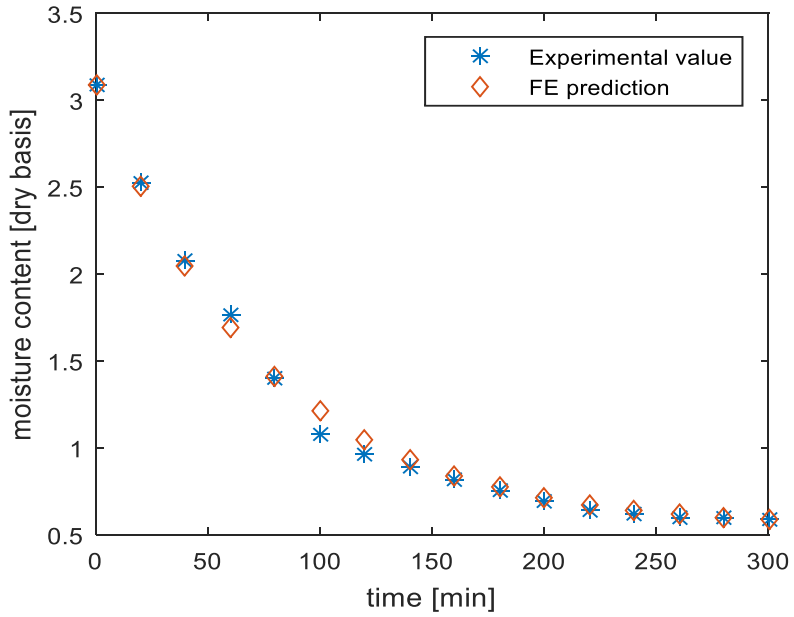


Figure 4.17.Measured moisture content and the FE predicted moisture content at heater temperature of 150ºC for the Rectangular cassava sample (a) results for a (b) results for a 5447-elements model

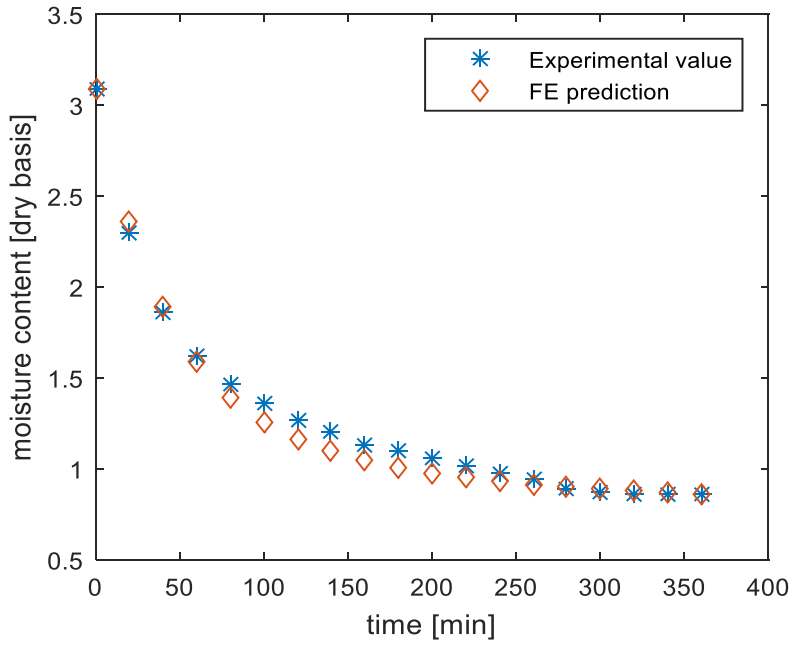


Figure 4.18.Measured moisture content and the FE predicted moisture content at heater temperature of 140ºC for the Rectangular cassava sample

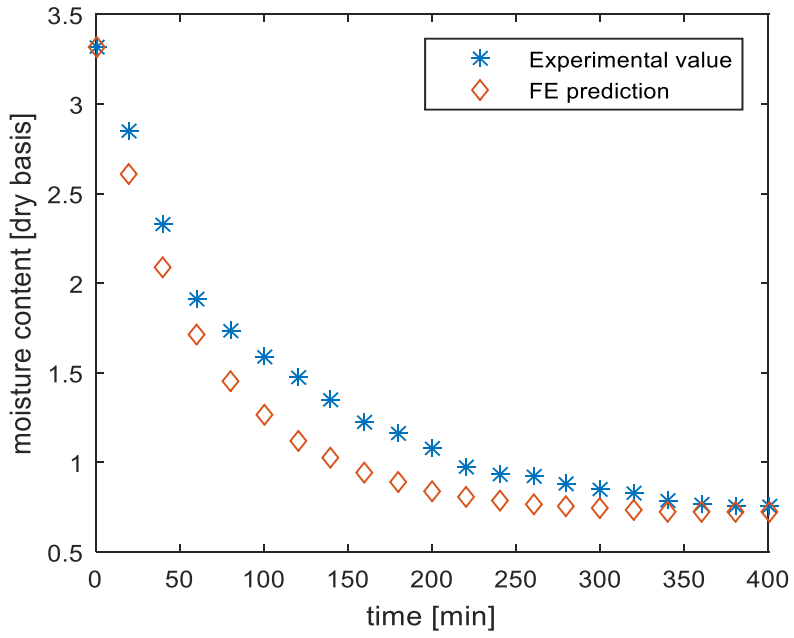


Figure 4.19.Measured moisture content and the FE predicted moisture content at heater temperature of 130ºC for the Rectangular cassava sample

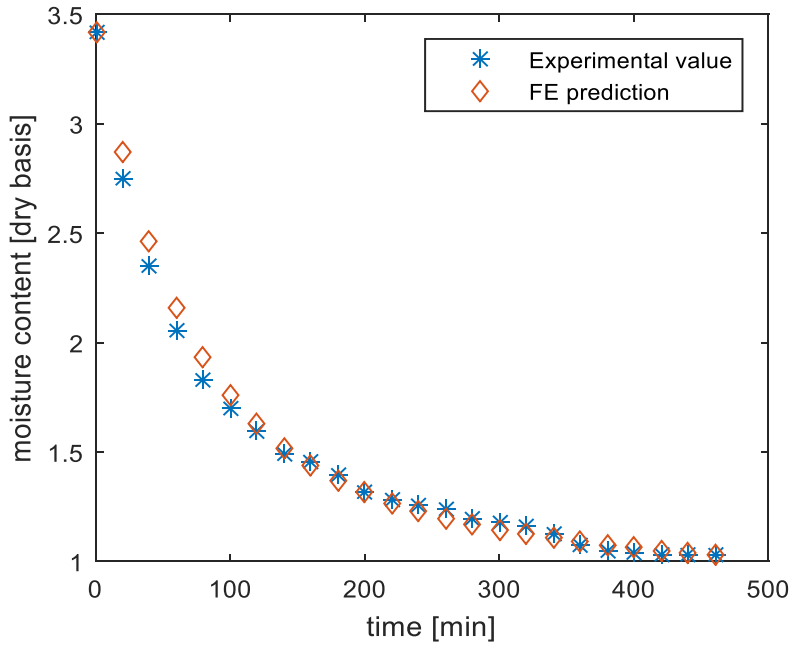


Figure 4.20.Measured moisture content and the FE predicted moisture content at heater temperature of 120$^{o}$C for the Rectangular cassava sample

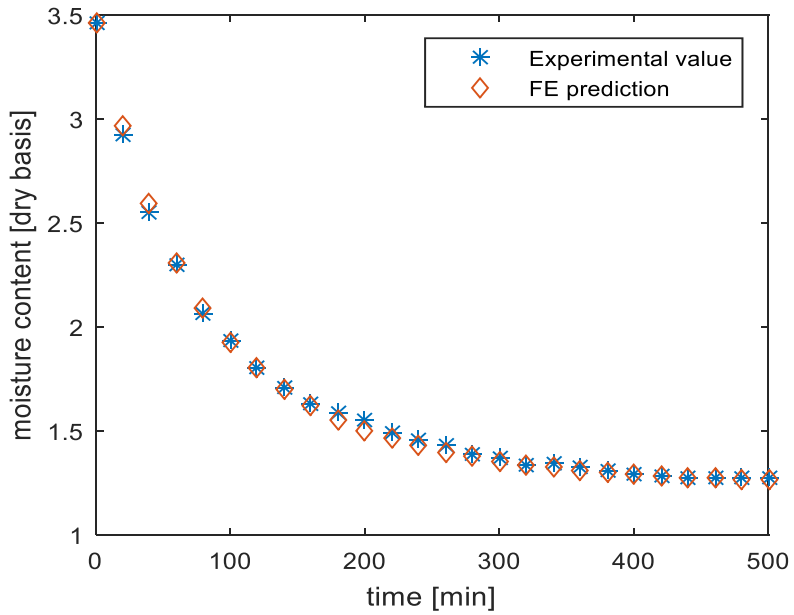


Figure 4.21.Measured moisture content and the FE predicted moisture content at heater temperature of 110$^{o}$C for the Rectangular cassava sample

Table 4.16. The statistical performance indices of the finite element prediction of cassava drying relative to the experimental measurements for the rectangular pellets

| Rectangular pellets | | | | |
|---|---|---|---|---|
| T [$^o$C] | $M_{eq}$<br>$M_0$ | $R^2$ | *RMSE* | *R* |
| 150 | 0.5400<br>3.0902 | 0.9340<br>0.9958 | **0.1924**<br>**0.0483** | 0.9912<br>0.9984 |
| 140 | 0.8380<br>3.0868 | 0.9877 | 0.0623 | 0.9963 |
| 130 | 0.7375<br>3.3151 | **0.9126** | 0.2077 | 0.9885 |
| 120 | 0.9410<br>3.4144 | 0.9924 | 0.0515 | 0.9978 |
| 110 | 1.2376<br>3.4577 | 0.9983 | 0.0224 | 0.9995 |

### 4.4.2. Circular Samples

For the circular samples drying at 150$^o$C, the corresponding equilibrium moisture content, effective diffusivity, convective mass transfer coefficient in Table 4.13 are inserted in the Equation (3.38). Since Equation (3.38) is a hybrid formulation of finite element and finite difference methods, the initial condition $M_0 = 3.8871$ is inserted from which the solution propagates. A very accurate moisture content kinetics is predicted as judged with $R^2 = 0.9870$, *RMSE*=0.0853 and $r$=0.9969. The graphical comparison of the predicted and measured kinetics are presented in Figure 4.22. At the other experimental temperatures, the predicted solutions agree with experimental solutions with a striking accuracy, especially for the experimental temperatures at 120 $^o$C and 110 $^o$C. The corresponding comparative graphical results

are presented in Figures 4.23 to 4.26. Figure 4.25 depicts the very accurate FE prediction, reflecting the very reliable indices $R^2 = 0.9954$, *RMSE*=0.0409 and $r$=0.9989, for the experimental drying at 120 $^{o}$C. Prediction accuracy improved with mesh refinement as seen in Figures 4.27 to 4.30. It is seen that in Figure 4.27 with 142 elements, the range of solution values as indicated in the colour map/bar is clearly outside the measured moisture values. A color bar provide a map of the different shades to the numerical values of the solution. When the number of elements increased to 539 elements as in Figure 4.28, the solution values indicated in the colour map showed improvement towards the experimental range for moisture content. Improvements continued with mesh refinement to 2095 element and 8255 elements as respectively seen in Figures 4.29 and 4.30 towards the experimental values. The parameters for the solutions and the goodness-of-fit parameters are summarized in Table 4.17.

These results show that the finite element method can predict cassava drying with a high degree of accuracy such that the costly case-by-case empirical approach, which is based on linear or non-linear regression analysis for parameter estimation, can be avoided.

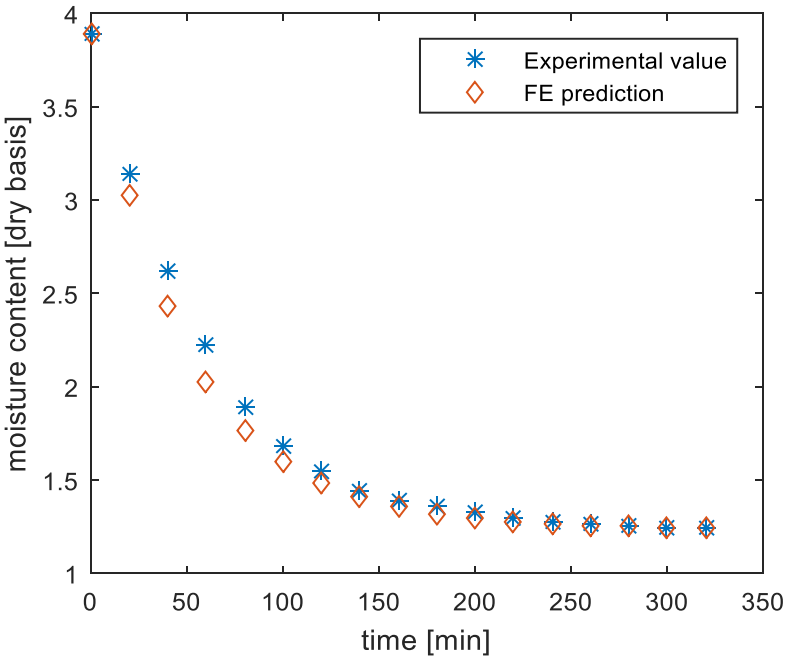


Figure 4.22. Measured moisture content and the FE predicted moisture content at heater temperature of 150ºC for the circular cassava sample

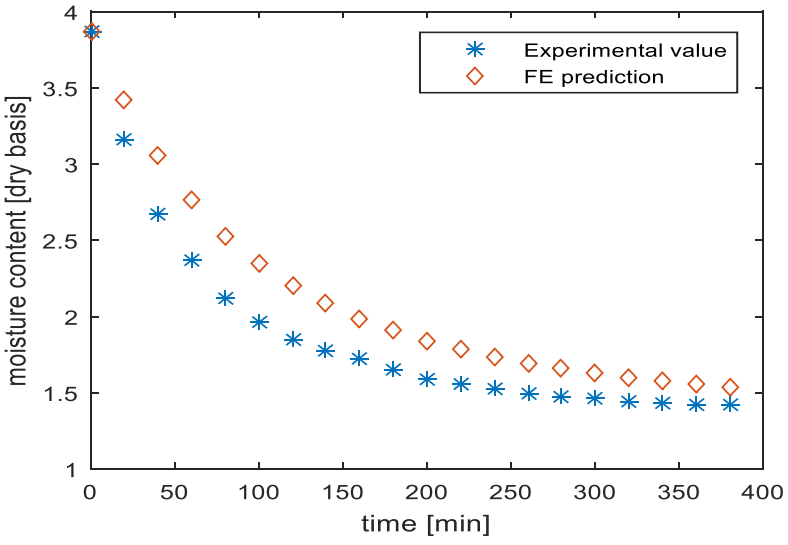


Figure 4.23.Measured moisture content and the FE predicted moisture content at heater temperature of 140ºC for the circular cassava sample

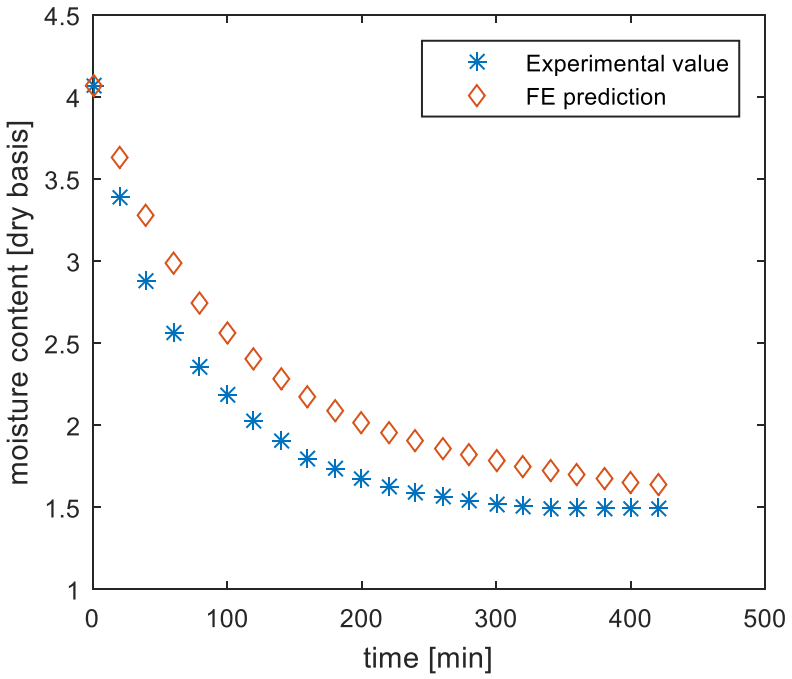


Figure 4.24.Measured moisture content and the FE predicted moisture content at heater temperature of 130ºC for the circular cassava sample

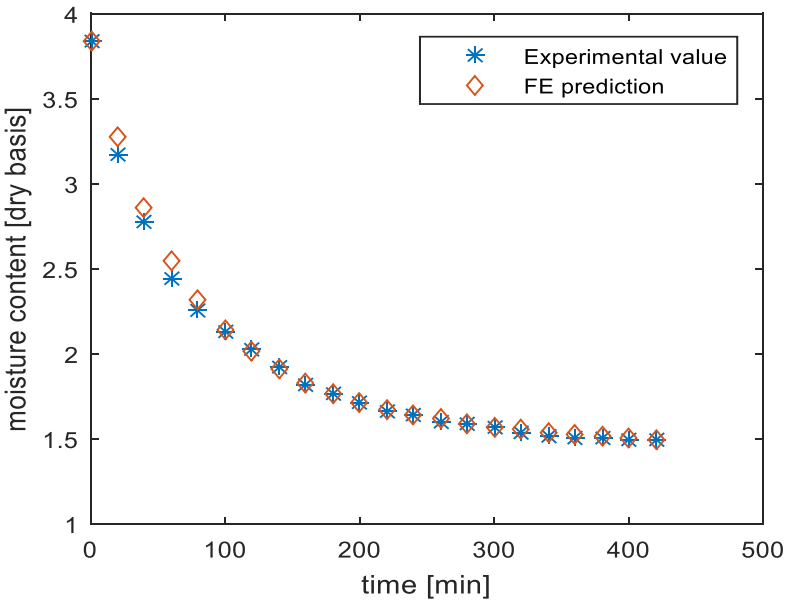


Figure 4.25.Measured moisture content and the FE predicted moisture content at heater temperature of 120ºC for the circular cassava sample

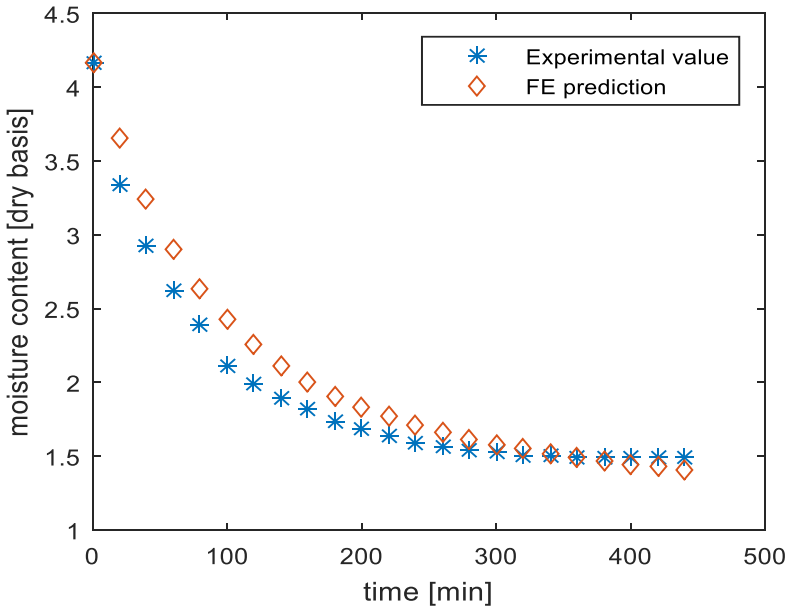


Figure 4.26. Measured moisture content and the FE predicted moisture content at heater temperature of 110ºC for the circular cassava sample

Table 4.17. The statistical performance indices of the finite element prediction of cassava drying relative to the experimental measurements for the circular pellets

| Circular Samples | | | | |
|---|---|---|---|---|
| T [ºC] | $M_{eq}$ $M_0$ | $R^2$ | *RMSE* | $r$ |
| 150 | 1.2402 3.8871 | 0.9870 | **0.0853** | 0.9969 |
| 140 | 1.3369 3.8703 | 0.8316 | 0.2634 | 0.9866 |
| 130 | 1.4377 4.0716 | 0.7976 | 0.3058 | 0.9889 |
| 120 | 1.4367 3.8412 | 0.9954 | 0.0409 | 0.9989 |
| 110 | 1.4359 4.1652 | 0.9341 | 0.1754 | 0.9882 |

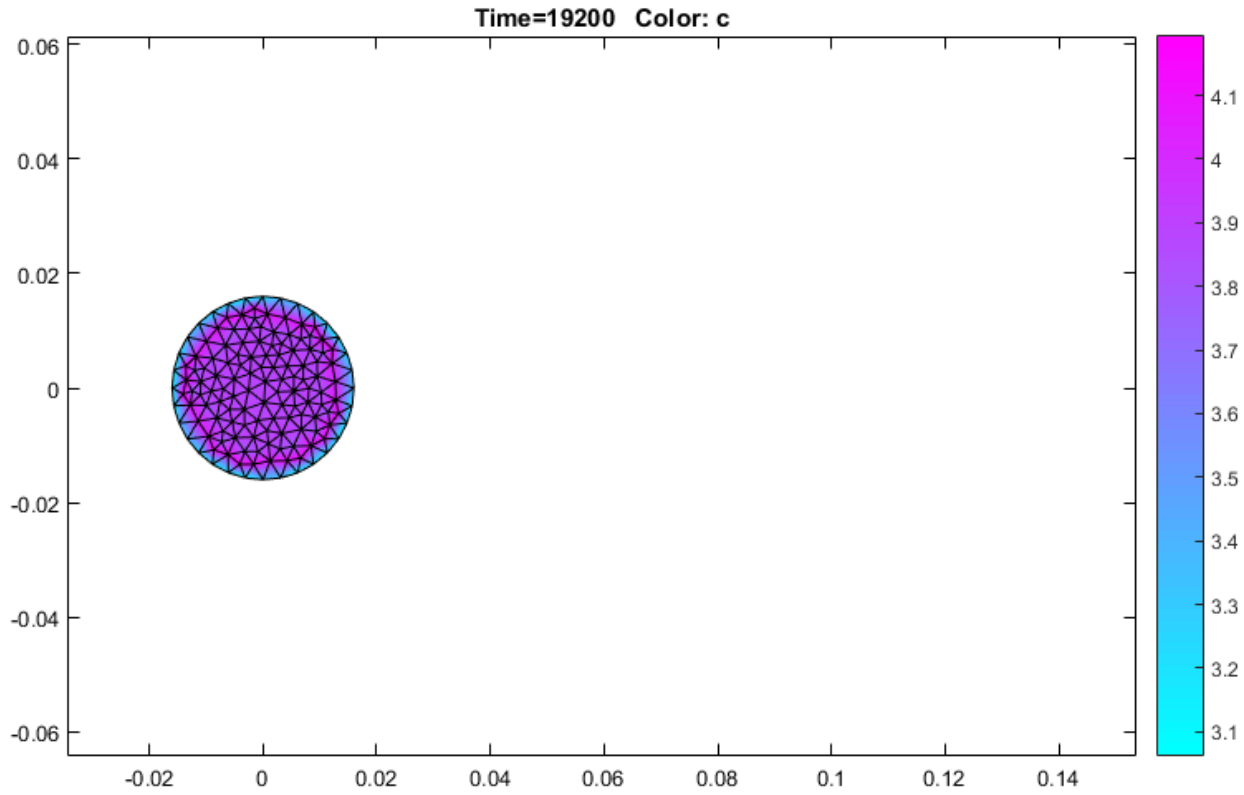


Figure 4.27. Solution showing the colour bar for 142-Finite Element model

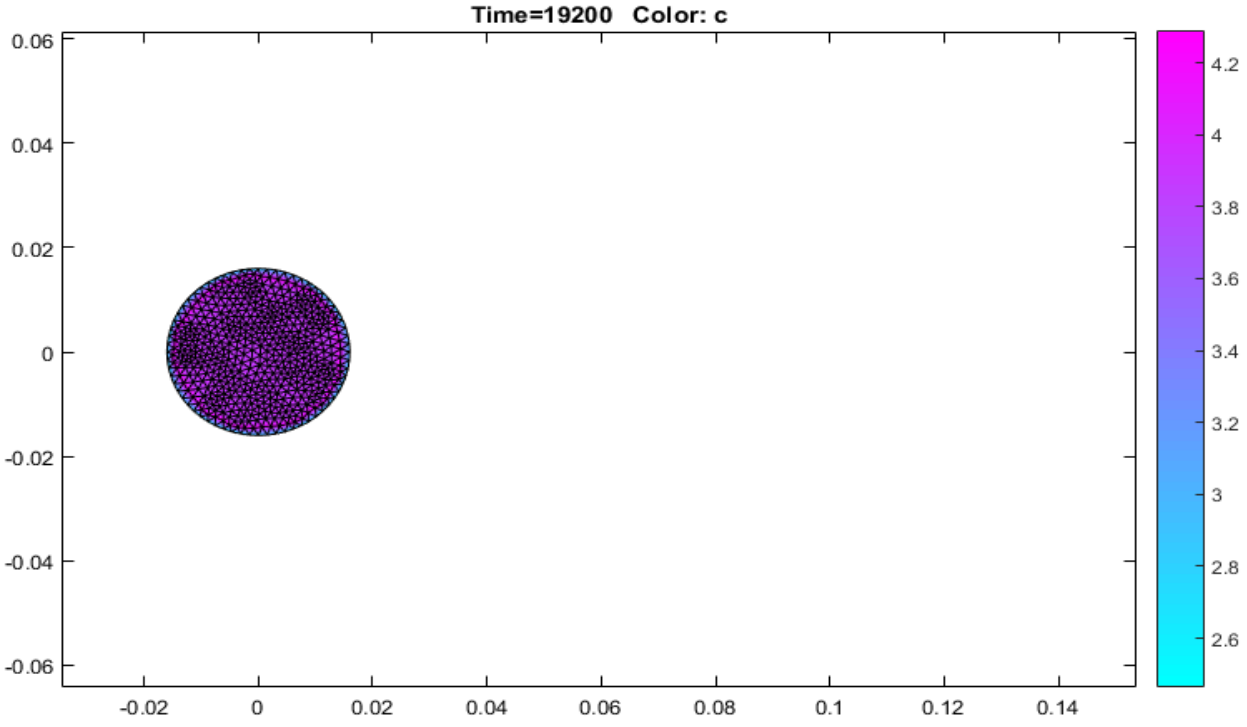


Figure 4.28. Solution showing the colour bar for 539-Finite Element model

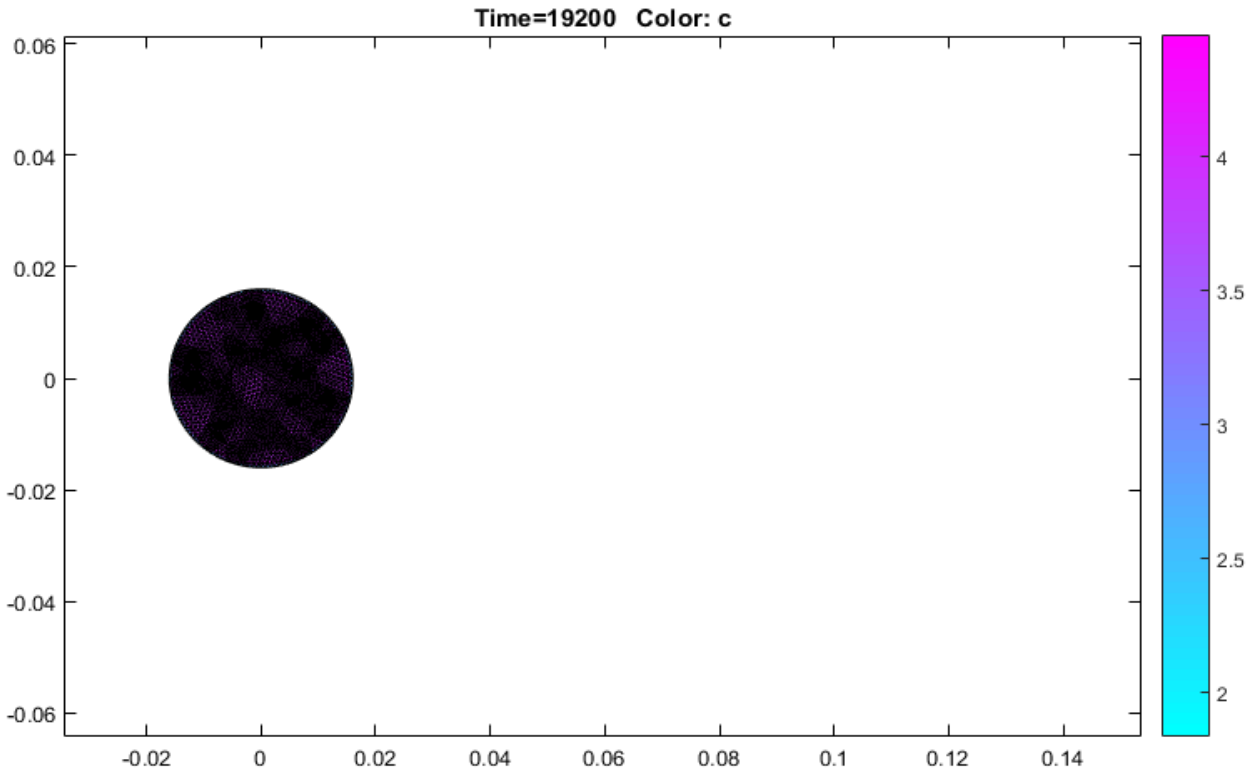


Figure 4.29. Solution showing the colour bar for 2095-Finite Element model

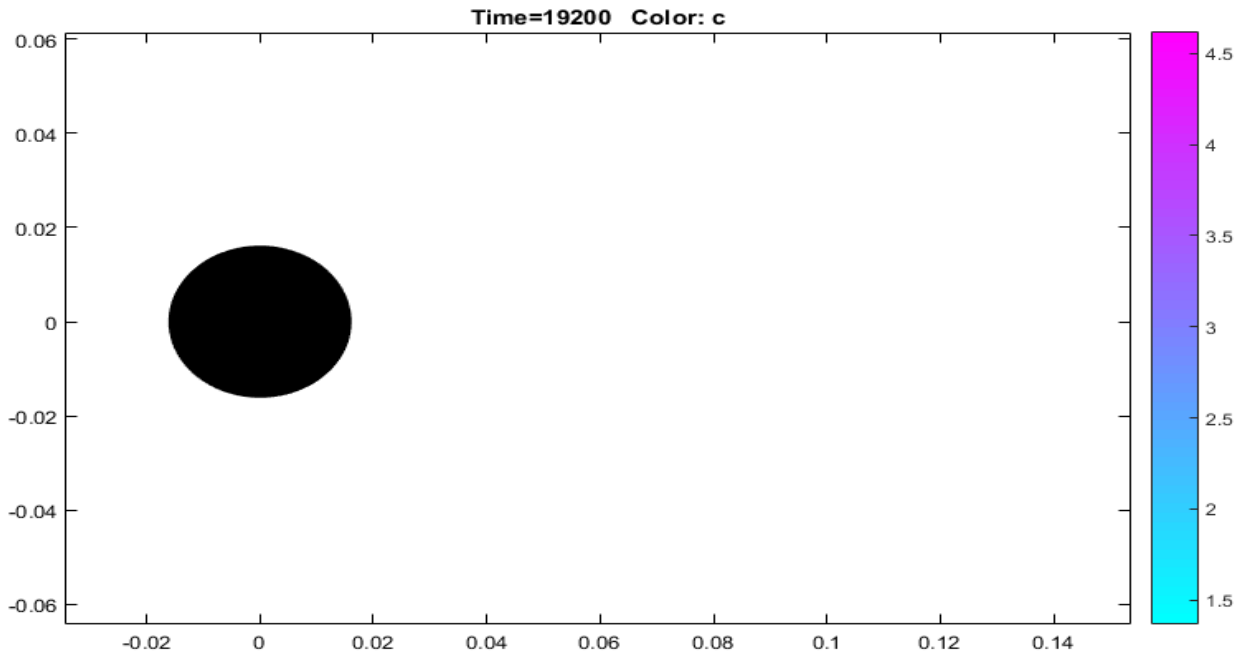


Figure 4.30. Solution showing the colour bar for 8255-Finite Element model

### 4.4.3 Standard Air Correlations.

Psychrometric chart could not be used in this work for predicting the conditions of standard air at various conditions. However, relevant correlations were employed as stated in section 3.3.7. Since the properties of air varies, the correlations for how these properties vary with temperature are generated. The table of properties of air in appendix iii was used in generating the relevant correlations.

Table 4.18: Table of Standard air correlations

| Temperature (K) | Density ρ (Kg/m$^3$) | Dynamic viscosity μ ($10^{-5}$ kg/ms) | kinematic viscosity v x$10^{-5}$ (m$^2$/s) | Thermal conductivity ($10^{-5}$ kW/mK) | Prandtl's Number Pr | Specific Heat Cp (kJ/kg.K) | Specific Heat Cv (kJ/kg.K) |
|---|---|---|---|---|---|---|---|
| 354 | 0.9982 | 2.092 | 2.098 | 3.033 | 0.696 | 1.0086 | 0.7215 |
| 351 | 1.0063 | 2.079 | 2.067 | 3.011 | 0.697 | 1.0083 | 0.7212 |
| 348 | 1.0152 | 2.066 | 2.036 | 2.988 | 0.698 | 1.0081 | 0.721 |
| 343 | 1.0306 | 2.044 | 1.986 | 2.951 | 0.698 | 1.0077 | 0.7206 |
| 338 | 1.0459 | 2.021 | 1.939 | 2.913 | 0.699 | 1.0073 | 0.7202 |

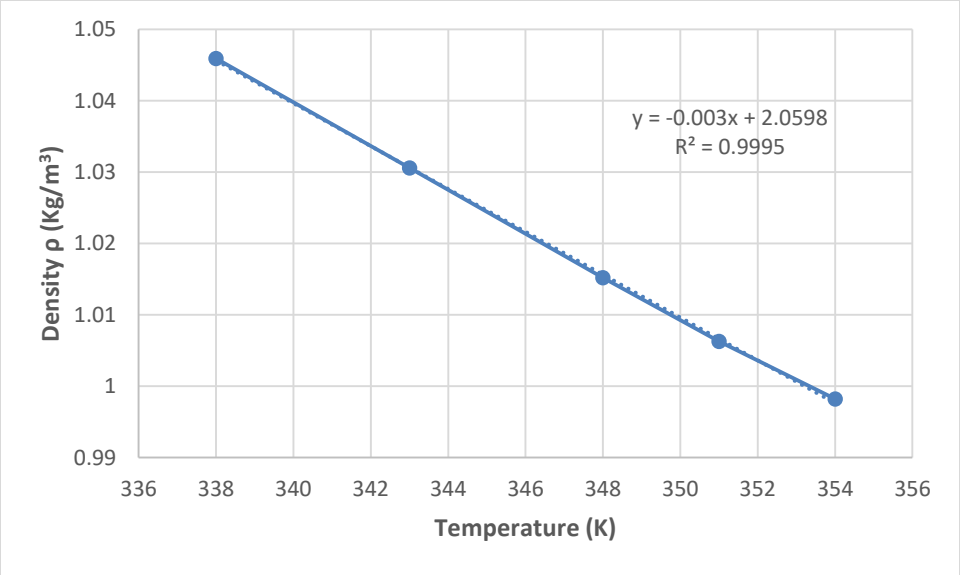


Fig. 4.31: Variation of air density with temperature

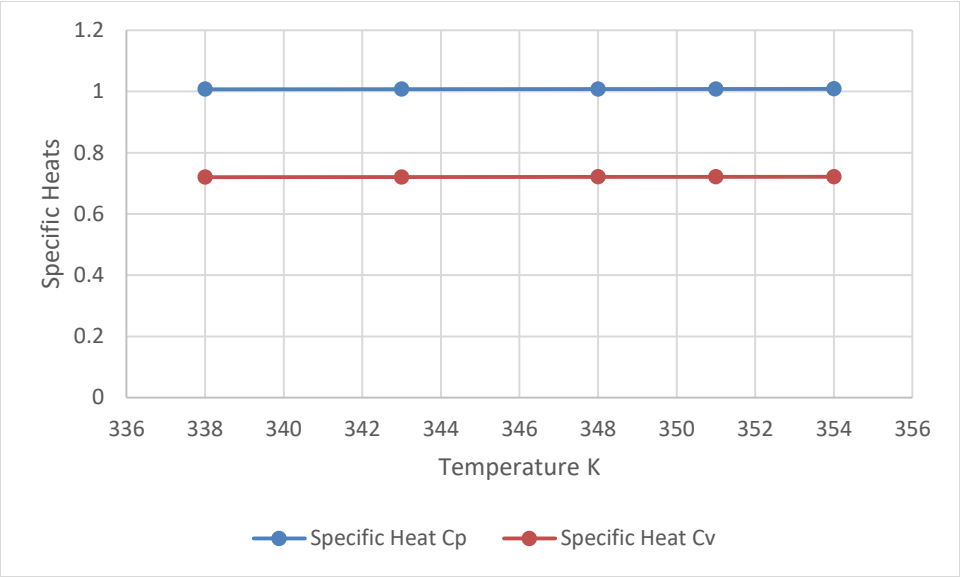


Fig. 4.32: Variation of air specific heats with temperature

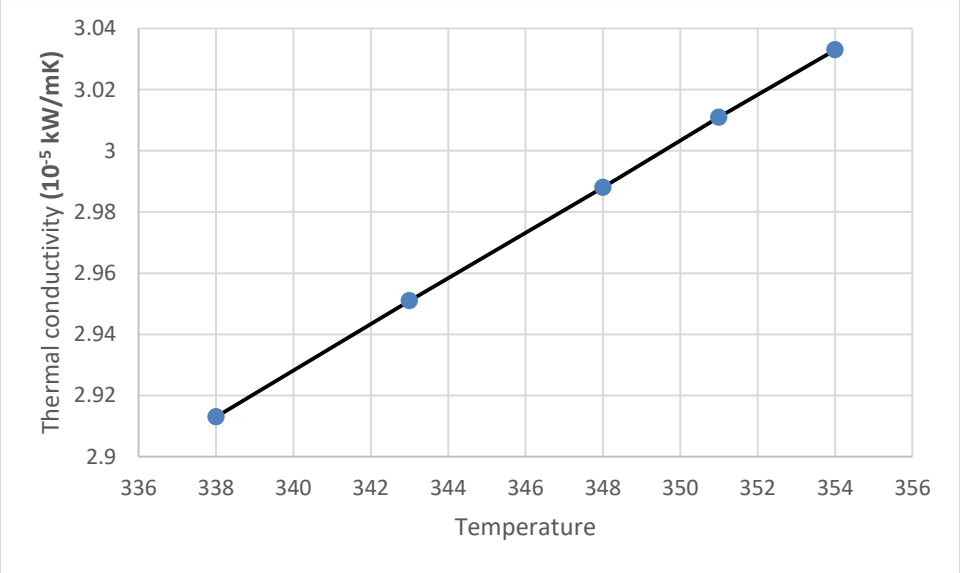


Fig. 4.33: Variation of air thermal conductivity with temperature

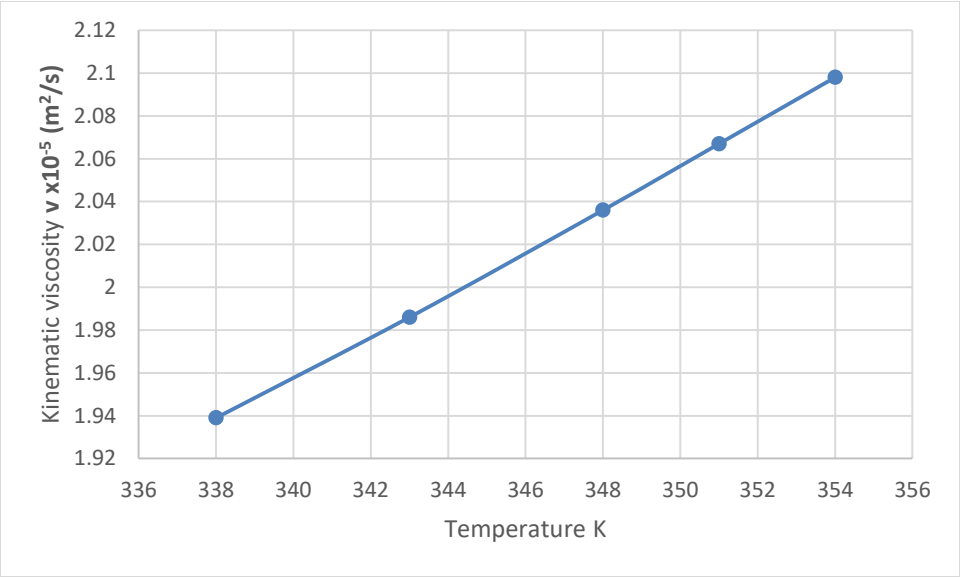


Fig. 4.34: Variation of air kinematic viscosity with temperature

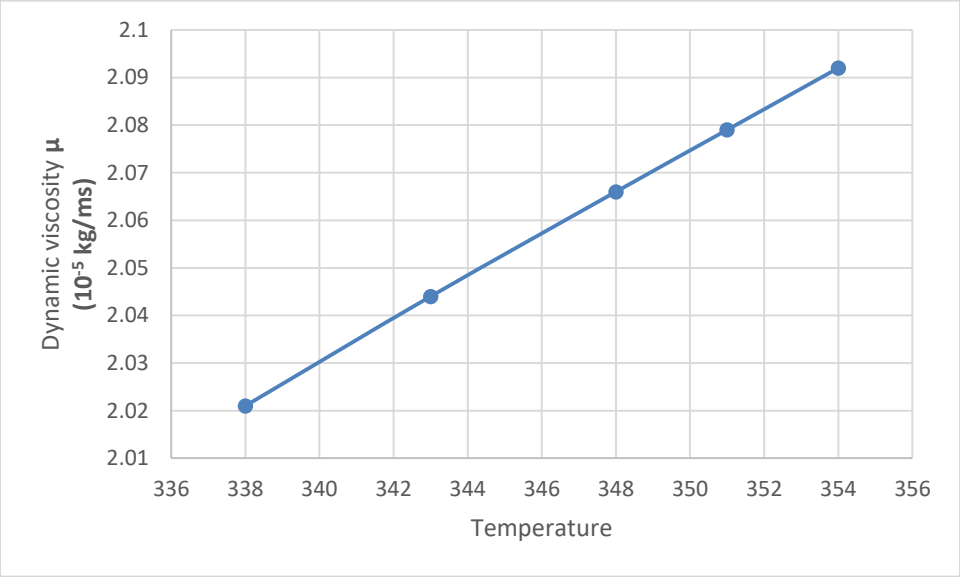


Fig. 4.35: Variation of air dynamic viscosity with temperature

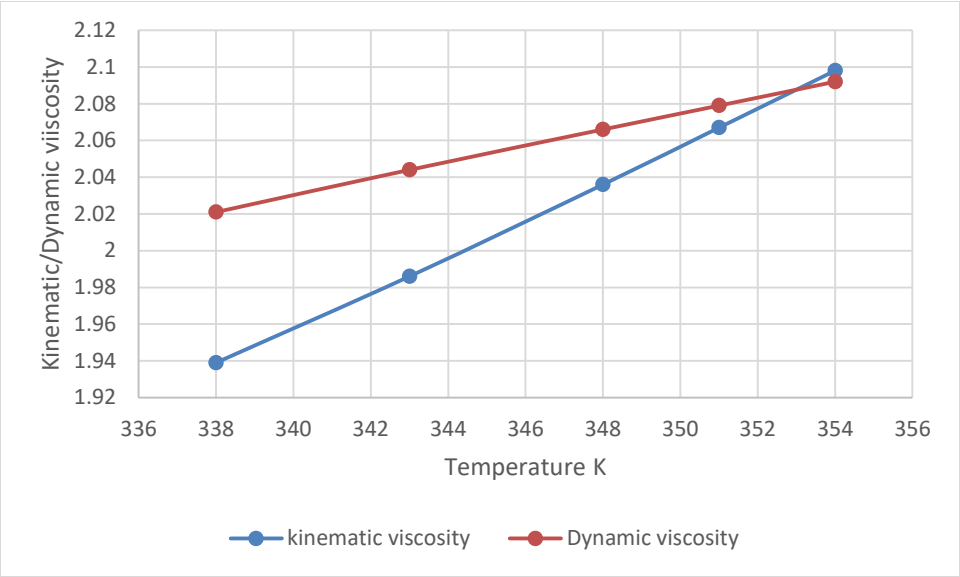


Fig. 4.36: Variation of air kinematic and dynamic viscosity with temperature

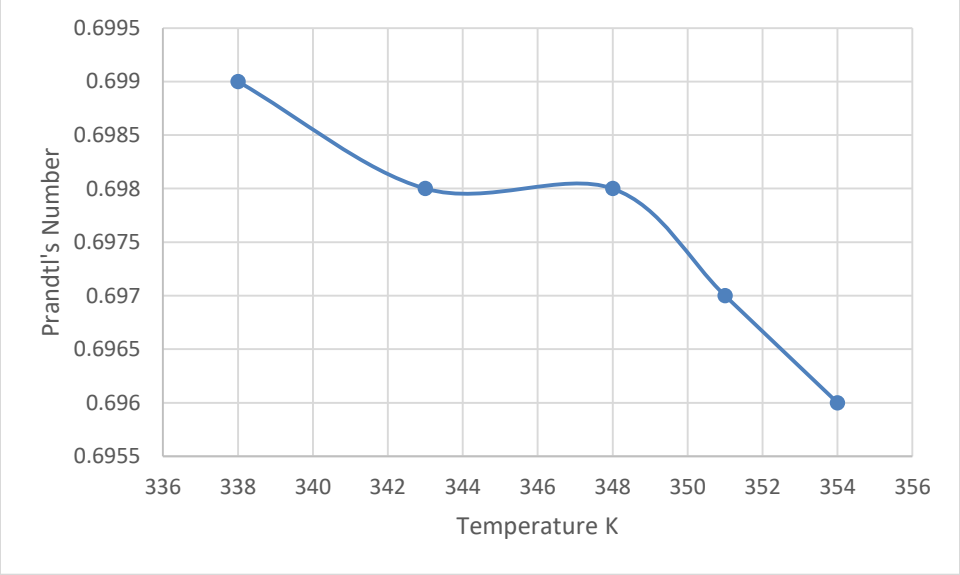


Fig. 4.37: Variation of air prandtl's number with temperature

### 4.4.4 Tabulated and graphical results of dimensionless properties

Table 4.17a & b shows the values of the dimensionless properties calculated from equations 3.40, 3.41 and 3.42. The parameters for calculating each property were obtained from the table of air properties (Appendix III) via linear interpolation (equation 3.43). Figure 4.38a & b displays the trends of Schimidt number in the direction of increasing temperature. This trend clearly explains that dynamic viscosity, density and effective diffusivity dictates the Sc values at any given drying temperature, and its best described using a 4th order polynomial equation $Sc = -5E+40T^4 + 2E+32T^3 - 4E+23T^2 + 3E+14T - 81222$ with $R^2 = 1$. Figure 4.39a & b indicates that Reynolds value decreases with increase in effective diffusivity which is a function both drying temperature and time. The Re values decreases with increase in temperature as a result of the increase in dynamic viscosity. The trend of figure 4.40 a & b also depicts that Sherwood number which is a function of hm and hydraulic diameter of the dryer decreases with increase in Deff. $Sh = 0.023\, Re^{0.83} Sc^{0.44}$ validates the trend of the graph. Figure 4.41a & b shows that hm which is dependent on Sherwood number and hydraulic diameter increases as Deff increases with respect to drying time. The values of hm obtained are within the range predicted using finite element analysis. A 3rd order polynomial equation $hm = -1E-20T^3+6E-12T^2-0.0008T+40242$ with $R^2 = 0.9999$ best describes the fit.

Table 4.19a: Table of dimensionless properties for rectangular pellets

| S/N | Teperature (K) | Deff x10 $^9$ | Schimidt Number (Sc) x10$^{-9}$ | Reynolds Number (Re) | Sheerwood Number (Sh) | hm |
|---|---|---|---|---|---|---|
| 1 | 354 | 2.3304 | 8.9932 x10$^{-10}$ | 78252.77 | 0.0277 | 1.5744 X10$^8$ |
| 2 | 351 | 2.1277 | 9.7099 x10$^{-10}$ | 79880.54 | 0.0292 | 1.5153 X10$^8$ |
| 3 | 348 | 2.0004 | 1.0173 x10$^{-9}$ | 80597.03 | 0.3001 | 1.4642 X10$^9$ |
| 4 | 343 | 1.1498 | 1.7249 x10$^{-9}$ | 82690.02 | 0.3867 | 1.0845 X10$^9$ |
| 5 | 338 | 1.4260 | 1.3551 x10$^{-9}$ | 84872.64 | 0.3554 | 1.2361 X10$^9$ |

Table 4.19b: Table of dimensionless properties for Circular pellets

| S/N | Teperature (K) | Deff x10 $^{9}$ | Schimidt Number (Sc) | Reynolds Number (Re) | Sheerwood Number (Sh) | hm |
|---|---|---|---|---|---|---|
| 1 | 354 | 3.1467 | 6.6602 x$10^{-10}$ | 78252.77 | 0.0243 | 1.8649 X$10^{8}$ |
| 2 | 351 | 1.4830 | 1.3931 x$10^{-9}$ | 79880.54 | 0.0342 | 1.2370 X$10^{8}$ |
| 3 | 348 | 1.6770 | 1.2135 x$10^{-9}$ | 80597.03 | 0.0324 | 1.3252 X$10^{8}$ |
| 4 | 343 | 1.4759 | 1.3438 x$10^{-9}$ | 82690.02 | 0.0347 | 1.2491 X$10^{8}$ |
| 5 | 338 | 1.5665 | 1.2335 x$10^{-9}$ | 84872.64 | 0.0341 | 1.3029 X$10^{8}$ |

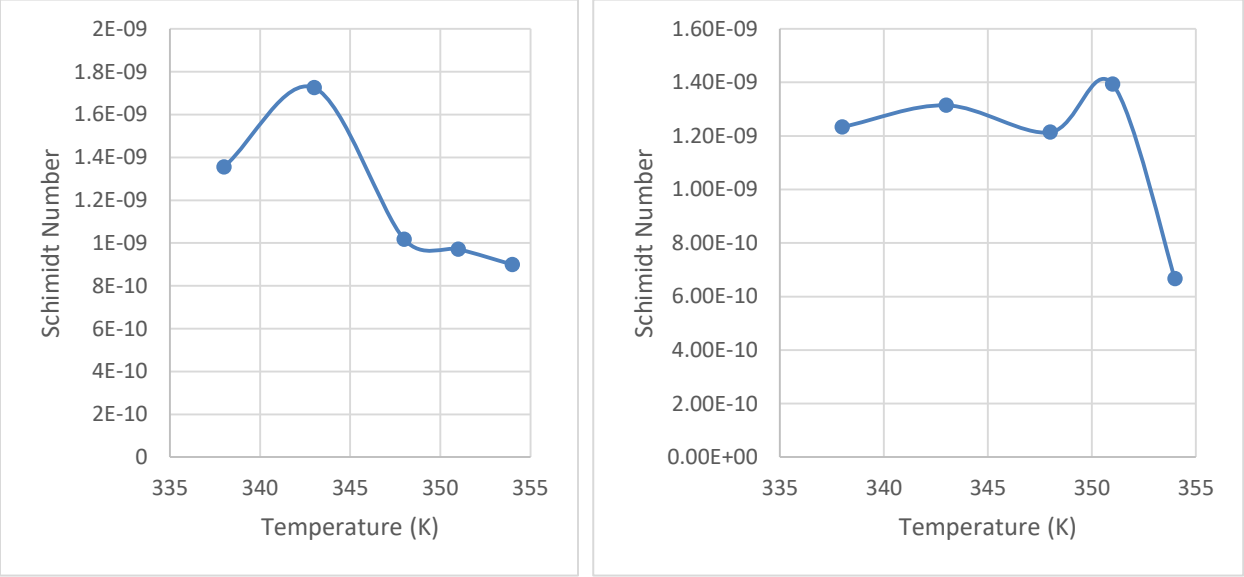


Figure 4.38: Graph of Schimidt against temperature for rectangular & circular pellets.

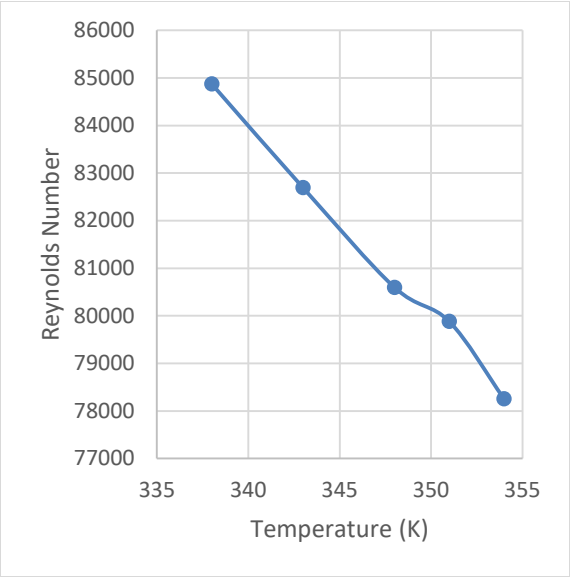


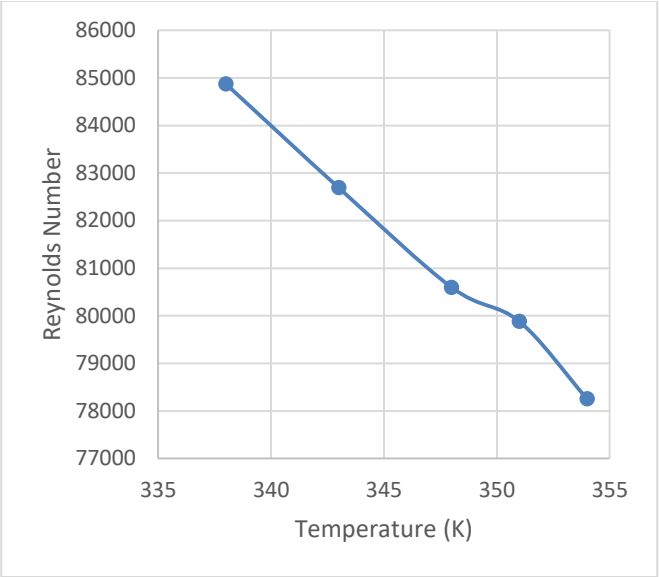


Figure 4.39: Graph of Reynolds number against temperature for rectangular & circular pellets

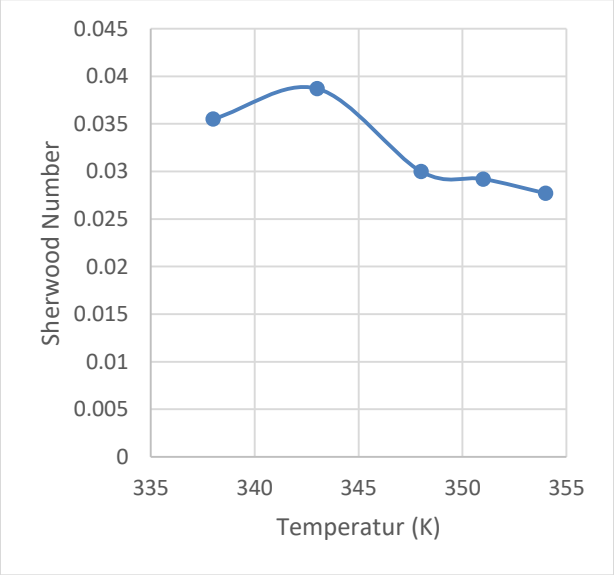


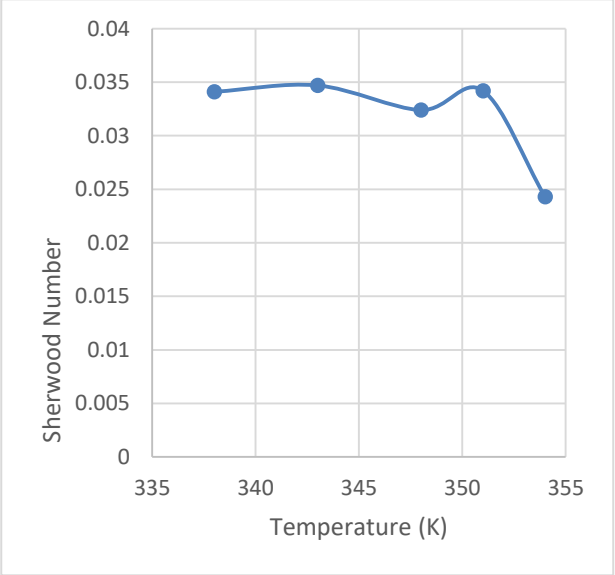


Figure 4.40: Graph of Sherwood against temperature for rectangular & circular pellets

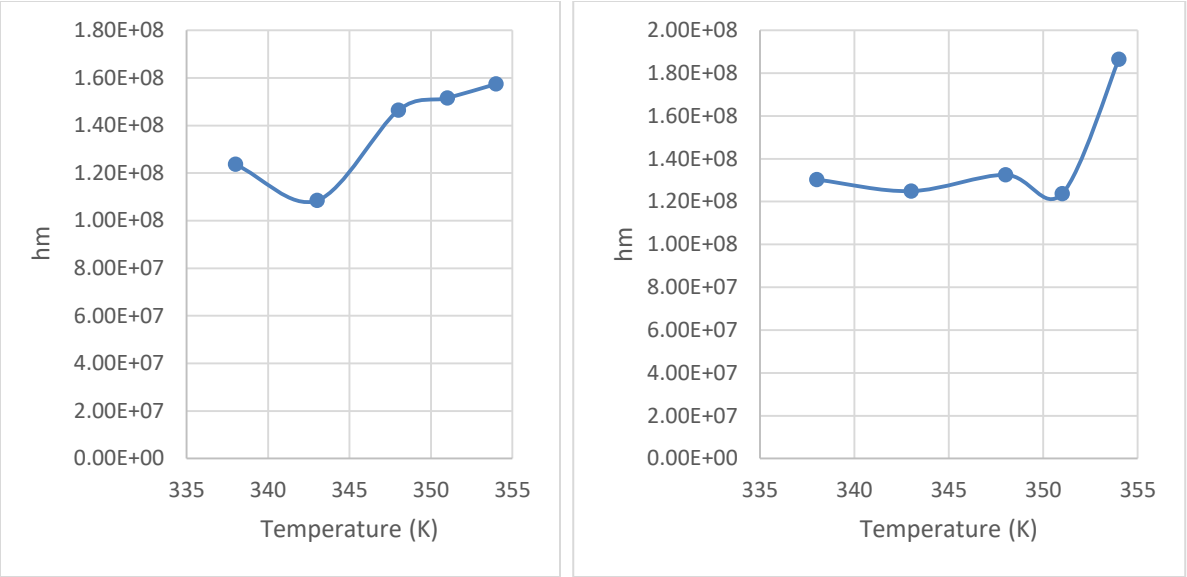


Figure 4.41: Graph of hm against temperature for rectangular & circular pellets

# CHAPTER FIVE

## 5.0 Conclusion and Recommendations

## 5.1 Conclusion

In this study, convective drying of Cassava Pellets was investigated experimentally and numerically. A two-dimensional finite element model was developed for the sample drying and programmed in MATLAB version 7.7.0 (R2008b) to simulate the process and predict the drying curves. Drying rate, moisture diffusivity and mass transfer coefficient of the samples were found to increase with the increment in drying air temperature. No constant rate period was seen and the entire drying process of the cassava occurred in the falling rate period at the applied air temperatures. The diffusivity of the samples were determined to be in range of $2.3304\times10^{9}$ - $1.4260\times10^{9}$ $m^2s^{-1}$ for rectangular pellets and $3.1469\times10^{9}$ - $1.5665\times10^{9}$ $m^2s^{-1}$for the circular pellets and both were perfectly described using a 3rd order polynomial as a function of air temperature. For each drying temperature, mass transfer coefficient of the samples were determined experimentally and found to be functions of the process time and moisture removal, respectively.

From the calculated $D_{eff}$ given in Table 4.1. , it was observed that an increment in drying temperature increased the effective diffusivity value. Thus, an increase in temperature causes a decrement in water viscosity and increases the activity of water molecules. These phenomena facilitate diffusion of water molecules in object capillaries and consequently, increase the moisture diffusivity. The results showed that the moisture diffusivity of cassava pellets can be expressed as a function of temperature using a 3rd order polynomial equation.

From the 5447-element model of the rectangular pellets, the comparison between FE predictions at the experimental intervals and the measured values gave a

corresponding statistical goodness of fit values. For the circular pellets, when the number of elements increased to 539 elements, the solution values indicated in the colour map showed improvement towards the experimental range for moisture content. Improvements continued with mesh refinement to 2095 element and 8255 elements respectively. The parameters for the solutions and the goodness-of-fit parameters showed that all the $R^2$ values for the rectangular and circular pellets are above 90%, where majority were up to 99% indicating high accuracy of FE prediction of cassava drying.

These results show that the finite element method can predict cassava drying kinetics with a high degree of accuracy such that the costly case-by-case empirical approach, which is based on linear or non-linear regression analysis for parameter estimation, can be avoided. The study could provide theoretical bases of the equipment design and process optimization for hot air drying of Cassava pellets.

## 5.2 Contribution to Knowledge

This research work made the following contribution to knowledge

- Developed a 2-dimensional model of coupled heat and mass transfer for the convective drying of rectangular and cylindrical cassava pellets.
- Provided a numerical algorithm for solving the thermophisical properties of cassava pellets using the model developed.
- Developed linear and seconder order polynomial models for the logarithmic constants and coefficients to account for the effect of drying air temperature.
- Generated data of standard air correlations which could aid in dryer design for optimal drying of cassava pellets.

## 5.3 Recommendations

This study showed that Fick's second law describes satisfactorily the drying process performed through the model validation with the drying kinetics and the temperature of the cassava pellets. By this, it is important to study this process after other mechanisms for the transport of water during drying, such as pressure driven and capillary flow during drying, transport mechanisms of drying of porous media, and evaporation condensation theory.

It would also research worthy to develop a fully 3-dimensional model for drying, modelled as three dimensional shapes. This is because a 3-dimensional model could be used to model the movement of water more accurately and it will be possible to calculate the contact area and the shrinkage volume of drying samples.

Research should be done on modeling and simulation of hot air dryer in order to obtain reliable data on the structural and mechanical behavior of dryer, detect possible damages when used at very high temperatures, maximize the drying process and optimize designs of parts. Also, modeling and simulation of the interaction between the dryer and the pellets in order to predict behavior of materials been dried during drying, storage and other processes is also of great importance to control post-harvest losses.

## References


Ademosun O.C., Jimoh M.O., Olukunle O.J. (2012). Effect of physical and mechanical properties of cassava tubers on the performance of an automated peeling machine. International Journal of Development and Sustainability. Volume 1 Number 3: Pages 810-822. ID: IJDS12080704.

Aghbashlo, M., et al., (2008). Energy and Exergy Analyses of Thin-Layer Drying of Potato Slices in a Semi-Industrial Continuous Band Dryer, Drying Technology, 26), 12, 4, pp. 1501-1508. https://doi.org/10.1080/07373930802412231.

Aguilera, J. M.; Stanley, D. W. (1990). Microstructural Principles of Food Processing and Engineering. London: Elsevier Science Publishers LTD. 1990

Akgun, N. A.; Doymaz, I. (2005). Modelling of Olive Cake Thin-Layer Drying Process. Journal of Food Engineering 68 (4), 5: 455-461.

Ahrne, L.; Prothon, F.; Funebo, T. (2003). Comparison of Drying Kinetics and Texture Effects of Two Calcium Pre-treatments before Microwave-Assisted Dehydration of Apple and Potato. International Journal of Food Science and Technology, Volume 38:411-420

Akinpelu, A.O. Amamgbo L.E.F, Olojede A.O, Oyekale A.S. (2011). Health Implications of Cassava Production and Consumption. Journal of Agriculture and Social Research (JASR) Vol. 11, No. 1.

Akpinar E. K., Bicer Y. and Midilli A. (2003). Modeling and experimental study on drying of apple slices in a convective cyclone dryer, Journal of Food Process Engineering, 26 (6) (2003) 515-541.

Akpinar E. K. (2005). Energy and exergy analyses of drying of eggplant slices in a cyclone type dryer. KSME International Journal (Journal of Mechanical Science and Technology), 19 (2005) 692-703.

Akgun, N. A.; Doymaz, I. (2005). Modelling of Olive Cake Thin-Layer Drying Process. Journal of Food Engineering 68 (4): 455-461

Armenica L. Lebensmittel-Wissenschaftund-Technologie (Food Science and Technology) 40 (5). 2007: 753-758

Amer B.M.A, Hossain M.A, Gottschalk K (2010). Design and performance evaluation of a new hybrid solar dryer for banana. Energy Conversion and Management. Vol 51,813–820.

Arabhosseini, A.; Huisman, W; Van-Boxtel, A.; Muller, J. (2007). Long-Term Effects of Drying Conditions on the Essential Oil and Color of Tarragon Leaves during Storage. Journal of Food Engineering 79 (2): 561-566.

Al-Duri, B.; Mcintyre, S. (1992). Comparison of Drying Kinetics of Foods Using a Fan- Assisted Convection Oven, a Microwave Oven and a Combined Microwave/Convection Oven. Journal of Food Engineering 15 (2): 139-155

Al-Juamily K.E.J, Khalifa A.J.N, Yassen T.A (2007). Testing of the performance of a fruit and vegetable solar drying system in Iraq. 209 (1–3):163–70.

Alzamora, S. M.; Chirife, J.; Voillaz, P. (1979). A Simplified Model for Predicting the Temperatures of Foods during Air Dehydration. Journal of Food Technology 14.1979: 369-380

Andrieu, J.; Stamatopoulos, A. (1986). Durum Wheat Pasta Drying Kinetics. Lebensmittel-Wissenschaft und-Technologie 19: 448-456

Ashrae (1974). ASHARE handbook and product dictionary Application. New York, USA: American Society of Heating, Refrigerating and Air-Conditioning Engineers (ASHRAE).

Aversa, M.; Curcio, S.; Calabrò, V.; Iorio G. (2007). An Analysis of the Transport Phenomena Occurring during Food Drying Process. Journal of Food Engineering 78 (3). 2007: 922-932

Babalis S.J, Belessiotis V.G. (2004). Influence of the drying conditions on the drying constants and moisture diffusivity during the thin-layer drying of figs. Journal of Food Engineering; 65: 449–458.

Barbosa-Canovas, G. V.; Vega-Mercado, H. (1996). Dehydration of Foods. New York: International Thomas Publishing.

Bennamoun L, Belhamri A. (2003). Design and simulation of a solar dryer for agriculture products. Journal of Food Engineering 59(2–3):259–266.

Bolaji B.O, Olalusi A.P, (2008). Performance evaluation of a mixed-mode solar dryer. AU Journal of Technology. Volume 11(4), 2008, 225–31.

Bolaji B.O, (2005). Development and performance evaluation of box-type absorber solar air collector for crop drying. Journal of Food Technology. Volume 3(4), 2005:515–600.

Bondaruk, J.; Markowski, M.; Blaszczak, W. (2007). Effect of Drying Conditions on the Quality of Vacuum-Microwave Dried Potato Cubes. Journal of Food Engineering 81 (2). 2007: 306-312

Brasiello A., Adiletta G., Russo P., Crescitelli S., Albanese D. and Di Matteo M. (2013). Mathematical modeling of eggplant drying: shrinkage effect. J. Food Eng. 114: 99-105.

Brennan, J. G. (2006). Evaporation and Dehydration. In: Brennan, J. G. (Edt): Food Processing Handbook. Weinheim: Willey-VCH Verlag GmbH & Co. 2006: 71-124

Brooker, D.B., Bakker-Arkema, F.W. and Hall, C.W. (1992). Drying and storage of grains and oilseeds. New York, Van Nostrand Reinhold.

Bruce, D. M. (1985). Exposed-Layer Barley Drying: Three Models Fitted to New Data Up to 150°C. Journal of Agricultural Engineering Research 32 (4): 337-348

Cassava Processing Research in Nigeria, IITA Research for Development (R4D) Review. http://r4dreview.iita.org/index.php/2011/11/13/cassava-processing-research-in-nigeria

Castell-Palou, A., Váquiro, H. A., Cárcel, J. A., Rosselló, C., Femenia, A., & Simal, S. (2012). Mathematical Modeling of Moisture Distribution and Kinetics in Cheese Drying. Drying Technology. http://doi.org/10.1080/07373937.2012.704465

Chen, J. Y.; Isobe, K.; Zhamg, H.; Matsunaga, R. (2000). Hot-Air Drying Model for Udon Noodles. Food Science Technology Research 6 (4): 284-287

Chua, K. J.; Mujumdar, A. S.; Chou, S. K.; Hawlader, M. N. A; Ho, J. C. (2000). Convective Drying of Banana, Guava and Potato Pieces: Effect of Cyclical Variations of Air Temperature on Drying Kinetics and Color Change. Drying Technology 18 (4-5). 2000: 907-936.

Dare Aderibigbe Adetan, Kolawole Adesola Oladejo and Surajudeen Olanrewaju Obayopo (2016). Development of a Multipurpose Solar Dryer. FUOYE Journal of Engineering and Technology, Volume 1, Issue 1, September 2016 ISSN: 2579-0625.

Datta A.K (2016). Toward Computer – Aided Food Engineering: Mechanistic frameworks for evolution of product, quality and safety during processing. Journal of Food Engineering, Volume 176, Pages 9-27. https://doi.org/10.1016/j.jfoodeng.2015.10.010.

Davidson, V. J.; Li X.; Brown, R. B. (2004). Forced-Air Drying of Ginseng Root, Effects of Air Temperature on Quality. Journal of Food Engineering 63 (4). 2004: 361-367

De Bonis, M. V., & Ruocco, G. (2008). A generalized conjugate model for forced convection drying based on an evaporative kinetics. Journal of Food Engineering. http://doi.org/10.1016/j.jfoodeng.2008.05.008.

Dagde Kenneth Kekpugile, Goodhead ThankGod Oweifa (2013). Analysis of Mass Transfer during Microwave Drying Of Yam Slabs. American Journal of Engineering Research (AJER, e-ISSN: 2320-0847 p-ISSN: 2320-0936, Volume-02, Issue-11, pp-267-271.

Demirel, D.; Turhan, M. (2003). Air-Drying Behavior of Dwarf Cavendish and Gros Michel Banana Slices. Journal of Food Engineering 59 (1): 1-11

Diamante L. M. and Munro P. A. Munro (1993). Mathematical modelling of thin layer solar drying of sweet potato slices, Solar Energy, 51: 271-276.

Dimitrios A. Tzempelikosa, Dimitris Mitrakosb, Alexandros P. Vourosc, Achilleas V. Bardakasd, Andronikos E. Filiose, Dionissios P. Margarisa (2015). Numerical modeling of heat and mass transfer during convective drying of cylindrical quince slices, Journal of Food Engineering, Volume 156, July 2015, Pages 10-21

Doymaz, I.; Tugrul, N.; Pala, M. (2006). Drying Characteristics of Dill and Parsley Leaves. Journal of Food Engineering 77 (3): 559-565

Doymaz, I. (2006). Drying Kinetics of Black Grapes Treated with Different Solutions. Journal of Food Engineering 76 (2): 212-217

Donsi, G.; Ferrari, G.; Nigro, R. (1996). Experimental Determination of Thermal Conductivity of Apple and Potato at Different Moisture Contents. Journal of Food Engineering 30 (3-4): 263-268

Doymaz I. (2005). Sun drying of figs: an experimental study, Journal of Food Engineering, 71 (4) (2005) 403-407.

Ekechukwu O V, Norton B (1997). Experimental studies of integral-type natural-circulation solar energy tropical crop dryers. Energy Conversion Management 1997; 38(14):1483–500.

El-Beltagi A, Gamea GR, Essa AHA (2007). Solar drying characteristics of strawberry. Journal of Food Engineering; 78; 2007, 456–64.

Enibe S. O. (2002). Performance of natural circulation solar air heating system with phase change material energy storage, Renewable Energy; 27: 69–86.

Food and Agricultural Organization (FAO) 2004. Proceedings of the validation forum on the global cassava development strategy, Volume 4. FAO, Rome, 26-28 April 2000.

Federal Ministry of Agriculture & Rural Development (2016). Nigeria's Staple Crop Processing Zones Available: https://www. afdb.org/fileadmin/uploads/afdb /Documents/GenericDocuments/Nigeria%E2%80%99s_staple_crop_processing_zones_by_dr._Niyi_odunlami.pdf

Fellows, J. P. (2000). Food Processing Technology: Cambridge: Woodhead Publishing Limited.

Ferguson, W. J., & Turner, I. W. (1996). A Control Volume Finite Element Numerical Simulation of the High Temperature Drying of Spruce. Journal of Computational Physics archive, Volume 125 Issue 1, Pages 59-70. doi>10.1006/jcph.1996.0079

Ferguson W. J. (2007). A Control Volume Finite Element Numerical Simulation of the High Temperature Drying of Spruce. International Journal of Drying Technology, Volume 13, 1995 - Issue 3, Pages 607-634, https://doi.org/10.1080/07373939508916977.

Fish, D. M. and Trim, D. S. (1993). A review of research into the drying of cassava chips. Journal of Tropical Science, Vol. 33 (2): 191 - 208.

Fortes, M.; Okos, M. R. (1981). Non-Equilibrium Thermodynamics Approach to Heat and Mass Transfer in Corn Kernels. Transactions of the ASAE. 1981: 761-769

Fontaine, J.; Ratti, C. (1999). Lumped-Parameter Approach for Prediction of Drying Kinetics in Foods. Journal of Food Process Engineering 22: 287-305

F.K. Forson; M.A.A. Nazha; F.O. Akuffo; H. Rajakaruna (2007). Design of mixed-mode natural convection solar crop dryers: Application of principles and rules of thumb, Renewable Energy 32, 2007, 2306–2319.

Freire, F.; Figueiredo, A.; Ferrao, P. (2001). Modelling High Temperature Thin Layer Drying Kinetics of Olive Bagasse. Journal of Agricultural Engineering Research 78 (4): 397-406

Fudholi A, Sopian K, Othman M, Ruslan M (2014). Energy and exergy analyses of solar drying system of red seaweed. Energy Build, 2014; 68:121–9.

Gastón, A. L., Abalone, R. M., & Giner, S. A. (2002). Wheat drying kinetics. Diffusivities for sphere and ellipsoid by finite elements. Journal of Food Engineering. http://doi.org/10.1016/S0260-8774(01)00121-2

G. Adiletta, C. Wijerathne, W. Senadeera, P. Russo, A. Crescitelli and M. Di Matteo (2018). Dehydration and Rehydration characteristics of pretreated pumpkin slices. Italian journal of food science, vol. 30, 684-706

García-Alvaradoa M.A., Pacheco-Aguirreab F.M., Ruiz-Lópezb I.I. (2014). Analytical solution of simultaneous heat and mass transfer equations during food drying. Elsevier Journal of Food Engineering, Volume 142, pp 39-45

Geankoplis, C. J. (2003). Transport Process and Separation Principles. New Jersey: Pearson Education, Inc.

Günhan T., Demir V., Hancioglu E. and Hepbasli A. (2005). Mathematical modelling of drying of bay leaves, Energy Conversion and Management, Volume 46, pp 11-12.

Haghi A. K. (2001). A Mathematical Model of the Drying Process. Acta Polytechnica Vol. 41, No. 3/2001

Haghighi K., Irudayaraj J., Stroshine R. L., Sokhansanj S. (1990). Grain kernel drying simulation using the finite element method. Journal of Transactions of the American Society of Agricultural Engineers, Vol 33, Issue 6, pp 1957-1965.

Hassini L., Azzouz S., Peczalski R., Belghith A. (2007). Estimation of potato moisture diffusivity from convective drying kinetics with correction for shrinkage. Journal of food engineering volume 79 no.1 pp. 47-56. DOI.10.1016/j.jfoodeng.2006.01.025

Hallström, B. (1992). Mass Transfer in Foods. In: Heldman, D. R.; Lund, D. B. (Edt): Handbook of Food Engineering. New York: Marcel Dekker, Inc. 1992: 317-339

Heldman, D.; Hartel, R. (1997). Principles of Food Processing. New York: International Thomson Publishing. ISBN 978-1-4615-6093-7.

Hellevang K.J. 1993. Natural Air/Low-temperature Crop Drying. North Dakota State University Extension. EB-35.

Hii C.L., Jangam S.V., Ong S.P. and Mujumdar A.S. (2009). Solar drying: Fundamentals, applications and innovations (ISBN: 978-981-07-3336-0, 2012).

Hii C.L., Law C.L., Cloke M. (2009). Modeling using a new thin layer drying model and product quality of cocoa. Journal of Food Engineering. http://doi:10.1016/j.jfoodeng.2008.06.022

Husain, A.; Chen, C. S.; Clayton, J. T.; Whitney, L. F. (1972). Mathematical Simulation of Mass and Heat Transfer in High Moisture Foods. Transactions of the ASAE 1972:732

https://oxfordbusinessgroup.com/analysis/leveraging-growth-agricultural-exports-are-although-various-hurdles-still-need-be-overcome

Ibarz, A; Barbosa-Canovas, G. V. (2003). Unit Operations in Food Engineering. Boca Raton: CRC Press LLC.

Iguaz, A.; San-Martín, M. B.; Maté, J. I.; Fernández, T.; Vírseda, P. (2003). Modelling Effective Moisture Diffusivity of Rough Rice (Lido Cultivar) at Low Drying Temperatures. Journal of Food Engineering 59 (2-3): 253-258

Irudayaraj, J., Haghighi, K., & Stroshine, R. L. (1992). Finite element analysis of drying with application to cereal grains. Journal of Agricultural Engineering Research. http://doi.org/10.1016/0021-8634 (92)80084-6

Janjai, S., Lamlert, N., Intawee, P., Mahayothee, B., Haewsungcharern, M., Bala, B. K., Muller, J. (2008). Finite element simulation of drying of longan fruit. Drying Technology. http://doi.org/10.1080/07373930802046088

Janjai, S., Lamlert, N., Intawee, P., Mahayothee, B., Haewsungcharern, M., Bala, B. K., & Müller, J. (2008). Finite element simulation of drying of mango. Biosystems Engineering. http://doi.org/10.1016/j.biosystemseng.2007.12.010

Janas, S., Boutry, S., Malumba, P., Vander Elst, L., & Béra, F. (2010). Modelling dehydration and quality degradation of maize during fluidized-bed drying. Journal of Food Engineering. http://doi.org/10.1016/j.jfoodeng.2010.05.001

Jamradloedluk, J.; Nathkaranakule, A.; Soponronnarit, Prachayawarakorn, S. (2007). Influences of Drying Medium and Temperature on Drying Kinetics and Quality Attributes of Durian Chip. Journal of Food Engineering 78 (1).2007: 198-205

Jayaraman, K. S. (1995). Critical Review on Intermediate Moisture Fruits and Vegetables. In: Barbosa-Canovas, G. V., Welti-Chanes, J. (Edt): Food Preservation by Moisture Control: Fundamentals and Applications. Lancaster: Technomic Publishing Company, Inc. 1995: 411-441

Jayaraman, K. S.; Das Gupta, D. K. (1995). Drying of Fruits and Vegetables. : Mujumdar, S. A. (Edt): Handbook of Industrial Drying (Volume 1). New York: Marcel Dekker, Inc. 1995: 643-690.

Jeannine Bonilla Lagos, Nivea M. Vicentini, Rodolfo M.C. Dos Santos, Ana Monica Q.B. Bittante, and Paulo J.A. Sobral (2015).Mechanical properties of cassava starch films as affected by different plasticizers and different relative humidity conditions. International Journal of Food Studies, Volume 4 pages 116-125.

Jie Chen, Ying Zhou, Sheng Fang, Yuecheng Meng, Xin Kang, Xuejiao Xu and Xiaobo Zuo (2013). Mathematical Modeling of Hot Air Drying Kinetics of Momordica charantia Slices and Its Color Change. Advance Journal of Food Science and Technology 5(9): 1214-1219, ISSN: 2042-4868; e-ISSN: 2042-4876.

Jittanit W, Saeteaw N, Charoenchaisri A. (2010). Industrial paddy drying and energy saving options. J Stored Prod Res 2010; 46(4):209–13.

Jompob Waewsa, Sirinuch Chindaruksa, Chantana Punlek (2006). A Mathematical Modeling Study of Hot Air Drying for Some Agricultural Products. Thammasat Int. J. Sc. Tech.Vol. II. No. l.

Kashaninejad, M.; Mortazavi, A.; Safekordi, A.; Tabil, L. G. (2007). Thin-Layer Drying Characteristics and Modeling of Pistachio Nuts. Journal of Food Engineering 78 (1): 98-108

Karathanos, V. T.; Belessiotis, V. G. (1997). Sun and Artificial Air Drying Kinetics of Some Agricultural Products. Journal of Food Engineering 31 (1): 35-46

Karathanos, V. T.; Belessiotis, V. G. (1999). Application of a Thin-Layer Equation to Drying Data of Fresh and Semi-Dried Fruits. Journal of Agricultural Engineering Research 74 (4): 355-361

Karel, M; Lund, D. B. (2003). Physical Principles of Food Preservation. New York: Marcel Dekker, Inc.

Kaya A., Aydin O. Dincer I. (2006). Journal of Heat Mass Transfer, Volume 49, pp. 3094-3103

Kaymak-Ertekin, F. (2002). Drying and Rehydrating Kinetics of Green and Red Peppers. Journal of Food Science 67 (1): 168-175

Karel M; Lund, D. B. (2003). Physical Principles of Food Preservation. New York: Marcel Dekker, Inc. 2003.

Karabulut, I.; Topcu, A.; Duran, A.; Turan, S.; Ozturk, B (2015). Effect of Hot Air Drying and Sun Drying on Color Values and ß-Carotene Content of Apricot (Prunus armenica L.). Interdisciplinary Centre for Mathematical and Computational Modelling. Http// doi10.1016/j.lwt.2006.05.001

Karathanos, V. T.; Villalobos, G.; Saravacos, G. D. (1990). Comparison of Two Methods of Estimation of the Effective Moisture Diffusivity from Drying Data. Journal of Food Science 55 (1): 218-223

Karsli Suleyman (2007). Performance analysis of new-design solar air collectors for drying applications. Renewable Energy, Elsevier, vol. 32(10), pages 1645-1660. http//doi: 10.1016/j.renene.2006.08.005

Karel, M; Lund, D. B. (2003). Physical Principles of Food Preservation. New York: Marcel Dekker, Inc.

Kashaninejad, M.; Mortazavi, A.; Safekordi, A.; Tabil, L. G. (2007). Thin-Layer Drying Characteristics and Modeling of Pistachio Nuts. Journal of Food Engineering 78 (1): 98-108

Kalogirou Soteris (2003). The potential of solar industrial process heat applications.

Applied Energy, 2003, vol. 76, issue 4, 337-361.

Kenneth J, Hellevang P. (2013). Grain drying. AE701; 2013. NDSU Extension Service. North Dakota State University, Fargo, North Dakota. Available from: (https://www.ag.ndsu.edu/publications/crops/grain-drying/ae701-grain-drying.pdf).

Khan, M. I. H., Kumar, C., Joardder, M. U. H., & Karim, M. A. (2017). Determination of appropriate effective diffusivity for different food materials. Drying Technology. http://doi.org/10.1080/07373937.2016.1170700

Khalil M. H., Khan M. A., Ramzan M., Rehman M. U., Khan M., Amin M. and Ali A. (2012). Drying of Apricots using a Proficient dish type solar air heater, World Applied Sciences Journal, Issue 18(8), pp 1102-1106.

K. Sacilik (2007). Effect of drying methods on thin-layer drying characteristics of hull-less seed pumpkin (Cucurbita pepo L.), Journal of Food Engineering, 79 (1) (2007) 23-30.

Kumar, D. G. P.; Hebbar, U. H.; Ramesh, M. N. (2006). Suitability of Thin Layer Models for Infrared-Hot Air-Drying of Onion Slices. Lebensmittel-Wissenschaft und-Technologie (Food Science and Technology) 39 (6): 700-705

Lateef A. Sanni, Oluseyi O. Oke, Faborode M. Oladimeji, Kolawole F. Ogbozomivaze (2016). Thermal Properties and Energy Utilization of Cassava Meal in Conductive Rotary Drying. American Journal of Food Science and Technology, Vol. 4, No. 6, 160-167.doi:10.12691/ajfst-4-6-1.

Lahsasni S., Kouhila M., Mahrouz M. and Jaouhari J. J. (2004). Thin layer convective solar drying and mathematical modeling of prickly pear peel (Opuntia Ficus Indica), Energy, 29: 211-224.

Lemus-Mondaca, R. A., Zambra, C. E., Vega-Gálvez, A., Moraga, N.O. (2013). Coupled 3D heat and mass transfer model for numerical analysis of drying process in papaya slices." Journal of Food Engineering. 116(1), pp. 109-117. https://doi.org/10.1016/j.jfoodeng.2012.10.050

Leniger, H. A.; Bruin, S. (1977). The State of the Art of Food Dehydration. In: Downey, W.K. (Edt): Food Quality and Nutrition. London: Applied Science Publishers. 1977: 265-295

Levy A. and Borde I. (1999). Steady State One Dimensional Flow Model for a Pneumatic Dryer. Chem Engr. Processing, Vol. 38, pp.121-130.

Lewis, M. J. (1987). Physical Properties of Foods and Food Processing Systems. Chichester: Ellis Horwood Ltd. 1987

Lewwicki, P. P. (2006). Design of Hot Air Drying for Better Foods. Trends in Food Science and Technology 17 (4). 2006: 153-163

Lomauro, G. J.; Bakshi, A. S. (1985). Finite Element Analysis of Moisture Diffusion in Stored Foods. Journal of Food Science 50 (2): 392-397

Madamba, P. S.; Driscoll, R. H.; Buckle, K. A. (1996). Thin-layer Drying Characteristics of Garlic Slices. Journal of Food Engineering 29 (1): 75-97

Madiouli J., Sghaier J., Lecomte D., Sammouda H. (2012). Food Bioprod. Process. 90 (2012) 43-51

Madhlopa A, Jones SA, Saka J.D.K (2002). A solar air heater with composite-absorber systems for food dehydration. Renewable Energy, 27: 27–37

Marinos-Kouris, D.; Maroulis, Z. B. (1995). Transport Properties in the Drying of Solids. In: Mujumdar, S. A. (Edt): Handbook of Industrial Drying (Volume 1). New York: Marcel Dekker, Inc: 113-160

Márquez, C. A.; De Michelis, A.; Giner, S. A. (2006). Drying Kinetics of Rose Hip Fruits (Rosa Eglanteria L.). Journal of Food Engineering 77 (3): 566-574

Menges H. O. and Ertekin C. (2006). Thin layer drying model for treated and untreated stanley plums, Energy Conversion and Management, 47 (15-16) (2006) 2337-2348.

Maskan, A.; Kaya, S.; Maskan, M. (2002). Hot Air and Sun Drying of Grape Leather (Pestil). Journal of Food Engineering. 54 (1): 81-88

Maskan, M. (2001). Drying, Shrinkage and Rehydration Characteristics of Kiwifruits during Hot Air and Microwave Drying. Journal of Food Engineering 48 (3):177-182

Marcelo S. Bacelosa, Paulo I.F. Almeidab (2001). Modelling of drying kinetic of potatoes taking into account shrinkage. 11th International Congress on Engineering and food (ICEF11), Procedia Food Science 1, 713–721. http//doi:10.1016/j.profoo.2011.09.108

Mennouchea D., Bouchekimaa B, Boubekri A., Boughali S., Bouguettaia H., Bechki D (2014). Valorization of rehydrated Deglet-Nour dates by an experimental investigation of solar drying processing method, Energy Conversion and Management; 84:481–487

Megha S. Sontakke, Prof. Sanjay P. Salve (2015). "Solar Drying Technologies: A review" International Refereed Journal of Engineering and Science (IRJES) ISSN 2319-183X, (Print) 2319-1821, Volume 4, Issue 4, PP.29-35

Methakhup, S.; Chiewchan, N.; Devahastin, S. (2005). Effects of Drying Methods and Conditions on Drying Kinetics and Quality of Indian Gooseberry Flake. Lebensmittel-Wissenschaft und Technologie (Food Science and Technology) 38 (6): 579-587

Midilli A., Kucuk H. and Yapar Z. (2002). A new model for single layer drying. Drying Technology, 20 (7), pp 1503-1513.

Midilli A. and Kucuk H. (2003). Mathematical modeling of thin layer drying of pistachio by using solar energy. Energy Conversion and Management, Volume 44, pp 1111-1122.

Midilli A (2001). Determination of Pistachio Drying Behavior and Conditions in a Solar Drying System, International Journal Of Energy Research, Vol.25, pp.7l 5-725.

Mishkin, M.; Saguy, I.; Karel, M. (1983). Dynamic Optimization of Dehydration Processes: Minimizing Browning in Dehydration of Potatoes. Journal of Food Science 48 (6):1617-1621

Maskan M. and Gogus F (1998). Sorption isotherms and drying characteristics of mulberry (Morus Alba), Journal of Food Engineering, 37. pp 437-449.

Mcminn W.A.M., Khraisheh M.A.M., Magee T.R.A. (2003). Modelling the mass transfer during convective, microwave and combined microwave convective drying of solid slabs and cylinders; Food Research International, 36: 977-983.

Motevali A, Minaei S, Khoshtagaza M.H (2011). Evaluation of energy consumption in different drying methods. Energy Convers Manage, 52(2):1192–9.

Mohsen Beigi1 (2017). Mathematical Modelling and Determination of Mass Transfer Characteristics of Celeriac Slices under Vacuum Drying. Periodica Polytechnica, Chemical Engineering, 61(2), pp. 109-116. https://doi.org/10.3311/PPch.9271

Mohsen Beigi (2017). Numerical Simulation of Potato Slices Drying using a Two-Dimensional Finite Element Model. Chemical Industry & Chemical Engineering Quarterly, 23(3), 431–440.

Moyers, C. G.; Baldwin, W. G. (1997). Psychrometry, Evaporative Cooling, and Solids Drying. In: Perry, H. R.; Green, D. W.; Maloney, J. O. (Edt): Perry's Chemical Engineers' Handbook (seventh editon). New York: McGraw Hill: 12.3-12.90

Mujumdar, A. S.; Beke, J. (2003). Grain Drying: Basic Principles. In: Amalendu, C.; Mujumdar, A. S.; Raghavan, G. S. V.; Ramaswamy, H. S. (Edt): Handbook of Postharvest Technology. New York: Marcel Dekker, Inc: 119-138

Murphy, R. Y.; Marks, B. P. (1999). Apparent Thermal Conductivity, Water Content, Density, and Porosity of Thermally-Processed Ground Chicken Patties. Journal of Food Process Engineering 22: 129-140

Naghavi Z., Moheb A., Ziaei-rad S. (2010). Numerical simulation of rough rice drying in a deep-bed dryer using non-equilibrium model. Energy Conversion and Management, Volume 51, Issue 2, Pages 258-264. https://doi.org/10.1016/j.enconman.2009.09.019

Nilnont, W., Thepa, S., Janjai, S., Kasayapanand, N., Thamrongmas, C., & Bala, B. K. (2012). Finite element simulation for coffee (Coffea arabica) drying. Food and Bioproducts Processing. http://doi.org/10.1016/j.fbp.2011.06.007

Njie D. N., Rumsey T. R. & Singh R. P. (1996) .Thermal Properties of Cassava, Yam and Plantain. Journal of Food Engineering 37 (1996) 63-76.PII:S0260-8774(98)00068-5.

North Dakota State University Extension Bulletin 35, "Natural Air/Low Temperature Crop Drying."

Okos, R. M.; Narsimhan, G.; Singh, R. K.; Weitnauer, A. C. (1992). Food Dehydration. In: Heldman, D.R.; Lund, D. B. (Edt): Handbook of Food Engineering. New York: Marcel Dekker, Inc: 437-562

Oladele Peter Kolawole (2012). Evaluation of Cassava Tuber Resistance to Deformation. Global Advanced Research Journal of Food Science and Technology Vol. 1(3) pp. 039-043.

Oladele P. Kolawole, Agboola Simeon Ogunlowo and Leo Agbetoye (2007). Strength and Elastic Properties of Cassava Tuber. International Journal of Food Engineering · doi: 10.2202/1556-3758.1225.

Olm-Olyne, (2004). Olm-Olyne Intertech Ventures Technical Report on Production of Cassava Chips and Pellets, Oshodi, Lagos.

Onyekwere, P. S. N., Ukpabi, U. J. and Ene, L. S. O. (1994). A study on the Quality of Cassava Pellets Produced with a Machine Fabricated in Nigeria. In: Root Crop for Food Security in Africa, Proceedings of the Fifth Technical Symposium of the International Society for Tropical Root Crops – African Branch Held at Kampala, Uganda, 22 - 28 November 1992. Edited by Akoroda M. O.

Ontario ministry of Agriculture, Food and Rural Affairs. http://www.omafra.gov.on.ca

Otuu Obinna, Sam Omenyi, Solomon Nwigbo (2013). Finite element modelling of cassava flash drying in a vertically upward pneumatic conveying dryer. Journal of Engineering and Applied Sciences 9: 24-41

Özilgen, M.; Guvenc, G.; Makaraci, M.; Tumer, I (1995). Colour Change and Weight Loss of Apple Slices during Drying. Zeitschrift für Lebensmittel-Untersuchung und- Forschung 201, 40-45

Ozoegwu, C. G., Eze, C., Onwosi, C. O., Mgbemene, C. A., & Ozor, P. A. (2017). Biomass and bioenergy potential of cassava waste in Nigeria : Estimations based partly on rural-level garri processing case studies. Renewable and Sustainable Energy Reviews, 72, 625–638. http://doi.org/10.1016/j.rser.2017.01.031

Panchariya, P. C.; Popovic, D.; Sharma, A. L. (2002). Thin-Layer Modelling of Black Tea Drying Process. Journal of Food Engineering 52: 349-357

Pan, Y. K.; Zhao, L. J.; Dong, Z. X.; Mujumdar, A. S.; Kudra, T. (1999). Intermittent Drying of Carrot in a Vibrated Fluid Bed: Effect on Product Quality. Drying Technology 17 (10). 2323-2340

Pan, Y. K.; Zhao, L. J.; Hu, W. B. (1999). Tempering-Intermittent Drying on Quality and Energy of Plant Materials'. Drying Technology 17 (9): 1795-1812

Pangavhane D.R, Sawhney R.L. (2002). Review of research and development work on solar dryers or grape drying. Energy Conversion Management 2002; 43:45–61.

Pangavhane D.R, Sawhney R.L, Sarsavadia P.N. (2002). Design development and performance testing of a new natural convection solar dryer. Energy 2002; 27:579-590. PII: S0 360-5442(02)00005-1.

Pavón-Melendez, G.; Hernández, J. A.; Salgado, M. A.; García, M. A. (2002). Dimensionless Analysis of the Simultaneous Heat and Mass Transfer in Food Drying. Journal of Food Engineering 51 (4): 347-353

Parry, J. L. (1985). Mathematical Modelling and Computer Simulation of Heat and Mass Transfer in Agricultural Grain Drying: A Review. Journal of Agricultural Engineering Research 32 (1): 1-29

Perussello, C. A., Mariani, V. C., Masson, M. L., & Castilhos, F. De. (2013). Determination of thermophysical properties of yacon (Smallanthus sonchifolius) to be used in a finite element simulation. International Journal of Heat and Mass Transfer. http://doi.org/10.1016/j.ijheatmasstransfer.2013.09.004

Phillips T.P, Taylor D.S, Sanni L, Akoroda M.O (2004). A cassava industrial revolution in Nigeria; the potential for a new industrial crop. The Global Cassava Development Strategy. IFAD/ FAO, Rome.

Prabhanjan, D. G.; Ramaswamy, H. S.; Raghavan, G. S. V. (1995). Microwave-Assisted Convective Air Drying of Thin-layer Carrots. Journal of Food Engineering (25) 2: 283-293

Prachayawarakorn, S.; Prachayawasin, P.; Soponronnarit, S. (2006). Heating Process of Soybean Using Hot-Air and Superheated-Steam Fluidized-Bed Dryers. Lebensmittel-Wissenschaft und-Technologie (Food Science and Technology) 39 (7). 2006: 770-778

Prakash O, Kumar A (2013). Historical Review and Recent Trends in Solar Drying Systems, International Journal of Green Energy (2013); 10:690–738.

Queiroz, R.; Gabas, A. L.; Telis, V. R. N. (2004). Drying Kinetics of Tomato by Using Electric Resistance and Heat Pump Dryers. Drying Technology 22 (7): 1603-1620

Ranjan, R., Irudayaraj, J., Reddy, J. N., & Mujumdar, A. S. (2004). Finite-element simulation and validation of stepwise drying of bananas. Numerical Heat Transfer; Part A: Applications. http://doi.org/10.1080/10407780490453963

Rahman, S. M.; Perera, O. C. (1999). Drying and Food Preservation. In: Rahman, S.M. (Edt): Handbook of Food Preservation. New York: Marcel Dekker, Inc: 173-216.

Rajamma, P., McFarlane, J. A. and Poulter, N. H. (1994). Susceptibility of Rhyzopertha Dominica (f.) (Coleoptera: Bostrichidae) and Tribolium Castaneum (Herbst) (Coleoptera: Tenebrionidae) to Cyanogens in Dried Cassava Products. Tropical Science, 34: 315 – 320.

Raji A.O, Kanwanya N, Wahabi B.A, Sanni L.A, Dixon A.G, Paul Ilona. (2008). Optimisation of Cassava Pellet Processing Method. Article in International Journal of Food Engineering · January 2008. DOI: 10.2202/1556-3758.1234

Ramesh, M. N. (2003). Moisture Transfer Properties of Cooked Rice during Drying. Lebensmittel-Wissenschaft und-Technologie 36 (2): 245-255

Ramswamy, H.; Marcotte, M (2006). Food Processing - Principles and Applications. London: Taylor and Francis Group. 2006

Ramadan ElGamala, Frederik Ronsse, Jan G. Pietersa (2001). Modeling Deep-Bed Grain Drying Using COMSOL Multiphysics. Excerpt from the Proceedings of the 2013 COMSOL Conference in Rotterdam.

Ratti, C. (2001). Hot Air and Freeze-Drying of High-Value Foods: A Review. Journal of Food Engineering 49 (4): 311-319

Rizvi, S. S. H. (1995). Thermodynamic Properties of Foods in Dehydration. In: Rao, M. A.; Rizvi, S. S. H. (Edt): Engineering Properties of Foods. New York: Marcel Dekker, Inc: 223-309

Rotstein, E.; Laura, P. A.; De Cemborain, M. E. (1974). Analytical Prediction of Drying Performance in Nonconventional Shapes. Journal of Food Science 39 (3): 627-631

Rayaguru, K. and Routray, W. (2012).Mathematical modeling of thin layer drying kinetics of stone apple slices. International Food Research Journal 19(4): 1503-1510.

Sabarez, H. T. (2012). Computational modelling of the transport phenomena occurring during convective drying of prunes. Journal of Food Engineering. http://doi.org/10.1016/j.jfoodeng.2012.02.021

Sabarez, H. T., Gallego-Juarez, J. A., & Riera, E. (2012). Ultrasonic-Assisted Convective Drying of Apple Slices. Drying Technology. http://doi.org/10.1080/07373937.2012.677083.

Sablani, S.; Rahman, S.; Al-Habsi, N. (2000). Moisture Diffusivity in Foods-An Overview. In: Mujumdar, S. A. (Edt): Drying Technology in Agriculture and Food Sciences. Enfield: Science Publishers, Inc: 35-50

Sacilik, K.; Elicin, A. K.; Unal, G. (2006). Drying Kinetics of Üryani Plum in a Convective Hot-Air Dryer. Journal of Food Engineering 76 (3): 362-368

Salemović, D. R., Aleksandar D J. Dedic , and Nenad L.J. Ćupric **"**Two-Dimensional Mathematical Model For Simulation of The Drying Process of Thick Layers of Natural Materials in a Conveyor-Belt Dryer. Thermal Science, 21 (2017), 3, pp. 1169-1378

Salemović, D. R., et al., A Mathematical Model and Simulation of the Drying Process of Thin Layers of Potatoes in a Conveyor-Belt Dryer, Thermal Science, 19 (2015), 3, pp. 1107-1118

Saravacos, G. D. (1995). Mass Transfer Properties of Foods. In: Rao, M. A.; Rizvi, S. S. H. (Edt): Engineering Properties of Foods. New York: Marcel Dekker, Inc:169-221

Saravacos, G.; Maroulis, Z. B. (2001). Transport Properties of Foods. New York: Marcel Dekker, Inc. 2001

Saravacos, G., D.; Kostaropoulos, A. E. (2002). Handbook of Food Processing Equipment. New York: Plenum Publishers.

Sarsavadia P.N. (2007). Development of a solar-assisted dryer and evaluation of energy requirement for the drying of onion. RenewEnergy 2007; 32(15):2529–47.

Sarsavadia P. N., Sawhney R. L., Pangavhane D. R., & Singh S. P. (1999). Drying behaviour of brined onion slices. Journal of Food Engineering, vol. 40, pp. 219-226. https://doi.org/10.1016/S0260-8774 (99)00058-8

Sayali Gaikwad and Khot M.V. (2016). Thermal Analysis of Solar Dryer. International Journal of Current Engineering and Technology (IJCET). E-ISSN 2277-4106, P-ISSN 2347-5161.

Schweiger H, Mendes J,Benz N, Hennecke K, Prieto G, Gusi M (2000). The potential of solar heat in industrial processes. A state of the art review for Spain and Portugal. In Proceedings of Eurosun 2000, Copenhagen, Denmark.

Senadeera, W.; Bhandari, B. R.; Young, G.; Wijesinghe, B. (2003). Influence of Shapes of Selected Vegetable Materials on Drying Kinetics during Fluidized Bed Drying. Journal of Food Engineering 58 (3): 277-283

Sharma G.P., Prasad S. (2004). Effective moisture diffusivity of garlic cloves undergoing microwave-convective drying. Journal of Food Engineering. 65 (2004) 609-617. http// doi:10.1016/j.jfoodeng.2004.02.027.

Shanmugam V, Natarajam E (2007). Experimental study of regenerative desiccant integrated solar dryer with and without reflective mirror. Applied Thermal Engineering 27, 2007, 1543–51.

Sharma V.K, Colangelo A, Spagna G. (1995). Experimental investigation of different solar dryers suitable for fruit and vegetable drying. Renewable Energy; 6(4): 413–24.

Sharma A, Chen C.R, Nguyen V (2009). Solar-energy drying systems: A review, Renewable and Sustainable Energy Reviews 2009; 13:1185–1210.

Shahin Rafiee, Alireza Keyhani and Ali Mohammadi (2008). Soybean Seeds Mass Transfer Simulation during Drying Using Finite Element Method. World Applied Sciences Journal 4 (2): 284-288.

Janjai S., Lamlert N., Intawee P., Mahayothee B., Haewsungcharern M., Bala B.K., Müller J., Biosystems Engineering. Issue 99, pages 523-531.

Simal S., Femenia A., Garau M. C. and Rosella C. (2005). Use of exponential, Page's and Diffusional models to simulate the drying kinetics of kiwi fruit, Journal of Food Engineering, 66 (3) 323-328.

Singh, R. P.; Heldman, R. D. (1993). Introduction to Food Engineering. London: Academic Press, Inc. 1993

Sokhansanj, S.; Jayas, D. S. (1995). Drying of Food Stuffs. In: Mujumdar, S. A. (Edt): Handbook of Industrial Drying (Volume 1). New York: Marcel Dekker, Inc.1995: 589-625

Srikiatden, J.; Roberts, J. S. (2005). Moisture Loss Kinetics of Apple during Convective Hot Air and Isothermal Drying. International Journal of Food Properties 8: 493-512

Stefano Curcio, Maria Aversa, Sudip Chakraborty, Vincenza Calabrò, Gabriele Iorio (2016). Formulation of a 3D conjugated multiphase transport model to predict drying process behavior of irregular-shaped vegetables. Elsevier Journal of Food Engineering, Volume 176, Pages 36-55.

Tarigan, E.; Prateepchaikul, G.; Yamsaengsung, R.; Sirichote, A.; Tekasakul, P (2007). Drying Characteristics of Unshelled Kernels of Candle Nuts. Journal of Food Engineering 79 (3): 828-833

Tang, Z.; Cenkowski, S. (2000). Dehydration Dynamics of Potatoes in Superheated Steam and Hot Air. Canadian Agricultural Engineering 42 (1): 1-13

Temmerman, J. D.; Verboven, P.; Nicolai, B.; Ramon, H. (2007). Modelling of Transient Moisture Concentration of Semolina Pasta during Air Drying. Journal of Food Engineering 80 (3): 892-903

Thijsen, H. A. C (1979). Optimization of Process Conditions during Drying with Regard to Quality Factors. Lebensmittel-Wissenschaft and Technologie 12: 308-317

Thakor N. J., Sokhansanj S., Sosulski F. W., and Yannacopoulos S. (1999). Mass and dimensional changes of single canola kernels during drying, Journal of Food Engineering, 40 (1999) 153-160.

Tiris C., Tiris M. and Dincer I. (1996). Energy efficiency of a solar drying system, International Journal of Energy Research. 20 (9): 767-770.

Togrul I. T. and Pehlivan D. (2004). Modelling of thin layer drying kinetics of some fruits under open-air sun drying process. Journal of Food Engineering, Volume 65, pp 413-425.

Torki-Harchegani, M., Ghasemi-Varnamkhasti, M., Ghanbarian, D, Sadeghi, M., Tohidi, M. (2016). Dehydration characteristics and mathematical modelling of

lemon slices drying undergoing oven treatment. Heat and Mass Transfer. 52, pp. 281-289. https://doi.org/10.1007/s00231-015-1546-y

Torki-Harchegani M., Ghanbarian D., Sadeghi M. (2015). Heat Mass Transfer 51 (2015) 1121-1129

Torki Harchegani M., Moheb A., Sadeghi M., Tohidi M., Naghavi Z. (2012). Experimental study of deep – bed drying kinetics of rough rice. Journal of Engineering Int: CIGR Journal, Vol. 14, No4

Tutuncu A. M. and Labuza T. P. (1996). Effect of geometry on the effective moisture transfer diffusion coefficient. Journal of Food Engineering, Volume 30, pp 433-447.

Us. P., Khan M.K. (2007). Heat Pump Drying of Food Materials: A critical Review. Journal of Food Science and Technology 44 (2): 119-124

Uzman, D.; Sahbaz, F. (2000). Drying Kinetics of Hydrated and Gelatinized Corn Starches in the Presence of Sucrose and Sodium Chloride. Journal of Food Science 65 (1): 115-122

Vaccarezza, L. M.; Lombardi, J. L.; Chirife, J. (1974). Kinetics of Moisture Movement during Air Drying of Sugar Beet Root. Journal of Food Technology 9: 317-327

Vagenas, G. K., & Marinos-Kouris, D. (1991). Finite element simulation of drying of agricultural products with volumetric changes. Applied Mathematical Modelling. http://doi.org/10.1016/0307-904X(91)90037-P

Vega, A.; Fito, P.; Andres, A.; Lemus, R. (2007). Mathematical Modeling of Hot-Air Drying Kinetics of Red Bell Pepper (Var. Lamuyo). Journal of Food Engineering 79 (4): 1460-1466

Wachiraphansakul, S.; Devahastin, S (2007). Drying Kinetics and Quality of Okara Dried in a Jet Spouted Bed of Sorbent Particles. Lebensmittel-Wissenschaft und-Technologie (Food Science and Technology) 40 (2): 207-219

Wagner, M. J.; Lucas, T.; Le Ray, D.; Trystram, G. (2007). Water Transport in Bread during Baking. Journal of Food Engineering 78 (4):1167-1173

Wang L., Sun D.W., (2003). Recent developments in numerical modelling of heating and cooling processes in the food industry – A review. Trends Food Sci. Technol. 14: 408-423

Wang, N.; Brennan, J. G. (1995). A Mathematical Model of Simultaneous Heat and Moisture Transfer during Drying of Potato. Journal of Food Engineering 24 (1):47-60

Welti-Chanes, J; Mujica-Paz, H; Valdez-Fragoso, A.; Leon-Cruz, R. (2003). Fundamentals of Mass Transport. In: Welti-Chanes, J.; Velez-Ruiz, F. J.; Barbosa-Canovas, G. V. (Edt): Transport Phenomena in Food Processing. Florida: CRC Press LLC: 3-23

Wisconsin Energy Efficiency and Renewable Energy, sasanford@wisc.edu.

Xanthopoulos, G, (2007). Applicability of a Single-Layer Drying Model to Predict the Drying Rate of Whole Figs, Journal of Food Engineering, 81, 3, pp. 553-559

Yaldız O., Ertekin C. and Uzun H. I. (2001). Mathematical modelling of thin layer solar drying of sultana grapes, Energy-An International Journal, 26 (2001) 457-465.

Young, W. P. (1996). Determination of Moisture and Ash Contents of Food. In: Nollet, M. L. L. (Edt): Handbook of Food Analysis (volume 1). New York: Marcel Dekker, Inc: 59-92

Yusheng, Z.; Poulsen, P. K.: Diffusion in Potato Drying. Journal of Food Engineering 7. 1988: 249-262

Zhang Shiwei, Ninghua Kong, Yufang Zhu, Zhijun Zhang, and Chenghai Xu (2013). 3D Model-Based Simulation Analysis of Energy Consumption in Hot Air Drying of Corn Kernels. Mathematical Problems in Engineering, Volume 2013, Article ID 579452,http://dx.doi.org/10.1155/2013/579452

Zare, D, Minaei, S, Khoshtaghaza, M H, and Mohamad Zadeh, M. (2006). Computer simulation of rough rice drying in a batch dryer. United Kingdom: N. p. Web. doi:10.1016/J.ENCONMAN.2006.02.021.

Zhe Liu, Zidan Wu, Xiaomeng Wang, Jia Song, and Wenfu Wu (2015), Numerical Simulation and Experimental Study of Deep Bed Corn Drying Based on Water Potential. Hindawi Publishing Corporation, Mathematical Problems in Engineering, Article ID 539846, 13 pages. http://dx.doi.org/10.1155/2015/539846.

# APPENDIX I

```
% Thermophysical Characterization

% Heater Temp 150C

M_d=22.12/1000;% Mass of dry matter

MC_eq=1.2402;% equilibrium moisture content

H=10/1000/2; % half thickness of the sample

Time=60*[0 20 40 60 80 100 120 140 160 180 200 220
    240 260 280 300 320]; % time

Mass1=10^(-3)*[113.255 101.72 90.631 81.888 72.797
    67.517 63.69 60.637 59.362 58.382 57.443
    56.706 56.161 55.804 55.32 55.229 55.22]; % mass of
sample replicate one

Mass2=10^(-3)*[102.952 81.65 69.581 60.833 54.87 51.125
    49.133 47.344 46.463 45.972 45.432 44.782
    44.469 44.428 44.339 44.249 44.24];% mass of sample
replicate two

Mass=(Mass1+Mass2)/2; % mean mass of sample

MC=(Mass-M_d)/M_d; % moisture content

MR=(MC-MC_eq)/(MC(1)-MC_eq); % moisture ratio

y=(4*H^2/pi/pi)*log(8./MR/pi/pi);

D_eff=inv(Time*Time')*y*Time' % effecttive diffusivity
```

```
plot(Time,log(MR))

xlabel('t [sec]');ylabel('log(MR)');


% Convective Mass Transfer Coefficient

R=16/1000;h=10/1000;% length width and height of each sample

ns=10;% number of samples

rhow=1000; % density of water

V1_1=10^(-6)*[0  153   150   149   148   217   217   215   214   213   210
      209   207   205   203   202   201]; % initial volume in the flask

V1_2=10^(-6)*[0  215   215   220   218   215   214   255   250   249   246
      238   236   234   228   225   220]; % initial volume in the flask

V1=(V1_1+V1_2)/2;

V_i=ns*pi*R^2*h;% initial volume

A_i=ns*2*(pi*R*h+pi*R^2);% initial area

V=V_i-(Mass(1)-Mass)/rhow;% volume at time t

V2=V1+V/ns; % volume of one sample at t

A=zeros(1,length(V));

for i=1:length(V)

   if V(i)>0

A(i)=(1-((Mass(1)-Mass(i))./V_i/rhow))^(2/3)*A_i; % area at time t
```

```
h_m(i)=V(i)*log(MR(i))/A(i)/Time(i)/60; % convective mass transfer coefficient
    else
        A(i)=0;
        h_m(i)=0;
    end
end
10^6*V1'
V'
10^6*V2'
A'
h_m'


% MODEL FOR h_m
for i=1:length(Time)-1
    t(i)=Time(i+1);
    hm(i)=h_m(i+1);
end
f = fit( t', -hm', 'poly2')% quadratic fit
Y=f(t); % fitted values at the indicated points of "time"
```

```
T=-hm';

Rsquared=1-sum((T-Y).^2)/sum((T-mean(T)).^2);

RMSE=sqrt(mean((Y-T).^2));

r=sum((Y-mean(Y)).*(T-mean(T)))/sqrt(sum((Y-mean(Y)).^2)*sum((T-
mean(T)).^2));

Stat=[Rsquared RMSE r]'


% Program for Plotting The Measured and the FEM predicted Kinetics

% Temp 150C

M_d=22.12/1000;% Mass of dry matter

MC_eq=1.2402;% equilibrium moisture content

H=10/1000/2; % half thickness of the sample

Time=60*[0 20 40 60 80 100 120 140 160 180 200 220
    240 260 280 300 320]; % time

Mass1=10^(-3)*[113.255 101.72 90.631 81.888 72.797
    67.517 63.69 60.637 59.362 58.382 57.443
    56.706 56.161 55.804 55.32 55.229 55.22]; % mass of
sample replicate one

Mass2=10^(-3)*[102.952 81.65 69.581 60.833 54.87 51.125
    49.133 47.344 46.463 45.972 45.432 44.782
```

```
44.469 44.428 44.339 44.249 44.24];% mass of sample replicate two

Mass=(Mass1+Mass2)/2; % mean mass of sample

MC=(Mass-M_d)/M_d; % moisture content

% predicted values

[m,n]=size(u);

MCred=zeros(1,n);

MCpred=u(562,:);

plot((1/60)*Time,MC,'*',(1/60)*Time,MCpred,'d')

xlabel('time [min]');ylabel('moisture content [dry basis]')

legend('Experimental value','FE prediction')

% error indices

T=MC;Y=MCpred;

Rsquared=1-sum((T-Y).^2)/sum((T-mean(T)).^2);

RMSE=sqrt(mean((Y-T).^2));

r=sum((Y-mean(Y)).*(T-mean(T)))/sqrt(sum((Y-mean(Y)).^2)*sum((T-mean(T)).^2));

Stat=[Rsquared RMSE r]'


% Heater Temp 140C
```

```
M_d=22.12/1000;% Mass of dry matter

MC_eq=1.3369;% equilibrium moisture content

H=10/1000/2; % half thickness of the sample

Time=60*[0 20 40 60 80 100 120 140 160 180 200 220
    240 260 280 300 320 340 360 380]; % time

Mass1=10^(-3)*[114.45 101.25 90.002 82.151 75.549
    70.872 67.357 65.086 63.247 61.673 59.932
    59.023 58.229 57.612 57.046 56.591 56.076
    55.617 55.599 55.591]; % mass of sample replicate one

Mass2=10^(-3)*[101.012 83.03 72.421 66.98 62.263 60.263
    58.517 57.601 57.063 55.764 54.756 53.992
    53.325 52.796 52.461 52.358 51.85 51.781
    51.701 51.7];% mass of sample replicate two

Mass=(Mass1+Mass2)/2; % mean mass of sample

MC=(Mass-M_d)/M_d; % moisture content

MR=(MC-MC_eq)/(MC(1)-MC_eq); % moisture ratio

y=(4*H^2/pi/pi)*log(8./MR/pi/pi);

D_eff=inv(Time*Time')*y*Time' % effecttive diffusivity

plot(Time,log(MR))

xlabel('t [sec]');ylabel('log(MR)');
```

```
% Convective Mass Transfer Coefficient

R=16/1000;h=10/1000;% length width and height of each sample

ns=10;% number of samples

rhow=1000; % density of water

V1_1=10^(-6)*[0  168   167   166   165   163   162   160   158   157   155
      154   153   152   151   150   149   149   147   146]; % initial volume in
the flask

V1_2=10^(-6)*[0  215   219   218   216   213   212   211   210   210   209
      204   204   203   201   200   198   197   195   193]; % initial volume in
the flask

V1=(V1_1+V1_2)/2;

V_i=ns*pi*R^2*h;% initial volume

A_i=ns*2*(pi*R*h+pi*R^2);% initial area

V=V_i-(Mass(1)-Mass)/rhow;% volume at time t

V2=V1+V/ns; % volume of one sample at t

A=zeros(1,length(V));

for i=1:length(V)

   if V(i)>0

A(i)=(1-((Mass(1)-Mass(i))./V_i/rhow))^(2/3)*A_i; % area at time t

h_m(i)=V(i)*log(MR(i))/A(i)/Time(i)/60; % convective mass transfer coefficient
```

```
    else
        A(i)=0;
        h_m(i)=0;
    end
end
10^6*V1'
V'
10^6*V2'
A'
h_m'

% MODEL FOR h_m
for i=1:length(Time)-1
    t(i)=Time(i+1);
    hm(i)=h_m(i+1);
end
f = fit( t', -hm', 'poly2')% quadratic fit
Y=f(t); % fitted values at the indicated points of "time"
T=-hm';
```

```
Rsquared=1-sum((T-Y).^2)/sum((T-mean(T)).^2);

RMSE=sqrt(mean((Y-T).^2));

r=sum((Y-mean(Y)).*(T-mean(T)))/sqrt(sum((Y-mean(Y)).^2)*sum((T-
mean(T)).^2));

Stat=[Rsquared RMSE r]'


% Program for Plotting The Measured and the FEM predicted Kinetics

% Temp 140C

M_d=22.12/1000;% Mass of dry matter

MC_eq=1.3369;% equilibrium moisture content

H=10/1000/2; % half thickness of the sample

Time=60*[0 20 40 60 80 100 120 140 160 180 200 220
    240 260 280 300 320 340 360 380]; % time

Mass1=10^(-3)*[114.45 101.25 90.002 82.151 75.549
    70.872 67.357 65.086 63.247 61.673 59.932
    59.023 58.229 57.612 57.046 56.591 56.076
    55.617 55.599 55.591]; % mass of sample replicate one

Mass2=10^(-3)*[101.012 83.03 72.421 66.98 62.263 60.263
    58.517 57.601 57.063 55.764 54.756 53.992
    53.325 52.796 52.461 52.358 51.85 51.781
    51.701 51.7];% mass of sample replicate two
```

```
Mass=(Mass1+Mass2)/2; % mean mass of sample

MC=(Mass-M_d)/M_d; % moisture content

% predicted values

[m,n]=size(u);

MCred=zeros(1,n);

MCpred=u(562,:);

plot((1/60)*Time,MC,'*',(1/60)*Time,MCpred,'d')

xlabel('time [min]');ylabel('moisture content [dry basis]')

legend('Experimental value','FE prediction')

% error indices

T=MC;Y=MCpred;

Rsquared=1-sum((T-Y).^2)/sum((T-mean(T)).^2);

RMSE=sqrt(mean((Y-T).^2));

r=sum((Y-mean(Y)).*(T-mean(T)))/sqrt(sum((Y-mean(Y)).^2)*sum((T-
mean(T)).^2));

Stat=[Rsquared RMSE r]'


% Heater Temp 130C

M_d=22.12/1000;% Mass of dry matter
```

```
MC_eq=1.4377;% equilibrium moisture content

H=10/1000/2; % half thickness of the sample

Time=60*[0 20 40 60 80 100 120 140 160 180 200 220
    240 260 280 300 320 340 360 380 400 420]; % time

Mass1=10^(-3)*[110.176 97.34 83.95 76.435 70.835 66.356
    62.619 59.869 56.751 55.001 53.719 52.483
    52.02 51.63 51.346 51.181 50.982 50.853 50.799
    50.789 50.789 50.789]; % mass of sample replicate one

Mass2=10^(-3)*[114.192 96.82 87.691 81.337 77.336 74.466
    71.031 68.571 67.135 65.813 64.681 63.484
    62.631 61.602 60.857 60.276 60.06 59.537 59.37
    59.357 59.349 59.341];% mass of sample replicate two

Mass=(Mass1+Mass2)/2; % mean mass of sample

MC=(Mass-M_d)/M_d; % moisture content

MR=(MC-MC_eq)/(MC(1)-MC_eq); % moisture ratio

y=(4*H^2/pi/pi)*log(8./MR/pi/pi);

D_eff=inv(Time*Time')*y*Time' % effecttive diffusivity

plot(Time,log(MR))

xlabel('t [sec]');ylabel('log(MR)');
```

```
% Convective Mass Transfer Coefficient

R=16/1000;h=10/1000;% length width and height of each sample

ns=9;% number of samples

rhow=1000; % density of water

V1_1=10^(-6)*[0  177  175  175  174  173  172  172  170  169  168
      167  165  164  162  160  159  158  157  155  154  153];      %
initial volume in the flask

V1_2=10^(-6)*[0  247  245  243  240  239  236  234  233  231  228
      225  225  224  223  222  221  220  215  214  213  212];      %
initial volume in the flask

V1=(V1_1+V1_2)/2;

V_i=ns*pi*R^2*h;% initial volume

A_i=ns*2*(pi*R*h+pi*R^2);% initial area

V=V_i-(Mass(1)-Mass)/rhow;% volume at time t

V2=V1+V/ns; % volume of one sample at t

A=zeros(1,length(V));

for i=1:length(V)

   if V(i)>0

A(i)=(1-((Mass(1)-Mass(i))./V_i/rhow))^(2/3)*A_i; % area at time t

h_m(i)=V(i)*log(MR(i))/A(i)/Time(i)/60; % convective mass transfer coefficient
```

```
    else
        A(i)=0;
        h_m(i)=0;
    end
end
10^6*V1'
V'
10^6*V2'
A'
h_m'


% MODEL FOR h_m
for i=1:length(Time)-1
    t(i)=Time(i+1);
    hm(i)=h_m(i+1);
end
f = fit( t', -hm', 'poly2')% quadratic fit
Y=f(t); % fitted values at the indicated points of "time"
T=-hm';
```

```
Rsquared=1-sum((T-Y).^2)/sum((T-mean(T)).^2);

RMSE=sqrt(mean((Y-T).^2));

r=sum((Y-mean(Y)).*(T-mean(T)))/sqrt(sum((Y-mean(Y)).^2)*sum((T-
mean(T)).^2));

Stat=[Rsquared RMSE r]'


% Program for Plotting The Measured and the FEM predicted Kinetics

% Temp 130C

M_d=22.12/1000;% Mass of dry matter

MC_eq=1.4377;% equilibrium moisture content

H=10/1000/2; % half thickness of the sample

Time=60*[0 20 40 60 80 100 120 140 160 180 200 220
    240 260 280 300 320 340 360 380 400 420]; % time

Mass1=10^(-3)*[110.176 97.34 83.95 76.435 70.835 66.356
    62.619 59.869 56.751 55.001 53.719 52.483
    52.02 51.63 51.346 51.181 50.982 50.853 50.799
    50.789 50.789 50.789]; % mass of sample replicate one

Mass2=10^(-3)*[114.192 96.82 87.691 81.337 77.336 74.466
    71.031 68.571 67.135 65.813 64.681 63.484
    62.631 61.602 60.857 60.276 60.06 59.537 59.37
    59.357 59.349 59.341];% mass of sample replicate two
```

```
Mass=(Mass1+Mass2)/2; % mean mass of sample

MC=(Mass-M_d)/M_d; % moisture content

% predicted values

[m,n]=size(u);

MCred=zeros(1,n);

MCpred=u(145,:);

plot((1/60)*Time,MC,'*',(1/60)*Time,MCpred,'d')

xlabel('time [min]');ylabel('moisture content [dry basis]')

legend('Experimental value','FE prediction')

% error indices

T=MC;Y=MCpred;

Rsquared=1-sum((T-Y).^2)/sum((T-mean(T)).^2);

RMSE=sqrt(mean((Y-T).^2));

r=sum((Y-mean(Y)).*(T-mean(T)))/sqrt(sum((Y-mean(Y)).^2)*sum((T-
mean(T)).^2));

Stat=[Rsquared RMSE r]'


% Heater Temp 120C

M_d=22.12/1000;% Mass of dry matter
```

```
MC_eq=1.4367;% equilibrium moisture content

H=10/1000/2; % half thickness of the sample

Time=60*[0 20 40 60 80 100 120 140 160 180 200 220
    240 260 280 300 320 340 360 380 400 420]; % time

Mass1=10^(-3)*[110.46397.75 90.021 81.29 75.564 71.893
    68.896 66.452 64.447 62.525 61.211 59.907
    58.897 58.125 57.464 56.812 56.121 55.992
    55.871 55.841 55.808 55.808]; % mass of sample replicate one

Mass2=10^(-3)*[103.71 86.6 76.921 70.98 68.364 66.437
    64.818 62.912 60.067 59.921 59 58.021
    57.924 57.07 56.934 56.621 56.285 55.421
    54.925 54.856 54.786 54.782];% mass of sample replicate two

Mass=(Mass1+Mass2)/2; % mean mass of sample

MC=(Mass-M_d)/M_d; % moisture content

MR=(MC-MC_eq)/(MC(1)-MC_eq); % moisture ratio

y=(4*H^2/pi/pi)*log(8./MR/pi/pi);

D_eff=inv(Time*Time')*y*Time' % effecttive diffusivity

plot(Time,log(MR))

xlabel('t [sec]');ylabel('log(MR)');
```

```
% Convective Mass Transfer Coefficient

R=16/1000;h=10/1000;% length width and height of each sample

ns=10;% number of samples

rhow=1000; % density of water

V1_1=10^(-6)*[0  178   173   172   171   169   168   167   166   164   164
      163   161   159   158   157   156   154   153   152   151   150];      %
initial volume in the flask

V1_2=10^(-6)*[0  190   189   204   203   202   201   200   198   197   196
      195   194   193   192   190   189   188   187   186   185   184];      %
initial volume in the flask

V1=(V1_1+V1_2)/2;

V_i=ns*pi*R^2*h;% initial volume

A_i=ns*2*(pi*R*h+pi*R^2);% initial area

V=V_i-(Mass(1)-Mass)/rhow;% volume at time t

V2=V1+V/ns; % volume of one sample at t

A=zeros(1,length(V));

for i=1:length(V)

   if V(i)>0

A(i)=(1-((Mass(1)-Mass(i))./V_i/rhow))^(2/3)*A_i; % area at time t

h_m(i)=V(i)*log(MR(i))/A(i)/Time(i)/60; % convective mass transfer coefficient
```

```
    else
        A(i)=0;
        h_m(i)=0;
    end
end
10^6*V1'
V'
10^6*V2'
A'
h_m'

% MODEL FOR h_m
for i=1:length(Time)-1
    t(i)=Time(i+1);
    hm(i)=h_m(i+1);
end
f = fit( t', -hm', 'poly2')% quadratic fit
Y=f(t); % fitted values at the indicated points of "time"
T=-hm';
```

```
Rsquared=1-sum((T-Y).^2)/sum((T-mean(T)).^2);

RMSE=sqrt(mean((Y-T).^2));

r=sum((Y-mean(Y)).*(T-mean(T)))/sqrt(sum((Y-mean(Y)).^2)*sum((T-
mean(T)).^2));

Stat=[Rsquared RMSE r]'


% Program for Plotting The Measured and the FEM predicted Kinetics

% Temp 120C

M_d=22.12/1000;% Mass of dry matter

MC_eq=1.4367;% equilibrium moisture content

H=10/1000/2; % half thickness of the sample

Time=60*[0 20 40 60 80 100 120 140 160 180 200 220
    240 260 280 300 320 340 360 380 400 420]; % time

Mass1=10^(-3)*[110.463 97.75 90.021 81.29 75.564 71.893
    68.896 66.452 64.447 62.525 61.211 59.907
    58.897 58.125 57.464 56.812 56.121 55.992
    55.871 55.841 55.808 55.808]; % mass of sample replicate
one

Mass2=10^(-3)*[103.71 86.6 76.921 70.98 68.364 66.437
    64.818 62.912 60.067 59.921 59 58.021
    57.924 57.07 56.934 56.621 56.285 55.421
```

```
54.925 54.856 54.786 54.782];% mass of sample replicate two

Mass=(Mass1+Mass2)/2; % mean mass of sample

MC=(Mass-M_d)/M_d; % moisture content

% predicted values

[m,n]=size(u);

MCred=zeros(1,n);

MCpred=u(2,:);

plot((1/60)*Time,MC,'*',(1/60)*Time,MCpred,'d')

xlabel('time [min]');ylabel('moisture content [dry basis]')

legend('Experimental value','FE prediction')

% error indices

T=MC;Y=MCpred;

Rsquared=1-sum((T-Y).^2)/sum((T-mean(T)).^2);

RMSE=sqrt(mean((Y-T).^2));

r=sum((Y-mean(Y)).*(T-mean(T)))/sqrt(sum((Y-mean(Y)).^2)*sum((T-mean(T)).^2));

Stat=[Rsquared RMSE r]'


% Heater Temp 110C
```

```
M_d=22.12/1000;% Mass of dry matter

MC_eq=1.4359;% equilibrium moisture content

H=10/1000/2; % half thickness of the sample

Time=60*[0 20 40 60 80 100 120 140 160 180 200 220
    240 260 280 300 320 340 360 380 400 420 440]; % time

Mass1=10^(-3)*[113.84995.462 86.064 79.473 74.247 70.06
    66.789 64.292 62.479 61.094 59.9 58.611
    57.795 57.211 56.708 55.987 55.2 55.073
    54.846 54.837 54.771 54.767 54.763]; % mass of
sample replicate one

Mass2=10^(-3)*[114.65896.281 87.421 80.781 75.942
    67.424 65.292 63.924 62.025 59.999 58.924
    57.977 56.941 56.381 55.812 55.781 55.687
    55.511 55.501 55.499 55.497 55.496 55.496];%
mass of sample replicate two

Mass=(Mass1+Mass2)/2; % mean mass of sample

MC=(Mass-M_d)/M_d; % moisture content

MR=(MC-MC_eq)/(MC(1)-MC_eq); % moisture ratio

y=(4*H^2/pi/pi)*log(8./MR/pi/pi);

D_eff=inv(Time*Time')*y*Time' % effecttive diffusivity

plot(Time,log(MR))

xlabel('t [sec]');ylabel('log(MR)');
```

```
% Convective Mass Transfer Coefficient

R=16/1000;h=10/1000;% length width and height of each sample

ns=10;% number of samples

rhow=1000; % density of water

V1_1=10^(-6)*[0  243   240   237   234   232   231   230   229   226   224
       223   222   220   221   223   219   220   219   219   218   220   218];
% initial volume in the flask

V1_2=10^(-6)*[0  158   157   156   155   154   154   153   153   152   151
       150   149   148   147   146   145   144   143   142   141   141   139];
% initial volume in the flask

V1=(V1_1+V1_2)/2;

V_i=ns*pi*R^2*h;% initial volume

A_i=ns*2*(pi*R*h+pi*R^2);% initial area

V=V_i-(Mass(1)-Mass)/rhow;% volume at time t

V2=V1+V/ns; % volume of one sample at t

A=zeros(1,length(V));

for i=1:length(V)

   if V(i)>0

A(i)=(1-((Mass(1)-Mass(i))./V_i/rhow))^(2/3)*A_i; % area at time t
```

```
h_m(i)=V(i)*log(MR(i))/A(i)/Time(i)/60; % convective mass transfer coefficient
    else
        A(i)=0;
        h_m(i)=0;
    end
end
10^6*V1'
V'
10^6*V2'
A'
h_m'


% MODEL FOR h_m
for i=1:length(Time)-1
    t(i)=Time(i+1);
    hm(i)=h_m(i+1);
end
f = fit( t', -hm', 'poly2')% quadratic fit
Y=f(t); % fitted values at the indicated points of "time"
```

```
T=-hm';

Rsquared=1-sum((T-Y).^2)/sum((T-mean(T)).^2);

RMSE=sqrt(mean((Y-T).^2));

r=sum((Y-mean(Y)).*(T-mean(T)))/sqrt(sum((Y-mean(Y)).^2)*sum((T-
mean(T)).^2));

Stat=[Rsquared RMSE r]'


% Program for Plotting The Measured and the FEM predicted Kinetics

% Temp 110C

M_d=22.12/1000;% Mass of dry matter

MC_eq=1.4359;% equilibrium moisture content

H=10/1000/2; % half thickness of the sample

Time=60*[0 20 40 60 80 100 120 140 160 180 200 220
    240 260 280 300 320 340 360 380 400 420 440]; % time

Mass1=10^(-3)*[113.84995.462 86.064 79.473 74.247 70.06
    66.789 64.292 62.479 61.094 59.9 58.611
    57.795 57.211 56.708 55.987 55.2 55.073
    54.846 54.837 54.771 54.767 54.763]; % mass of
sample replicate one

Mass2=10^(-3)*[114.65896.281 87.421 80.781 75.942
    67.424 65.292 63.924 62.025 59.999 58.924
```

```
        57.977    56.941    56.381    55.812    55.781    55.687
        55.511    55.501    55.499    55.497    55.496    55.496];%
mass of sample replicate two

Mass=(Mass1+Mass2)/2; % mean mass of sample

MC=(Mass-M_d)/M_d; % moisture content

% predicted values

[m,n]=size(u);

MCred=zeros(1,n);

MCpred=u(1,:);

plot((1/60)*Time,MC,'*',(1/60)*Time,MCpred,'d')

xlabel('time [min]');ylabel('moisture content [dry basis]')

legend('Experimental value','FE prediction')

% error indices

T=MC;Y=MCpred;

Rsquared=1-sum((T-Y).^2)/sum((T-mean(T)).^2);

RMSE=sqrt(mean((Y-T).^2));

r=sum((Y-mean(Y)).*(T-mean(T)))/sqrt(sum((Y-mean(Y)).^2)*sum((T-
mean(T)).^2));

Stat=[Rsquared RMSE r]'
```

## APPENDIX II

```
% This script is written and read by pdetool and should NOT be edited.
% There are two recommended alternatives:
 % 1) Export the required variables from pdetool and create a MATLAB script
 %    to perform operations on these.
 % 2) Define the problem completely using a MATLAB script. See
 %    http://www.mathworks.com/help/pde/examples/index.html for examples
 %    of this approach.
function pdemodel
[pde_fig,ax]=pdeinit;
pdetool('appl_cb',10);
pdetool('snapon','on');
set(ax,'DataAspectRatio',[1.5 1 16]);
set(ax,'PlotBoxAspectRatio',[1 0.67080746008002234 0.67080746008002234]);
set(ax,'XLim',[-0.034150843881856935 0.15334915611814307]);
set(ax,'YLim',[-0.063946759259259328 0.061053240740740672]);
set(ax,'XTickMode','auto');
set(ax,'YTickMode','auto');
```

```
% Geometry description:
pdeellip(0,0,0.016,0.016,...
0,'E1');
set(findobj(get(pde_fig,'Children'),'Tag','PDEEval'),'String','E1')

% Boundary conditions:
pdetool('changemode',0)
pdesetbd(4,...
'neu',...
1,...
'-4.104*10^(-18)* t^2-1.421*10^(-13) *t+1.247*10^(-8)',...
'1.2402*(-4.104*10^(-18)* t^2-1.421*10^(-13) *t+1.247*10^(-8))')
pdesetbd(3,...
'neu',...
1,...
'-4.104*10^(-18)* t^2-1.421*10^(-13) *t+1.247*10^(-8)',...
'1.2402*(-4.104*10^(-18)* t^2-1.421*10^(-13) *t+1.247*10^(-8))')
pdesetbd(2,...
'neu',...
```

```
1,...
'-4.104*10^(-18)* t^2-1.421*10^(-13) *t+1.247*10^(-8)',...
'1.2402*(-4.104*10^(-18)* t^2-1.421*10^(-13) *t+1.247*10^(-8))')
pdesetbd(1,...
'neu',...
1,...
'-4.104*10^(-18)* t^2-1.421*10^(-13) *t+1.247*10^(-8)',...
'1.2402*(-4.104*10^(-18)* t^2-1.421*10^(-13) *t+1.247*10^(-8))')

% Mesh generation:
setappdata(pde_fig,'Hgrad',1.3);
setappdata(pde_fig,'refinemethod','regular');
setappdata(pde_fig,'jiggle',char('on','mean',''));
setappdata(pde_fig,'MesherVersion','preR2013a');
pdetool('initmesh')
pdetool('refine')
pdetool('refine')
pdetool('refine')
```

```
% PDE coefficients:
pdeseteq(2,...
'3.1467*10^(-20)',...
'0.0',...
'0',...
'1.0',...
'0:20*60:320*60',...
'3.8871',...
'0.0',...
'[0 100]')
setappdata(pde_fig,'currparam',...
['3.1467*10^(-20)';...
'0              '])

% Solve parameters:
setappdata(pde_fig,'solveparam',...
char('0','24384','10','pdeadworst',...
'0.5','longest','0','1E-4','','fixed','Inf'))
```

```
% Plotflags and user data strings:
setappdata(pde_fig,'plotflags',[1 1 1 1 1 1 1 1 0 1 0 17 1 0 0 0 0 1]);
setappdata(pde_fig,'colstring','');
setappdata(pde_fig,'arrowstring','');
setappdata(pde_fig,'deformstring','');
setappdata(pde_fig,'heightstring','');

% Solve PDE:
pdetool('solve')
```

# APPENDIX III

Table of Air properties (www.engineeringtoolbox.com/dry-air-properties-d_973.html)

| Temperature (*K*) | Specific Heat | | Ratio of Specific Heats - $k$ - ($c_p/c_v$) | Dynamic Viscosity - $\mu$ - ($10^{-5}$ kg/m s) | Thermal Conductivity ($10^{-5}$ kW/m K) | Prandtl Number | Kinematic Viscosity[1] - $\nu$ - ($10^{-5}$ $m^2/s$) | Density[1] - $\rho$ - ($kg/m^3$) | Thermal Diffusivity - $\alpha$ - ($10^{-6} m^2/s$) |
|---|---|---|---|---|---|---|---|---|---|
| | - $c_p$ - (kJ/kgK) | - $c_v$ - (kJ/kgK) | | | | | | | |
| 175 | 1.0023 | 0.7152 | 1.401 | 1.182 | 1.593 | 0.744 | 0.586 | 2.017 | |
| 200 | 1.0025 | 0.7154 | 1.401 | 1.329 | 1.809 | 0.736 | 0.753 | 1.765 | 10.17 |
| 225 | 1.0027 | 0.7156 | 1.401 | 1.467 | 2.020 | 0.728 | 0.935 | 1.569 | |
| 250 | 1.0031 | 0.7160 | 1.401 | 1.599 | 2.227 | 0.720 | 1.132 | 1.412 | 15.67 |
| 275 | 1.0038 | 0.7167 | 1.401 | 1.725 | 2.428 | 0.713 | 1.343 | 1.284 | |
| 300 | 1.0049 | 0.7178 | 1.400 | 1.846 | 2.624 | 0.707 | 1.568 | 1.177 | 22.07 |
| 325 | 1.0063 | 0.7192 | 1.400 | 1.962 | 2.816 | 0.701 | 1.807 | 1.086 | |
| 350 | 1.0082 | 0.7211 | 1.398 | 2.075 | 3.003 | 0.697 | 2.056 | 1.009 | 29.18 |
| 375 | 1.0106 | 0.7235 | 1.397 | 2.181 | 3.186 | 0.692 | 2.317 | 0.9413 | |
| 400 | 1.0135 | 0.7264 | 1.395 | 2.286 | 3.365 | 0.688 | 2.591 | 0.8824 | 36.94 |
| 450 | 1.0206 | 0.7335 | 1.391 | 2.485 | 3.710 | 0.684 | 3.168 | 0.7844 | |
| 500 | 1.0295 | 0.7424 | 1.387 | 2.670 | 4.041 | 0.680 | 3.782 | 0.7060 | |
| 550 | 1.0398 | 0.7527 | 1.381 | 2.849 | 4.357 | 0.680 | 4.439 | 0.6418 | |
| 600 | 1.0511 | 0.7640 | 1.376 | 3.017 | 4.661 | 0.680 | 5.128 | 0.5883 | |
| 650 | 1.0629 | 0.7758 | 1.370 | 3.178 | 4.954 | 0.682 | 5.853 | 0.5430 | |
| 700 | 1.0750 | 0.7879 | 1.364 | 3.332 | 5.236 | 0.684 | 6.607 | 0.5043 | |

| | | | | | | | | | |
|---|---|---|---|---|---|---|---|---|---|
| 750 | 1.0870 | 0.7999 | 1.359 | 3.482 | 5.509 | 0.687 | 7.399 | 0.4706 | |
| 800 | 1.0987 | 0.8116 | 1.354 | 3.624 | 5.774 | 0.690 | 8.214 | 0.4412 | |
| 850 | 1.1101 | 0.8230 | 1.349 | 3.763 | 6.030 | 0.693 | 9.061 | 0.4153 | |
| 900 | 1.1209 | 0.8338 | 1.344 | 3.897 | 6.276 | 0.696 | 9.936 | 0.3922 | |
| 950 | 1.1313 | 0.8442 | 1.340 | 4.026 | 6.520 | 0.699 | 10.83 | 0.3716 | |
| 1000 | 1.1411 | 0.8540 | 1.336 | 4.153 | 6.754 | 0.702 | 11.76 | 0.3530 | |
| 1050 | 1.1502 | 0.8631 | 1.333 | 4.276 | 6.985 | 0.704 | 12.72 | 0.3362 | |
| 1100 | 1.1589 | 0.8718 | 1.329 | 4.396 | 7.209 | 0.707 | 13.70 | 0.3209 | |
| 1150 | 1.1670 | 0.8799 | 1.326 | 4.511 | 7.427 | 0.709 | 14.70 | 0.3069 | |
| 1200 | 1.1746 | 0.8875 | 1.323 | 4.626 | 7.640 | 0.711 | 15.73 | 0.2941 | |
| 1250 | 1.1817 | 0.8946 | 1.321 | 4.736 | 7.849 | 0.713 | 16.77 | 0.2824 | |
| 1300 | 1.1884 | 0.9013 | 1.319 | 4.846 | 8.054 | 0.715 | 17.85 | 0.2715 | |
| 1350 | 1.1946 | 0.9075 | 1.316 | 4.952 | 8.253 | 0.717 | 18.94 | 0.2615 | |
| 1400 | 1.2005 | 0.9134 | 1.314 | 5.057 | 8.450 | 0.719 | 20.06 | 0.2521 | |
| 1500 | 1.2112 | 0.9241 | 1.311 | 5.264 | 8.831 | 0.722 | 22.36 | 0.2353 | |
| 1600 | 1.2207 | 0.9336 | 1.308 | 5.457 | 9.199 | 0.724 | 24.74 | 0.2206 | |
| 1700 | 1.2293 | 0.9422 | 1.305 | 5.646 | 9.554 | 0.726 | 27.20 | 0.2076 | |
| 1800 | 1.2370 | 0.9499 | 1.302 | 5.829 | 9.899 | 0.728 | 29.72 | 0.1961 | |
| 1900 | 1.2440 | 0.9569 | 1.300 | 6.008 | 10.233 | 0.730 | 32.34 | 0.1858 | |

# APPENDIX IV

Table 4.1. The effective diffusivity at various heater temperatures for the rectangular and circular samples

| Rectangular Samples | | | Circular Samples | | |
|---|---|---|---|---|---|
| Heater Temperature [$^o$C] | $M_{eq}$ | $D_{eff} \times 10^9$ | Heater Temperature [$^o$C] | $M_{eq}$ | $D_{eff} \times 10^9$ |
| 150 | 0.5400 | 2.3304 | 150 | 0.5375 | 3.1467 |
| 140 | 0.8380 | 2.1277 | 140 | 0.8375 | 1.4830 |
| 130 | 0.7375 | 2.0004 | 130 | 0.7375 | 1.6770 |
| 120 | 0.9410 | 1.1498 | 120 | 0.9375 | 1.4759 |
| 110 | 1.2376 | 1.4260 | 110 | 1.2375 | 1.5665 |

Table 4.2. Heater temperature: 150$^o$C; air temperature 81$^o$C, initial weight of gauze = 15.360g, mass of one Pellets = 10.326g

| S/N | Time | W | V1[ml] | V2[ml] | V$\times 10^4$=$n_s$(V2-V1) $\times 10^4$[m$^3$] | A [m$^2$] | $h_m \times 10^8$ |
|---|---|---|---|---|---|---|---|
| 0 | 0 | 91.486 | 0 | 8.0000 | 0.9600 | 0.0336 | NaN |
| 1 | 20 | 78.052 | 70.7500 | 77.7059 | 0.8347 | 0.0306 | 0.9503 |
| 2 | 40 | 67.868 | 69.7500 | 75.8886 | 0.7366 | 0.0282 | 0.9145 |
| 3 | 60 | 60.974 | 69.2500 | 74.8029 | 0.6663 | 0.0263 | 0.8597 |
| 4 | 80 | 52.565 | 68.5000 | 73.3892 | 0.5867 | 0.0242 | 0.9110 |
| 5 | 100 | 47.728 | 68.2500 | 72.5453 | 0.5154 | 0.0222 | 0.9985 |
| 6 | 120 | 45.130 | 65.0000 | 69.0760 | 0.4891 | 0.0214 | 0.9483 |

| | | | | | | | |
|---|---|---|---|---|---|---|---|
| 7 | 140 | 42.843 | 64.5000 | 68.4442 | 0.4733 | 0.0210 | 0.8867 |
| 8 | 160 | 41.060 | 63.7500 | 67.5582 | 0.4570 | 0.0205 | 0.8578 |
| 9 | 180 | 39.988 | 63.2500 | 66.9374 | 0.4425 | 0.0200 | 0.8457 |
| 10 | 200 | 38.850 | 62.5000 | 66.0837 | 0.4300 | 0.0197 | 0.8469 |
| 11 | 220 | 36.927 | 61.2500 | 64.7429 | 0.4191 | 0.0193 | 0.8665 |
| 12 | 240 | 36.151 | 60.5000 | 63.9479 | 0.4137 | 0.0192 | 0.8551 |
| 13 | 260 | 35.251 | 60.0000 | 63.4081 | 0.4090 | 0.0190 | 0.8552 |
| 14 | 280 | 35.246 | 59.2500 | 62.6567 | 0.4088 | 0.0190 | 0.7967 |
| 15 | 300 | 35.240 | 59.0000 | 62.3912 | 0.4069 | 0.0190 | 0.7719 |

Tables 4.3. Heater temperature: 140$^{o}$C; air temperature 78$^{o}$C, initial weight of gauze = 13.781g, mass of one Pellets =9.590g

| S/N | Time | W | V1[ml] | V2[ml] | V× $10^4$=$n_s$(V2-V1) × $10^4$[$m^3$] | A [$m^2$] | $h_m$ × $10^7$ |
|---|---|---|---|---|---|---|---|
| 0 | 0 | 87.349 | 0 | 8.0000 | 0.9600 | 0.0336 | NaN |
| 1 | 20 | 68.673 | 75.2500 | 81.7928 | 0.7851 | 0.0294 | 0.1607 |
| 2 | 40 | 59.167 | 74.0000 | 79.7327 | 0.6879 | 0.0269 | 0.1405 |
| 3 | 60 | 55.641 | 74.0000 | 79.2962 | 0.6355 | 0.0255 | 0.1217 |
| 4 | 80 | 53.112 | 73.0000 | 78.0060 | 0.6007 | 0.0246 | 0.1087 |
| 5 | 100 | 51.341 | 72.2500 | 77.0608 | 0.5773 | 0.0239 | 0.0982 |
| 6 | 120 | 48.894 | 71.5000 | 76.1358 | 0.5563 | 0.0234 | 0.0920 |
| 7 | 140 | 47.534 | 71.0000 | 75.5192 | 0.5423 | 0.0230 | 0.0857 |

| | | | | | | | |
|---|---|---|---|---|---|---|---|
| 8 | 160 | 45.313 | 70.2500 | 74.6464 | 0.5276 | 0.0225 | 0.0826 |
| 9 | 180 | 44.751 | 69.5000 | 73.8354 | 0.5202 | 0.0223 | 0.0774 |
| 10 | 200 | 43.917 | 68.5000 | 72.7635 | 0.5116 | 0.0221 | 0.0745 |
| 11 | 220 | 43.107 | 67.7500 | 71.9349 | 0.5022 | 0.0218 | 0.0735 |
| 12 | 240 | 42.877 | 67.2500 | 71.3509 | 0.4921 | 0.0215 | 0.0746 |
| 13 | 260 | 42.107 | 66.5000 | 70.5502 | 0.4860 | 0.0213 | 0.0742 |
| 14 | 280 | 41.866 | 66.0000 | 69.9448 | 0.4734 | 0.0210 | 0.0855 |
| 16 | 300 | 41.505 | 65.2500 | 69.1539 | 0.4685 | 0.0208 | 0.0920 |
| 17 | 320 | 41.497 | 64.7500 | 68.6510 | 0.4681 | 0.0208 | 0.0874 |
| 18 | 340 | 41.489 | 64.0000 | 67.9004 | 0.4680 | 0.0208 | 0.0825 |
| 19 | 360 | 41.481 | 63.5000 | 67.3998 | 0.4680 | 0.0208 | 0.0781 |

Tables 4.4. Heater temperature: 130$^{o}$C; air temperature 75$^{o}$C, initial weight of gauze = 15.360g, mass of one Pellets = 10.723g

| S/N | Time | W | V1[ml] | V2[ml] | V$\times 10^4$=$n_s$(V2-V1) $\times$ $10^4$[m$^3$] | A [m$^2$] | $h_m$ $\times 10^8$ |
|---|---|---|---|---|---|---|---|
| 0 | 0 | 96.929 | 0 | 8.0000 | 0.9600 | 0.0336 | NaN |
| 1 | 20 | 84.669 | 79.7500 | 86.8975 | 0.8577 | 0.0312 | 0.7558 |
| 2 | 40 | 72.520 | 79.0000 | 85.1848 | 0.7422 | 0.0283 | 0.8765 |
| 3 | 60 | 65.753 | 78.5000 | 83.9195 | 0.6503 | 0.0259 | 0.9099 |
| 4 | 80 | 61.351 | 78.0000 | 83.0939 | 0.6113 | 0.0249 | 0.8072 |
| 5 | 100 | 58.342 | 77.5000 | 82.3227 | 0.5787 | 0.0240 | 0.7407 |
| 6 | 120 | 55.943 | 76.5000 | 81.1025 | 0.5523 | 0.0232 | 0.6906 |

| | | | | | | | |
|---|---|---|---|---|---|---|---|
| 7 | 140 | 52.167 | 75.7500 | 80.1238 | 0.5248 | 0.0225 | 0.6677 |
| 8 | 160 | 49.071 | 75.0000 | 79.1448 | 0.4974 | 0.0217 | 0.6645 |
| 9 | 180 | 47.212 | 74.2500 | 78.2803 | 0.4836 | 0.0213 | 0.6331 |
| 10 | 200 | 45.221 | 73.5000 | 77.3705 | 0.4645 | 0.0207 | 0.6335 |
| 11 | 220 | 44.111 | 73.0000 | 76.6840 | 0.4421 | 0.0200 | 0.6658 |
| 12 | 240 | 43.079 | 72.2500 | 75.8547 | 0.4326 | 0.0197 | 0.6569 |
| 13 | 260 | 42.987 | 71.7500 | 75.3358 | 0.4303 | 0.0197 | 0.6180 |
| 14 | 280 | 42.381 | 71.0000 | 74.5053 | 0.4206 | 0.0194 | 0.6283 |
| 16 | 300 | 41.789 | 70.5000 | 73.9543 | 0.4145 | 0.0192 | 0.6278 |
| 17 | 320 | 41.022 | 69.7500 | 73.1637 | 0.4096 | 0.0190 | 0.6273 |
| 18 | 340 | 39.212 | 69.2500 | 72.5795 | 0.3995 | 0.0187 | 0.7098 |
| 19 | 360 | 38.877 | 68.5000 | 71.8076 | 0.3969 | 0.0186 | 0.7208 |
| 20 | 380 | 38.571 | 68.0000 | 71.2890 | 0.3947 | 0.0186 | 0.7401 |
| 21 | 400 | 38.520 | 67.2500 | 70.5317 | 0.3938 | 0.0185 | 0.7323 |

Tables 4.5. Heater temperature: 120$^{o}$C, air temperature 70$^{o}$C, initial weight of gauze = 15.360g, mass of one Pellets = 10.792g

| S/N | Time | W | V1[ml] | V2[ml] | V× $10^4$=$n_s$(V2-V1) × $10^4$[$m^3$] | A [$m^2$] | $h_m$ × $10^7$ |
|---|---|---|---|---|---|---|---|
| 0 | 0 | 96.781 | 0 | 8.0000 | 0.9600 | 0.0336 | NaN |
| 1 | 20 | 83.591 | 79.7500 | 86.5305 | 0.8137 | 0.0301 | 0.1167 |

| | | | | | | | |
|---|---|---|---|---|---|---|---|
| 2 | 40 | 74.802 | 82.2500 | 88.2930 | 0.7252 | 0.0279 | 0.1011 |
| 3 | 60 | 68.556 | 80.5000 | 85.9864 | 0.6584 | 0.0261 | 0.0933 |
| 4 | 80 | 63.729 | 80.0000 | 85.0712 | 0.6085 | 0.0248 | 0.0874 |
| 5 | 100 | 61.147 | 79.2500 | 84.0902 | 0.5808 | 0.0240 | 0.0791 |
| 6 | 120 | 59.020 | 77.5000 | 82.1445 | 0.5573 | 0.0234 | 0.0733 |
| 7 | 140 | 56.565 | 76.7500 | 81.2060 | 0.5347 | 0.0227 | 0.0698 |
| 8 | 160 | 55.815 | 76.0000 | 80.3877 | 0.5265 | 0.0225 | 0.0636 |
| 9 | 180 | 54.621 | 75.5000 | 79.7754 | 0.5130 | 0.0221 | 0.0605 |
| 10 | 200 | 53.370 | 74.2500 | 78.3879 | 0.4965 | 0.0217 | 0.0596 |
| 11 | 220 | 52.494 | 73.5000 | 77.5702 | 0.4884 | 0.0214 | 0.0568 |
| 12 | 240 | 51.820 | 72.7500 | 76.7727 | 0.4827 | 0.0212 | 0.0539 |
| 13 | 260 | 51.266 | 71.7500 | 75.7425 | 0.4791 | 0.0211 | 0.0509 |
| 14 | 280 | 50.494 | 70.7500 | 74.6651 | 0.4698 | 0.0209 | 0.0503 |
| 16 | 300 | 50.061 | 70.2500 | 74.1312 | 0.4657 | 0.0207 | 0.0483 |
| 17 | 320 | 49.589 | 69.7500 | 73.5965 | 0.4616 | 0.0206 | 0.0467 |
| 18 | 340 | 48.671 | 68.7500 | 72.5302 | 0.4536 | 0.0204 | 0.0469 |
| 19 | 360 | 47.412 | 67.2500 | 70.9427 | 0.4431 | 0.0201 | 0.0489 |
| 20 | 380 | 46.112 | 66.5000 | 70.1408 | 0.4369 | 0.0199 | 0.0497 |
| 21 | 400 | 45.911 | 65.7500 | 69.3688 | 0.4343 | 0.0198 | 0.0489 |
| 22 | 420 | 45.834 | 65.2500 | 68.8603 | 0.4332 | 0.0198 | 0.0472 |
| 23 | 440 | 45.821 | 63.2500 | 66.8589 | 0.4331 | 0.0198 | 0.0451 |
| 24 | 460 | 45.821 | 62.7500 | 66.3583 | 0.4330 | 0.0198 | 0.0432 |

Tables 4.6. Heater temperature: 110$^{o}$C; air temperature 66$^{o}$C, initial weight of gauze = 15.360g, mass of one Pellets =10.884g

| S/N | Time | W | V1[ml] | V2[ml] | V× $10^4$=$n_s$(V2-V1) × $10^4$[$m^3$] | A [$m^2$] | $h_m$ × $10^7$ |
|---|---|---|---|---|---|---|---|
| 0 | 0 | 100.736 | 0 | 8.0000 | 0.9600 | 0.0336 | NaN |
| 1 | 20 | 85.262 | 78.2500 | 85.2615 | 0.8414 | 0.0308 | 0.1050 |
| 2 | 40 | 77.732 | 77.5000 | 83.8280 | 0.7594 | 0.0287 | 0.0964 |
| 3 | 60 | 72.602 | 76.7500 | 82.6190 | 0.7043 | 0.0273 | 0.0877 |
| 4 | 80 | 68.723 | 76.2500 | 81.6811 | 0.6517 | 0.0260 | 0.0862 |
| 5 | 100 | 65.770 | 75.2500 | 80.4318 | 0.6218 | 0.0252 | 0.0801 |
| 6 | 120 | 63.514 | 74.5000 | 79.4465 | 0.5936 | 0.0244 | 0.0772 |
| 7 | 140 | 61.683 | 74.0000 | 78.7801 | 0.5736 | 0.0238 | 0.0738 |
| 8 | 160 | 60.078 | 73.2500 | 77.8834 | 0.5560 | 0.0233 | 0.0715 |
| 9 | 180 | 59.046 | 72.5000 | 77.0521 | 0.5462 | 0.0231 | 0.0675 |
| 10 | 200 | 58.200 | 71.7500 | 76.2415 | 0.5390 | 0.0229 | 0.0637 |
| 11 | 220 | 57.143 | 70.2500 | 74.6276 | 0.5253 | 0.0225 | 0.0639 |
| 12 | 240 | 56.373 | 70.0000 | 74.3127 | 0.5175 | 0.0223 | 0.0622 |
| 13 | 260 | 55.511 | 68.7500 | 73.0041 | 0.5105 | 0.0221 | 0.0611 |
| 14 | 280 | 54.950 | 67.7500 | 71.9265 | 0.5012 | 0.0218 | 0.0621 |
| 16 | 300 | 54.489 | 67.2500 | 71.4043 | 0.4985 | 0.0217 | 0.0597 |
| 17 | 320 | 53.067 | 66.7500 | 70.8398 | 0.4908 | 0.0215 | 0.0617 |

| | | | | | | | |
|---|---|---|---|---|---|---|---|
| 18 | 340 | 53.526 | 66.2500 | 70.3484 | 0.4918 | 0.0215 | 0.0572 |
| 19 | 360 | 52.921 | 65.2500 | 69.3170 | 0.4880 | 0.0214 | 0.0571 |
| 20 | 380 | 52.352 | 64.5000 | 68.5379 | 0.4845 | 0.0213 | 0.0573 |
| 21 | 400 | 51.866 | 64.0000 | 68.0034 | 0.4804 | 0.0212 | 0.0591 |
| 22 | 420 | 51.604 | 63.2500 | 67.2349 | 0.4782 | 0.0211 | 0.0594 |
| 23 | 440 | 51.504 | 62.5000 | 66.4776 | 0.4773 | 0.0211 | 0.0581 |
| 24 | 460 | 51.431 | 62.0000 | 65.9740 | 0.4769 | 0.0211 | 0.0563 |
| 25 | 480 | 51.430 | 61.5000 | 65.4720 | 0.4766 | 0.0211 | 0.0543 |
| 26 | 500 | 51.430 | 61.0000 | 64.9713 | 0.4766 | 0.0211 | 0.0523 |

Tables 4.7. Heater temperature: 150$^{o}$C; air temperature 81$^{o}$C, initial weight of gauze = 15.360g, mass of one Pellets =11.641g

| S/N | Time | W | V1[ml] | V2[ml] | V× $10^4$=$n_s$(V2-V1) × $10^4$[$m^3$] | A [$m^2$] | $h_m$ × $10^7$ |
|---|---|---|---|---|---|---|---|
| 0 | 0 | 113.255 | 0 | 8.0425 | 0.8042 | 0.0261 | NaN |
| 1 | 20 | 101.720 | 184.0000 | 190.4006 | 0.6401 | 0.0224 | 0.1303 |
| 2 | 40 | 90.631 | 182.5000 | 187.7427 | 0.5243 | 0.0197 | 0.1205 |
| 3 | 60 | 81.888 | 184.5000 | 188.8682 | 0.4368 | 0.0174 | 0.1148 |
| 4 | 80 | 72.797 | 183.0000 | 186.6155 | 0.3615 | 0.0153 | 0.1155 |
| 5 | 100 | 67.517 | 216.0000 | 219.1642 | 0.3164 | 0.0140 | 0.1122 |
| 6 | 120 | 63.690 | 215.5000 | 218.3733 | 0.2873 | 0.0132 | 0.1084 |
| 7 | 140 | 60.637 | 235.0000 | 237.6312 | 0.2631 | 0.0124 | 0.1085 |

| | | | | | | | |
|---|---|---|---|---|---|---|---|
| 8 | 160 | 59.362 | 232.0000 | 234.5234 | 0.2523 | 0.0121 | 0.1037 |
| 9 | 180 | 58.382 | 231.0000 | 233.4498 | 0.2450 | 0.0118 | 0.0992 |
| 10 | 200 | 57.443 | 228.0000 | 230.3759 | 0.2376 | 0.0116 | 0.0978 |
| 11 | 220 | 56.706 | 223.5000 | 225.8065 | 0.2307 | 0.0114 | 0.0998 |
| 12 | 240 | 56.161 | 221.5000 | 223.7636 | 0.2264 | 0.0112 | 0.1013 |
| 13 | 260 | 55.804 | 219.5000 | 221.7437 | 0.2244 | 0.0112 | 0.0998 |
| 14 | 280 | 55.320 | 215.5000 | 217.7151 | 0.2215 | 0.0111 | 0.1064 |
| 16 | 300 | 55.229 | 213.5000 | 215.7060 | 0.2206 | 0.0110 | 0.1065 |
| 17 | 320 | 55.220 | 210.5000 | 212.7051 | 0.2205 | 0.0110 | 0.1007 |

Tables 4.8. Heater temperature: 140$^{o}$C; air temperature 78$^{o}$C, initial weight of gauze = 15.360g, mass of one Pellets =13.536g

| S/N | Time | W | V1[ml] | V2[ml] | V× $10^4$=$n_s$(V2-V1) × $10^4$[$m^3$] | A [$m^2$] | $h_m$ × $10^7$ |
|---|---|---|---|---|---|---|---|
| 0 | 0 | 114.450 | 0 | 8.0425 | 0.8042 | 0.0261 | NaN |
| 1 | 20 | 101.250 | 191.5000 | 197.9834 | 0.6483 | 0.0226 | 0.1297 |
| 2 | 40 | 90.002 | 193.0000 | 198.3905 | 0.5391 | 0.0200 | 0.1199 |
| 3 | 60 | 82.151 | 192.0000 | 196.7259 | 0.4726 | 0.0183 | 0.1069 |
| 4 | 80 | 75.549 | 190.5000 | 194.6600 | 0.4160 | 0.0168 | 0.1012 |
| 5 | 100 | 70.872 | 188.0000 | 191.8261 | 0.3826 | 0.0159 | 0.0931 |

| | | | | | | | |
|---|---|---|---|---|---|---|---|
| 6 | 120 | 67.357 | 187.0000 | 190.5631 | 0.3563 | 0.0152 | 0.0872 |
| 7 | 140 | 65.086 | 185.5000 | 188.9037 | 0.3404 | 0.0147 | 0.0806 |
| 8 | 160 | 63.247 | 184.0000 | 187.2849 | 0.3285 | 0.0144 | 0.0749 |
| 9 | 180 | 61.673 | 183.5000 | 186.6412 | 0.3141 | 0.0140 | 0.0721 |
| 10 | 200 | 59.932 | 182.0000 | 185.0038 | 0.3004 | 0.0136 | 0.0706 |
| 11 | 220 | 59.023 | 179.0000 | 181.9201 | 0.2920 | 0.0133 | 0.0680 |
| 12 | 240 | 58.229 | 178.5000 | 181.3471 | 0.2847 | 0.0131 | 0.0660 |
| 13 | 260 | 57.612 | 177.5000 | 180.2898 | 0.2790 | 0.0129 | 0.0640 |
| 14 | 280 | 57.046 | 176.0000 | 178.7447 | 0.2745 | 0.0128 | 0.0620 |
| 16 | 300 | 56.591 | 175.0000 | 177.7168 | 0.2717 | 0.0127 | 0.0596 |
| 17 | 320 | 56.076 | 173.5000 | 176.1657 | 0.2666 | 0.0125 | 0.0593 |
| 18 | 340 | 55.617 | 173.0000 | 175.6393 | 0.2639 | 0.0124 | 0.0577 |
| 19 | 360 | 55.599 | 171.0000 | 173.6344 | 0.2634 | 0.0124 | 0.0549 |
| 20 | 380 | 55.591 | 169.5000 | 172.1339 | 0.2634 | 0.0124 | 0.0520 |

Table 4.9. Heater temperature: 130$^{o}$C, air temperature 75$^{o}$C, initial weight of gauze = 15.360g, mass of one Pellets =12.486g

| S/N | Time | W | V1[ml] | V2[ml] | V× $10^4$=$n_s$(V2-V1) × $10^4$[$m^3$] | A [$m^2$] | $h_m$ × $10^7$ |
|---|---|---|---|---|---|---|---|
| 0 | 0 | 110.176 | 0 | 8.0425 | 0.7238 | 0.0235 | NaN |

| | | | | | | | |
|---|---|---|---|---|---|---|---|
| 1 | 20 | 97.340 | 212.0000 | 218.3643 | 0.5728 | 0.0201 | 0.1186 |
| 2 | 40 | 83.950 | 210.0000 | 215.1132 | 0.4602 | 0.0174 | 0.1107 |
| 3 | 60 | 76.435 | 209.0000 | 213.3427 | 0.3908 | 0.0156 | 0.0983 |
| 4 | 80 | 70.835 | 207.0000 | 210.8093 | 0.3428 | 0.0143 | 0.0884 |
| 5 | 100 | 66.356 | 206.0000 | 209.4010 | 0.3061 | 0.0133 | 0.0810 |
| 6 | 120 | 62.619 | 204.0000 | 207.0026 | 0.2702 | 0.0122 | 0.0773 |
| 7 | 140 | 59.869 | 203.0000 | 205.7131 | 0.2442 | 0.0114 | 0.0737 |
| 8 | 160 | 56.751 | 201.5000 | 203.9601 | 0.2214 | 0.0107 | 0.0714 |
| 9 | 180 | 55.001 | 200.0000 | 202.2895 | 0.2061 | 0.0102 | 0.0686 |
| 10 | 200 | 53.719 | 198.0000 | 200.1554 | 0.1940 | 0.0098 | 0.0662 |
| 11 | 220 | 52.483 | 196.0000 | 198.0202 | 0.1818 | 0.0094 | 0.0653 |
| 12 | 240 | 52.020 | 195.0000 | 196.9471 | 0.1752 | 0.0091 | 0.0630 |
| 13 | 260 | 51.630 | 194.0000 | 195.8683 | 0.1681 | 0.0089 | 0.0621 |
| 14 | 280 | 51.346 | 192.5000 | 194.3111 | 0.1630 | 0.0087 | 0.0610 |
| 16 | 300 | 51.181 | 191.0000 | 192.7696 | 0.1593 | 0.0086 | 0.0597 |
| 17 | 320 | 50.982 | 190.0000 | 191.7466 | 0.1572 | 0.0085 | 0.0577 |
| 18 | 340 | 50.853 | 189.0000 | 190.7104 | 0.1539 | 0.0084 | 0.0574 |
| 19 | 360 | 50.799 | 186.0000 | 187.6981 | 0.1528 | 0.0083 | 0.0553 |
| 20 | 380 | 50.789 | 184.5000 | 186.1968 | 0.1527 | 0.0083 | 0.0525 |
| 21 | 400 | 50.789 | 183.5000 | 185.1964 | 0.1527 | 0.0083 | 0.0500 |
| 22 | 420 | 50.789 | 182.5000 | 184.1959 | 0.1526 | 0.0083 | 0.0476 |

Table 4.10. Heater temperature: 120°C, air temperature 70°C, initial weight of gauze = 11.638g, mass of one Pellets =13.244g

| S/N | Time | W | V1[ml] | V2[ml] | V× $10^4$=$n_s$(V2-V1) × $10^4$[$m^3$] | A [$m^2$] | $h_m$ × $10^7$ |
|---|---|---|---|---|---|---|---|
| 0 | 0 | 110.463 | 0 | 8.0425 | 0.8042 | 0.0261 | NaN |
| 1 | 20 | 97.750 | 184.0000 | 190.5513 | 0.6551 | 0.0228 | 0.1313 |
| 2 | 40 | 90.021 | 181.0000 | 186.6809 | 0.5681 | 0.0207 | 0.1117 |
| 3 | 60 | 81.290 | 188.0000 | 192.9473 | 0.4947 | 0.0189 | 0.1057 |
| 4 | 80 | 75.564 | 187.0000 | 191.5302 | 0.4530 | 0.0178 | 0.0953 |
| 5 | 100 | 71.893 | 185.5000 | 189.7503 | 0.4250 | 0.0171 | 0.0863 |
| 6 | 120 | 68.896 | 184.5000 | 188.5195 | 0.4020 | 0.0165 | 0.0798 |
| 7 | 140 | 66.452 | 183.5000 | 187.3020 | 0.3802 | 0.0159 | 0.0759 |
| 8 | 160 | 64.447 | 182.0000 | 185.5595 | 0.3560 | 0.0152 | 0.0753 |
| 9 | 180 | 62.525 | 180.5000 | 183.9561 | 0.3456 | 0.0149 | 0.0710 |
| 10 | 200 | 61.211 | 180.0000 | 183.3444 | 0.3344 | 0.0146 | 0.0685 |
| 11 | 220 | 59.907 | 179.0000 | 182.2302 | 0.3230 | 0.0142 | 0.0674 |
| 12 | 240 | 58.897 | 177.5000 | 180.6749 | 0.3175 | 0.0141 | 0.0645 |
| 13 | 260 | 58.125 | 176.0000 | 179.0936 | 0.3094 | 0.0138 | 0.0637 |
| 14 | 280 | 57.464 | 175.0000 | 178.0537 | 0.3054 | 0.0137 | 0.0615 |
| 16 | 300 | 56.812 | 173.5000 | 176.5055 | 0.3005 | 0.0136 | 0.0603 |
| 17 | 320 | 56.121 | 172.5000 | 175.4541 | 0.2954 | 0.0134 | 0.0601 |

| | | | | | | | |
|---|---|---|---|---|---|---|---|
| 18 | 340 | 55.992 | 171.0000 | 173.9045 | 0.2904 | 0.0133 | 0.0605 |
| 19 | 360 | 55.871 | 170.0000 | 172.8736 | 0.2874 | 0.0132 | 0.0601 |
| 20 | 380 | 55.841 | 169.0000 | 171.8687 | 0.2869 | 0.0131 | 0.0575 |
| 21 | 400 | 55.808 | 168.0000 | 170.8635 | 0.2864 | 0.0131 | 0.0551 |
| 22 | 420 | 55.808 | 167.0000 | 169.8633 | 0.2863 | 0.0131 | 0.0525 |

Table 4.11. Heater temperature: 110$^{o}$C, air temperature 66$^{o}$C, initial weight of gauze = 11.638g, mass of one Pellets =12.583g

| S/N | Time | W | V1[ml] | V2[ml] | V× $10^4$=$n_s$(V2-V1) × $10^4$[$m^3$] | A [$m^2$] | $h_m$ × $10^7$ |
|---|---|---|---|---|---|---|---|
| 0 | 0 | 113.849 | 0 | 8.0425 | 0.8042 | 0.0261 | NaN |
| 1 | 20 | 95.462 | 200.5000 | 206.7043 | 0.6204 | 0.0220 | 0.1423 |
| 2 | 40 | 86.064 | 198.5000 | 203.7914 | 0.5291 | 0.0198 | 0.1130 |
| 3 | 60 | 79.473 | 196.5000 | 201.1298 | 0.4630 | 0.0181 | 0.0987 |
| 4 | 80 | 74.247 | 194.5000 | 198.6266 | 0.4127 | 0.0168 | 0.0895 |
| 5 | 100 | 70.060 | 193.0000 | 196.4913 | 0.3491 | 0.0150 | 0.0907 |
| 6 | 120 | 66.789 | 192.5000 | 195.7212 | 0.3221 | 0.0142 | 0.0841 |
| 7 | 140 | 64.292 | 191.5000 | 194.5279 | 0.3028 | 0.0136 | 0.0783 |
| 8 | 160 | 62.479 | 191.0000 | 193.8423 | 0.2842 | 0.0131 | 0.0746 |
| 9 | 180 | 61.094 | 189.0000 | 191.6718 | 0.2672 | 0.0125 | 0.0725 |
| 10 | 200 | 59.900 | 187.5000 | 190.0583 | 0.2558 | 0.0122 | 0.0697 |

| | | | | | | | |
|---|---|---|---|---|---|---|---|
| 11 | 220 | 58.611 | 186.5000 | 188.9465 | 0.2447 | 0.0118 | 0.0684 |
| 12 | 240 | 57.795 | 185.5000 | 187.8539 | 0.2354 | 0.0115 | 0.0674 |
| 13 | 260 | 57.211 | 184.0000 | 186.2967 | 0.2297 | 0.0113 | 0.0656 |
| 14 | 280 | 56.708 | 184.0000 | 186.2431 | 0.2243 | 0.0112 | 0.0645 |
| 16 | 300 | 55.987 | 184.5000 | 186.7055 | 0.2206 | 0.0110 | 0.0631 |
| 17 | 320 | 55.200 | 182.0000 | 184.1615 | 0.2161 | 0.0109 | 0.0630 |
| 18 | 340 | 55.073 | 182.0000 | 184.1463 | 0.2146 | 0.0108 | 0.0608 |
| 19 | 360 | 54.846 | 181.0000 | 183.1345 | 0.2134 | 0.0108 | 0.0587 |
| 20 | 380 | 54.837 | 180.5000 | 182.6339 | 0.2134 | 0.0108 | 0.0556 |
| 21 | 400 | 54.771 | 179.5000 | 181.6305 | 0.2131 | 0.0108 | 0.0532 |
| 22 | 420 | 54.767 | 180.5000 | 182.6303 | 0.2130 | 0.0108 | 0.0507 |
| 23 | 440 | 54.763 | 178.5000 | 180.6301 | 0.2130 | 0.0108 | 0.0484 |